POLITECNICO DI MILANO
School of Civil, Environmental and Land Management Engineering
Master of Science in Civil Engineering

3D Seismic Base Isolation of Large Structures using Elastomeric Bearings

Supervisor: Prof. Luca Martinelli

Master's Thesis by:
Giulia Pecchillo, 881283

Academic Year 2018-2019

Contents

List of Figures

List of Tables

Abstract

Elastomeric bearing-based isolation system is one of the most adopted solutions to protect structures from intense earthquakes. This kind of isolation systems have been designed with great results for horizontal isolation. The field of the 3D isolation, i.e. elastomeric bearings systems that guarantee isolation in horizontal *and* vertical directions, is continuously evolving. In this thesis, a design approach for a 3D isolation system made of high damping rubber bearings with low shape factor ($S < 5$) is proposed relaxing the more conservative procedure prescribed by European Standards. To validate the approach, a case study is presented and isolated at the base. The European Extremely Large Telescope, E-ELT, is selected thank to its great importance both in terms of dimension of the structure and sensitivity to vibrations in every direction. To verify the designed 3D isolation system, a model of the single bearing is created and analyzed on OpenSees using the `ElastomericX` element by Kumar [2016], that models the bearing behaviour considering the coupling between vertical and horizontal responses. The analyses evidence the complexity of elastomeric bearing response and the difficulty to predict its actual behaviour through a simplified model. However, for the E-ELT case study, the bearing response can be modelled in horizontal directions by an idealized hysteresis cycle whereas in vertical direction as linear elastic. The whole isolated structure model is created and analyzed on SAP2000. The results highlight the beneficial effects of the designed 3D isolation system. The absolute accelerations undergo an overall reduction, in particular in horizontal directions. Vertical isolation is particularly effective in the high-frequency range, eliminating risks of resonance with the research equipment. The analysis is performed with El Centro seismic action so the 3D isolation proposal must be considered as a preliminary design for which further analyses are required. Due to the more complex setting and the relatively smaller amount of experimental and theoretical studies, 3D isolation continues to be an open field for the research of widespread practical and economical solutions [Kelly and Lee, 2018].

Sommario

Sistemi di isolamento composti da isolatori elastomerici rappresentano una delle soluzioni piú adottate per proteggere le strutture da forti sismi. Questi sistemi sono stati progettati con ottimi risultati per l'isolamento orizzontale. L'isolamento 3D, ovvero isolatori elastomerici che garantiscono isolamento in orizzontale e verticale, é in continuo sviluppo. In questo lavoro di tesi viene proposto un approccio per progettare un sistema di isolamento 3D composto da isolatori elastomerici ad elevato smorzamento con basso fattore di forma ($S < 5$), che permette di rilassare le prescrizioni piú conservative imposte da normativa Europea. Per validare la procedura proposta, essa viene applicata ad un caso di studio. L'E-ELT viene selezionato grazie alla sua imponenza e sensitivitá alle vibrazioni in ogni direzione. Per verificare il sistema di isolamento 3D progettato, viene creato ed analizzato il modello di un singolo isolatore su OpenSees usando l'elemento `ElastomericX` implementato da Kumar [2016], che riproduce il comportamento dell'isolatore considerando l'accoppiamento tra risposta orizzontale e verticale. Le analisi evidenziano la complessitá della risposta dell'isolatore e la difficoltá nel predire il suo comportamento attraverso un modello semplificato. Tuttavia, nel caso dell'E-ELT, la risposta dell'isolatore puó essere modellata da un ciclo idealizzato di isteresi in direzione orizzontale e come lineare elastica in direzione verticale. La struttura isolata viene poi modellata e analizzata su SAP2000. I risultati evidenziano gli effetti benefici del sistema di isolamento 3D progettato. Le accelerazioni assolute della struttura subiscono una generale riduzione, in particolare in direzione orizzontale. L'isolamento verticale é particolarmente efficace per le alte frequenze, eliminando rischi di risonanza con la strumentazione di ricerca. L'analisi viene svolta con azione sismica di El Centro perció la proposta si considera come progetto preliminare per cui sono necessarie ulteriori analisi. A causa della maggior complessitá del comportamento dell'isolatore 3D e il minor numero di studi teorici e sperimentali, l'isolamento 3D continua ad essere un campo aperto per la ricerca di soluzioni pratiche ed economiche [Kelly and Lee, 2018].

Acknowledgements

I would like to thank professor Luca Martinelli for the helpfulness and the patience, for sharing time and knowledge, for giving me support every moment, especially the discouraged ones.

A special and infinite thank to my family who made me the person I am and sustain me in every step of my life. Your love is my energy.

A lovely thank to Marco, my best friend and my love. With you my life is full of colours.

Chapter 1

Introduction

Humans are continuously fighting against the power of nature. Among the possible natural disasters, earthquakes are one of the most dangerous and unpredictable. An earthquake is the result of a sudden release of stored energy in the Earth's crust that creates an intense shaking of the ground. Depending on its magnitude, the seismic event could cause great destruction and risk for the population living in the interested zone. Structures need to be protected from the effects of strong ground motions. Considering a structure during earthquake shaking, conventional seismic design requires lateral force resisting system to absorb and dissipate energy in a stable way for a large number of cycles. The design approach is based on the creation of ductile plastic regions, the so-called *plastic hinges*, where the energy dissipation occurs and damage of the gravity frame is concentrated, which often is irreparable. Nevertheless, the performance of the structure is considered acceptable because structural collapse is prevented and life safety is ensured [Constantinou et al., 1998]. When a structure must remain functional even after a strong earthquake, as the case of important structures (e.g. bridges, hospitals, nuclear power plants), the conventional design approach is not applicable.

To fulfill this need, engineers started to work on the design of earthquake protective systems since a century ago [Warn and Ryan, 2012]. The first citation of a *"earthquake-proof building"* has been found into the patent by Jules Touaillon of San Francisco filed in the US Patent Office in February 1870, referring to a structure on steel balls which roll inside shallow dishes. The modern era of isolation is considered to have begun in the mid-seventies in New Zealand with the construction of a stepping, high-level, rail bridge having elements of flexibility in the columns at the pile cap. Construc-

tion of seismically isolated buildings has increased at an almost exponential rate since the 1980s starting principally from Japan and China and rapidly spreading to United States, France, United Kingdom, South Africa and Italy [Buckle, 2000]. In the last decades, several solutions have been studied and developed.
One of the most widespread solution consists of isolation made by elastomeric bearings, that are multiple bonded layers of vulcanized elastomer and steel shims. The elastomer is a macromolecular material which returns to approximately its initial dimensions and shape after substantial deformation by a weak stress and release of stress, having low horizontal stiffness and large deformation capacity. The steel shims provide vertical stiffness and restrain the rubber at the bond surface. Elastomeric bearings carry gravity load and provide flexibility to the system necessary to reduce the amount of seismic forces transmitted to the isolated structure. Isolators behave as rigid constraint for serviceability load levels and assure the dissipation of a significant portion of the energy induced by earthquakes. The amount of energy dissipation is defined by the effective viscous damping parameter that allows to distinguish the elastomeric bearings in two different categories: low damping rubber (LDR) bearings and high damping rubber (HDR) bearings. The latter provides a higher level of energy dissipation due to the addition of carbon black or other material fillers to the rubber compound during the manufacturing process.

Elastomeric bearing-based isolation systems have been already designed with great results for the horizontal isolation. The field of the three-dimensional isolation, i.e. an elastomeric bearings system that guarantees isolation in horizontal *and* vertical directions, is continuously evolving. Kelly et al. [1989] proposed the use of low shape factor elastomeric bearings, that is bearings with thick rubber layers that provide a low vertical stiffness in concert with low horizontal stiffness, to achieve a 3D isolation. Nevertheless, if the vertical input to be eliminated is ambient ground vibration, the natural rubber isolation system can provide great results for 3D isolation but if the vertical input is seismic, the situation becomes considerably more complicated. Because of this complication and expense, these systems have not been accepted for civil construction and the search for a practical and inexpensive system continues [Kelly and Lee, 2018]. However, structures exist in which the protection from vertical vibrations is considered as important as the protection from horizontal vibrations, to the point where vertical isolation is considered to be essential. For these structures, a three-dimensional isolation system is required.

In this thesis, a design approach based on an initial hypothesis that relax the more conservative design approach prescribed by European Standards for a 3D isolation system made of high damping rubber bearings with low shape factor is proposed to protect large structures from damaging effects of intense earthquake shaking. To validate the procedure, a case study is presented and an elastomeric bearing-based isolation system is designed to reduce the values of the seismic forces and accelerations transmitted to the structure in both horizontal and vertical directions. The European Extremely Large Telescope, E-ELT for short, is selected as a suitable case study thank to its great importance both in terms of dimension of the structure and sensitivity to vibrations in every direction of the contained research technology. To verify the reliability of the designed 3D isolation system, models of the single elastomeric bearing and of the whole isolated structure are created and analyzed through commercial structural software.

This document is organized in eight chapters, the first of which is the Introduction read right now. Chapter 2 provides the basic knowledge required to better understand the context of three-dimensional seismic base isolation. The existing mathematical and numerical model for elastomeric bearings are deeply discussed in Chapter 3. Then, Chapter 4 proposes a design procedure for a high damping rubber bearing-based 3D isolation system and Chapter 5 describes a case study and the application of the aformentioned proposal to that structure. The OpenSees analyses performed on a single isolator and the obtained results are reported in Chapter 6. Then, Chapter 7 describes the model of the whole structure created on SAP2000 and the results obtained through its analysis. Finally, Chapter 8 discusses the conclusions of this thesis on the 3D seismic base isolation of large structures using elastomeric bearings.

Chapter 2

Literature Review of 3D Seismic Isolation

Elastomeric bearing-based isolation system is one of the most adopted solution to protect the structures from the damaging effects of earthquakes. Different solutions are possible but not considered in detail in this report. However, it is good practice to understand the context to which the use of elastomeric bearings belongs. To this aim, Section 2.1 introduces the field of earthquake protection systems focusing on seismic base isolation and Section 2.2 briefly describes the main devices diffused worldwide. Section 2.3 highlights advantages and problems related to three-dimensional seismic isolation systems. Then, in Section 2.4 and Section 2.5 are reported the stability theory and the physical model of rubber bearings that represent the fundamental background on which the model described in Chapter 3 is based.

2.1 Earthquake Protective Systems Overview

Conventional seismic design relies on the dissipation of earthquake-induced energy through inelastic response in selected components of the structural frame, so non linear behaviour and deformation of the structure are expected. This approach is associated with structural damage that in most cases is unrecoverable or causes a huge money loss due to repairing. Seismic protection systems are intended to mitigate earthquake hazard. Mitigation is defined as the action taken to reduce the consequences of earthquakes, e.g. seismic strengthening or upgrading, installation of a seismic isolation or energy dissipation system [Buckle and Mayes, 1990].

The family of control systems includes passive, hybrid and active systems, as shown in Figure 2.1.

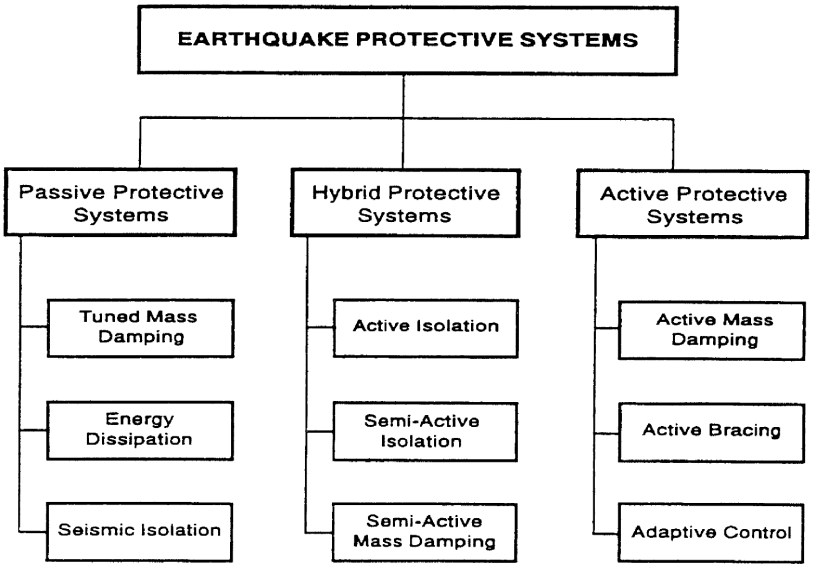

Figure 2.1: Family of earthquake protective systems (adapted from [Buckle, 2000]).

In the semi-active and active systems field, the motion of a structure is controlled or modified through the action of a control system that requires some external energy supply. Generally, semi-active systems derive from passive control systems modified to allow for adjustment of their mechanical properties by means of a nominal power demand, whereas active systems are able to provide energy to the structure. Nowadays actual systems of these types have been designed, fabricated and installed in full-scale structures [Blanford et al., 2010].

Passive systems comprise seismic base isolation and passive mechanical energy dissipation. The latter consists in passive energy dissipation devices that, once incorporated into the superstructure of a building, absorb or consume a portion of the input energy, thereby energy dissipation demand on primary structural members is reduced and possible structural damage is minimized. They can be distinguished as hysteretic, or displacement-dependent, and viscoelastic, or velocity-dependent, dissipators. Energy dissipation systems which cannot be classified by one of the basic types are considered as other systems. A subset of passive energy dissipators consists of tuned mass damper (TMD) and tuned liquid damper (TLD). These vibration absorbers are tuned to a particular dominant mode of vibration of the

structure and transfer kinetic energy among vibrating modes. They allow to control wind vibrations in elastic structures and provide a small amount of damping in tall structures, sufficient to guarantee comfort of occupants during wind storms but ineffective for earthquakes, because of the de-tuning of the absorbers and the narrowness of the provided damping when inelastic actions occur [Buckle, 2000]. Due to their performance, passive energy dissipation devices can be effective both against wind-induced and earthquake-induced motions, thus they are applicable to a wider range of structures, especially those sensitive to long period ground motions. However, it is worth noting that these devices provide additional strength and stiffness to the structure that could assume value such that the contributions become large compared to the structure itself, offsetting the advantages generated by the increase in damping. Moreover, even if they are less intrusive than base isolation in retrofit situations, the limitation of the structural damage is not as significant as the one provided by seismic base isolation [Constantinou et al., 1998].

Seismic base isolation originates from the idea that it is possible to uncouple a structure from its foundation, so the term *"base"* is referred to the plane where the isolation devices are placed to protect the so-called *superstructure* from damaging effects of earthquake ground motions (Figure 2.2).

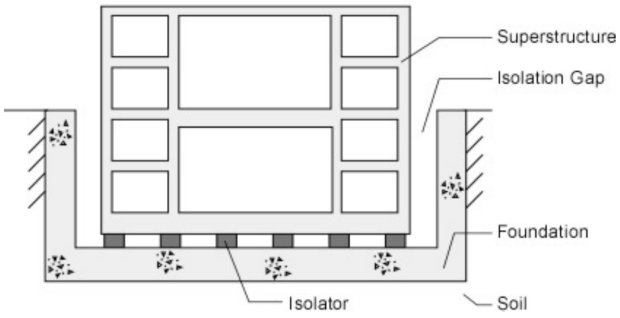

Figure 2.2: Components of a base isolated structure (adapted from [Blanford et al., 2010]).

The introduction of isolators, that are flexible elements, at the base of the structure reduces the stiffness of the system and shifts the fundamental natural period of the structure to the long period range, e.g. two to four seconds. Therefore, when a seismic event occurs, the superstructure is subjected to decreased floor acceleration and inter-story drift with respect to the corresponding conventional non-isolated structure, that experiences deformations within each story of the structure and amplified accelerations at

upper floor levels, as shown in Figure 2.3. The reduction of demands allow the superstructure to remain in the elastic, or nearly elastic, range and minimize the risk of damage to displacement sensitive and acceleration sensitive equipment, nonstructural components, and content. As a consequence of these advantages, isolated structures experience deformation primarily at the isolation interface and the accelerations are relatively uniform over the height [Warn and Ryan, 2012].

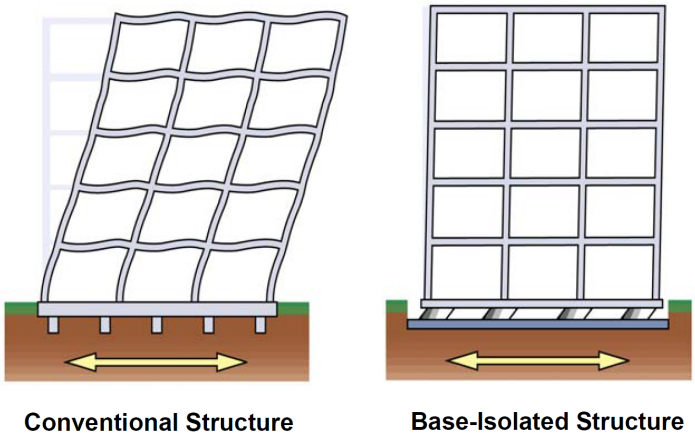

Figure 2.3: Conventional and base isolated structure deformations (adapted from [Symans, 2009]).

The isolation devices are designed to sustain large deformations without damage and to return the structure to its original configuration. The design of the isolator system must include sufficient space for free movement of the structure during earthquake and for access to inspect, and eventually replace, individual element, defined as *"isolation gap"* in Figure 2.2. While lateral flexibility is required to isolate against seismic loads, rigidity must be provided under frequent low load levels, such as minor earthquakes or wind loads, to avoid the structural system to vibrate in a perceptible manner. The efficiency of an isolation system is based on its capacity to alter the fundamental period of the structure, so that it is significantly larger than the one of the non-isolated structure, inducing a response that is far from the acceleration-sensitive region of the earthquake spectrum. Hence, base isolation is preferable for structures with low non-isolated fundamental periods placed in environments where damaging earthquake motions are expected to have short predominant excitation periods, i.e. structures on stiff soil [Symans, 2009].

To sum up, the benefits of seismic base isolation are:

- **Flexibility**. The addition of flexibility to the system increases the fundamental period of vibration and thus reduces values of design forces. The increased flexibility implies larger displacements of the system with inelastic deformation concentrated in the isolation devices, allowing elastic design of the superstructure.
- **Energy dissipation**. A significant portion of the earthquake-induced energy is dissipated by the isolation system, enhancing the aforementioned advantages coming from the additional flexibility, i.e. reduction of the shear forces and limitation of the maximum displacement demand.
- **Resistance for service loads**. Isolation system provide enough stiffness to protect the superstructure from movements due to frequent and low load levels, such as less intense earthquakes and wind loads.

2.2 Seismic Base Isolation

Seismic base isolation is a design strategy based on the introduction of flexible elements moving the period of the structure away from the predominant period of the ground motion. Seismic isolation devices could be classified as:

- **Elastomeric bearings**
  - Low-damping rubber bearings
  - High-damping rubber bearings
  - Lead rubber bearings
- **Sliding bearings**
  - Friction pendulum
  - Triple pendulum

On one hand, elastomeric bearings consist of multiple bonded layers of elastomer and steel shims that carry gravity load of the isolated structure and provide the horizontal flexibility necessary to decrease the amount of seismic forces transmitted to the superstructure (Figure 2.4). In fact, the rubber has low horizontal stiffness and large deformation capacity whereas

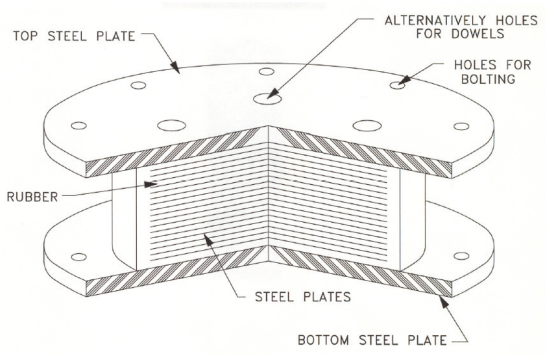

Figure 2.4: Cross section of an elastomeric bearing (adapted from Constantinou et al. [2006]).

the steel shims provide vertical stiffness, restraining the rubber at the bond surface [Kelly et al., 1989].

The construction procedure starts by placing un-vulcanized natural or synthetic rubber sheets and steel shims in a mold, then the mold is subjected to high values of temperature and pressure that simultaneously vulcanize and bond the rubber. A rubber cover is provided to protect the internal rubber layers and steel plates from environmental degradation due to ozone attack and corrosion, respectively [Symans, 2009]. An elastomeric bearing deformed in horizontal direction and the possible actions on it are shown in Figure 2.5.

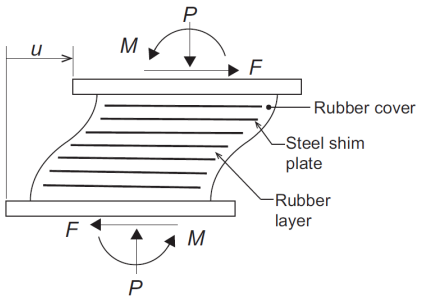

Figure 2.5: Deformed configuration of an elastomeric bearing (adapted from Warn and Ryan [2012]).

An important property of elastomeric bearing is the **shape factor**, S, i.e. the ratio between the loaded area and the total force-free area, that for a circular bearing results:

$$S = \frac{D}{4t_r} \tag{2.1}$$

Low damping rubber (LDR) bearings are natural rubber bearings with normal energy-absorbing capacities, which provide base-isolated buildings with damping ratios that range between 2% and 4% at 100% shear strain. To control, or limit, displacements across the isolation interface, external supplemental damping devices are added [Fujita, 1998].

High damping rubber (HDR) bearings are composed of layers of an elastomeric compound, typically a natural or synthetic rubber with the addition of carbon black, oils, resins and other fillers to provide energy dissipation under cycling loading, without the need for additional dampers. Due to this, the stress-strain behaviour is non linear and causes high horizontal stiffness for low shear strains that occur under service conditions, maintaining forces and deformations in the elastic range. In a moderate seismic event, the HDR bearing deforms and dissipates energy, isolating the structure, while for extreme earthquake loading the shear modulus increases and the stiffened behaviour limits the deformation in the bearing reducing the risk of bearing instability. Damping ratios generally range between 10% and 20% of the critical one at 100% shear strain [Grant et al., 2005]. The dynamic properties of high damping rubber bearings are sensitive to loading conditions, e.g. scragging, that is a reduction in stiffness and damping during the initial cycles of motion with the behavior stabilizing as the number of cycles increases. The behavior under virgin conditions could be strongly different from that under scragged conditions. After a sufficient amount of time, the initial properties are recovered [Warn and Ryan, 2012].

Lead rubber (LR) bearings differ from low-damping rubber bearings only by the addition of a lead-plug that is press-fit into a central hole in the bearing (Figure 2.6). The elastomer provides the isolation component and the lead core, with diameter ranging between 15% and 33% of the bonded diameter of the bearing, provides the energy dissipation or damping component, due to the plastic deformation of the lead [Fujita, 1998]. Particular attention must be paid on the effect of heating in the lead-core with repeated cycling that leads to degradation in the characteristic strength. Fatigue of the lead could be disregarded since lead recrystallizes at normal temperatures [Constantinou et al., 1998].

On the other hand, sliding bearings sustain the weight of the structure through a bearing that rests on a sliding interface. Most of them use polytetrafluorethylene (PTFE) type material and stainless steel for the bearing material at the sliding interface. Horizontal flexibility is provided by sliding,

Figure 2.6: Cross section of a lead rubber bearing (adapted from Blanford et al. [2010]).

while vertical stiffness is provided by direct contact of the bearing elements. The sliding interface is designed with a low coefficient of friction, which limits the resistance to horizontal forces and the amount of force transferred to the superstructure. Restoring force is provided either by additional damping devices or through geometry [Warn and Ryan, 2012].

Friction pendulum consists of a base-plate made of ductile iron, an articulated slider made of ductile iron with bonded PTFE type bearing material and a spherical concave dish made of cast steel with stainless steel overlay, which radius of curvature provides restoring force (Figure 2.7). When an earthquake occurs causing horizontal displacement of the superstructure, the concave surface of the bearing leads to an upward movement of the whole system, against gravity, reducing vertical displacement. Moreover, it ensures the re-centering property of the bearing. The radius of the concave contact surface and the friction coefficient are the parameters designed to give the Friction Pendulum bearings desirable dynamic properties, such that very high axial loads could be supported at large lateral displacements [Warn and Ryan, 2012].

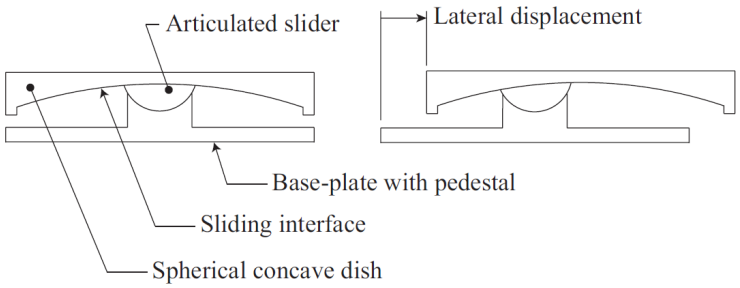

Figure 2.7: Friction Pendulum bearing undeformed and deformed configurations (adapted from Warn and Ryan [2012]).

Triple pendulum is a multi-spherical sliding bearings. This device consists of four spherical sliding surfaces and three independent pendulum mechanisms, as shown in Figure 2.8. In particular, the response during low intensity seismic event is controlled by the internal pendulum mechanism, with two concave plates and a rigid slider, whereas the outer stainless steel concave surfaces provide two independent pendulum mechanisms that control the response during medium or high level of ground motions [Zayas et al., 2016].

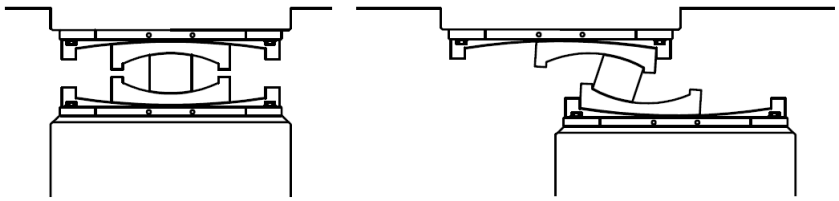

Figure 2.8: Triple Pendulum bearing undeformed and deformed configurations (adapted from Zayas et al. [2016]).

2.3 3D Seismic Isolation

Elastomeric bearing systems can be subdivided in two categories:

1. Elastomeric bearings with additional extrinsic devices to improve the overall damping of the isolation system;
2. Elastomeric bearings that provide the needed amount of damping due to their mechanical properties.

The latter contains the lead rubber bearings, in which the supplemental damping contribution is given by the inelastic deformation of the lead core, and the high damping rubber bearing, in which filler materials enhance the damping and stiffness properties of the rubber compound.
An important characterization of the bearings can be made through the shape factor: high values of S represent thin layers of rubber, that implies high vertical stiffness, while low values represent thick layers of rubber, that implies low vertical stiffness. Therefore, high shape factor bearings are designed to guarantee only horizontal isolation and low shape factor bearings are designed to guarantee horizontal *and* vertical isolation, thanks to the low stiffness in vertical direction in addition to the low horizontal stiffness.

Hence, elastomeric bearings characterized by low value of the shape factor could be adopted to design a three-dimensional seismic isolation system.

The behaviour of elastomeric bearings in horizontal shear and vertical compression has been largely studied in the last decades and mathematical models has been implemented and experimentally validated. However, 3D seismic isolation through only elastomeric bearings is rarely adopted. This is because a lower value of the vertical stiffness implies a lower value of the critical buckling load, that leads to an increasing importance of the stability problem under lateral deformation. Despite this, structures exist in which vibrations in vertical direction could be as undesirable as vibrations in horizontal direction.
The critical buckling load capacity is influenced either by the vertical stiffness and by the lateral displacement of the bearing. The latter leads to a coupling of horizontal and vertical motions in addition to the coupling of bidirectional motions in orthogonal horizontal directions.

The bearing properties that must be determined to design an elastomeric bearing-based seismic isolation system are:

- **Horizontal stiffness** of the bearing, linked to a specific horizontal natural frequency;
- **Vertical stiffness** of the bearing, linked to a predominant vertical frequency;
- **Stability** of the bearing under combined vertical load and lateral displacement.

To shed light on vertical response in general, and on the stability problem, the following sections are focused on the theoretical background of the mathematical existing model for elastomeric bearing: the Haringx's theory of bearing stability and the Two-spring model for elastomeric bearing. The formulations for the computation of horizontal and vertical stiffness of a bearing are deeply discussed in Chapter 3, with particular attention on the coupling between horizontal and vertical motions and their reciprocal influence. [Kelly et al., 1989; Kumar et al., 2015]

2.4 Haringx's Theory of Rubber Bearing Stability

The buckling behaviour of an elastomeric bearing is analogous to the one of a slender column with low shear stiffness. Haringx [1948], Haringx [1949a] and Haringx [1949b] are three of the six papers written by Haringx about

highly compressible helical springs and rubber rods and their application for vibration-free mountings. Some decades later, Gent [1964] recognized that in these three papers, and in particular in Haringx [1949b], Haringx treated for the first time the instability problem of elastomeric bearings. Gent [1964] proved that the Haringx's theory of stability can be applied to predict buckling loads, the interaction of vertical load and horizontal shear stiffness and the influence of vertical load on the damping of a bearing. The linearity of the theory does not allow to consider the strain-softening effect in highly filled rubbers, so this must be introduced in an approximate way [Kelly et al., 1989]. According to the Timoshenko's theory of buckling of columns accounting for shear deformations [Timoshenko and Gere, 1961], the bearing is considered as a beam and it is assumed that plane sections normal to the undeformed central axis remain plane but not necessarily normal to the deformed axis.

Consider an elastic column of length l subjected to a compression load P. The column is fixed at the bottom and restrained against rotation at the top, so a reaction moment, M_0, can arise. To reproduce the actual boundary conditions of a bearing, the upper end is free to move in the horizontal direction and a horizontal force F can be applied or not. The system is shown in Figure 2.9.

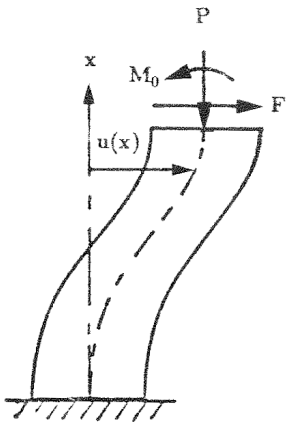

Figure 2.9: Haringx column in deformed configuration (adapted from Kelly et al. [1989]).

The problem is described by:

- the displacement of the central axis, $v(x)$

- the rotation of a face originally normal to the undeformed axis, $\Phi(x)$

Thus, the deformation of the system is given by:

- the shear deformation, $v'(x) - \Phi(x)$
- the curvature, $\Phi'(x)$

Equilibrium equations, derived from Figure 2.10, result:

$$M(x) = M_0 - Pu(x) + H_0 x \tag{2.2}$$

$$V(x) = P\Phi(x) - H_0 \tag{2.3}$$

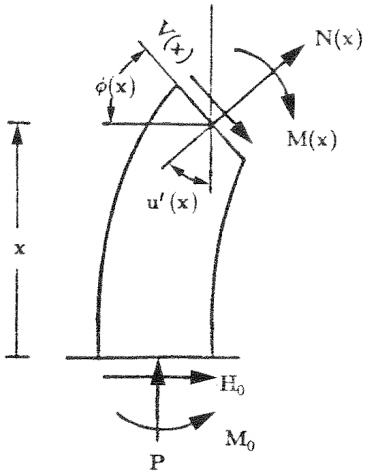

Figure 2.10: Internal forces in a generic cross section of the deformed column (adapted from Kelly et al. [1989]).

Constitutive equations are:

$$M(x) = EI_{eff}\Phi'(x) \tag{2.4}$$

$$V(x) = GA_{eff}[v'(x) - \Phi(x)] \tag{2.5}$$

Where the effective properties, introduced because of the presence of the reinforcing shims in the rubber, are defined as $EI_{eff} = E_r I_s$ and $GA_{eff} = GA_s$.

Kelly [1993] suggests a more specific interpretation of the introduced parameters. In particular, even if the steel shims do not deform in shear, their height contributes to the slenderness of the bearing so the area of the bonded rubber, A, and the inertia of the bonded rubber, I, must be modified multiplying them by a factor h/T_r, where h is the total height of the rubber layers, T_r, summed with the total height of the shims. Moreover, the modulus of elasticity must be considered as the rotation modulus $E_r = E_c/3$.
To sum up, the effective properties can be computed as:

$$EI_{eff} = E_r I_s = \frac{E_c}{3} I \frac{h}{T_r} \tag{2.6}$$

$$GA_{eff} = GA_s = GA \frac{h}{T_r} \tag{2.7}$$

Being E_c the compression modulus and G the shear modulus of the rubber bearing.

To obtain the governing equations, equilibrium and constitutive equations can be combined. In particular, Φ is obtained from the combination of Equation (2.3) and Equation (2.5). Then, Φ can be substituted in the combination of Equation (2.2) and Equation (2.4) to give the following governing differential equation in term of $v(x)$:

$$\frac{EI}{1 + \frac{P}{GA_s}} v'' + Pu = H_0 x + M_0 \tag{2.8}$$

The corresponding governing differential equation in term of Φ results:

$$\frac{EI}{1 + \frac{P}{GA_s}} \Phi'' + P\Phi = H_0 \tag{2.9}$$

The general solutions of the governing equations are

$$v(x) = A \cos \alpha x + B \sin \alpha x + \frac{H_0}{P} x + \frac{M_0}{P} \tag{2.10}$$

$$\Phi(x) = C \cos \alpha x + D \sin \alpha x \frac{H_0}{P} \tag{2.11}$$

Where $\alpha^2 = \frac{P}{EI_{eff}}(1 + \frac{P}{GA_s})$.

A relation among the four constants is obtainable, since they are not independent each other. To solve the problem, it is necessary to impose the boundary conditions, illustrated in Figure 2.9:

$$\begin{cases} v(0) = 0 \\ \Phi(0) = 0 \\ H_0(0) = 0 \\ \Phi(l) = 0 \end{cases}$$

These lead to $\alpha l = \pi$ that, elevating to the second power and substituting the definition of α, gives:

$$P\left(1 + \frac{P}{GA_s}\right) = \frac{\pi^2 EI_{eff}}{l^2} \tag{2.12}$$

Thus, the buckling load can be computed as:

$$P_{cr} = \frac{P_s}{2}\left(\sqrt{1 + 4\frac{P_E}{P_s}} - 1\right) \tag{2.13}$$

Where $P_s = GA_s$ and $P_E = \pi^2 EI_{eff}/l^2$ is the Eulerian critical load of the elastomeric bearing.
This solution can be approximated as:

$$P_{cr} = \sqrt{P_E P_s} \tag{2.14}$$

.

2.5 The Two-Spring Model of an Elastomeric Bearing

The Haringx's theory of stability describes the buckling behaviour of a bearing in the undeformed configuration, i.e. for zero lateral displacement. However, an acceptable physical model of an elastomeric isolator must take into account that the height of the bearing reduces when lateral displacement occurs. According to this need, Koh and Kelly [1988] proposed a Two-spring physical model to couple vertical stiffness to lateral displacement and then Kelly [1993] described the exact solution related to it. These theoretical development are presented following the formulation in [Constantinou et al., 2006].

Consider a rigid column of length h equal to the total height of the rubber layers and the steel shims. The column is put on a rigid plate on two

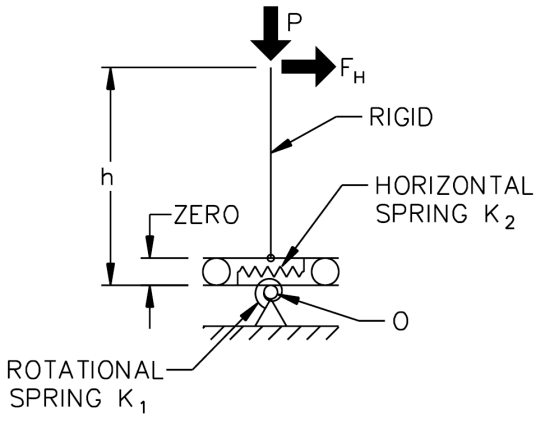

Figure 2.11: The two-spring model (adapted from Constantinou et al. [2006]).

frictionless rollers of negligible dimension, which in turn sit on another rigid plate. A horizontal spring, characterized by a stiffness K_2 (force per unit length), constrains the relative displacement, s, between the two plates. The bottom plate is simply supported in the middle and the relative rotation, θ, is constrained by a rotational spring, characterized by a stiffness K_1 (moment per unit radian). A vertical compression load P and a horizontal force F_H are applied at the free end of the column [Kelly et al., 1989]. Figure 2.11 illustrates the considered physical model.

According to the small displacement assumption, the kinematics of the simplified model results:

$$u = s + h\theta \tag{2.15}$$

$$v = s\theta + h\frac{\theta^2}{2} \tag{2.16}$$

Where u is the horizontal displacement of the top of the column and v is the height reduction.

Equilibrium of forces in the direction of displacement s and of moments about point O, referring to Figure 2.12, are:

$$P\theta + F_H + K_2 s = 0 \tag{2.17}$$

$$Pu + F_H h - K_1\theta = 0 \tag{2.18}$$

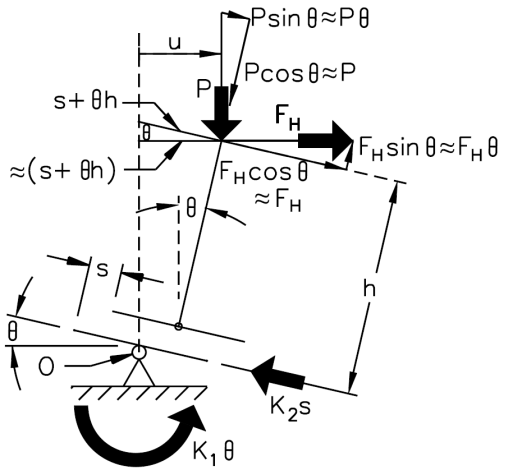

Figure 2.12: Forces and moments acting on the deformed configuration of the Two-spring model (adapted from Constantinou et al. [2006]).

Expression for each one of the two stiffnesses is obtainable considering that the other one tends to infinite. The two relations are given by:

$$\begin{cases} K_1 = P_E h \\ K_2 = \frac{GA_s}{h} = \frac{GA}{T_r} \end{cases}$$

Where P_E is the Eulerian critical load. Solutions of Equation (2.17) and Equation (2.18) in terms of deformation s and θ are:

$$\theta = \frac{F_H}{GA_s} \frac{GA_s + P}{P_E - P(1 + \frac{P}{GA_s})} \tag{2.19}$$

$$\frac{s}{h} = \frac{F_H}{GA_s} \frac{P_E}{P_E - P(1 + \frac{P}{GA_s})} \tag{2.20}$$

Assuming $P_E >> P$ and $P_E >> GA_s$, Equation (2.19) and Equation (2.20) are substituted in the equation $K_H = F_H/u$ so the horizontal stiffness of the bearing, including the effect of the vertical load and neglecting the higher order terms, turns out to be:

$$K_H = \frac{GA}{T_r}\left(1 - \frac{P^2}{P_{cr}^2}\right) \tag{2.21}$$

Where P_{cr} is the critical load computed as reported in Section 2.4, in particular using Equation (2.14). The total vertical displacement v_{tot} is the sum of two terms:

$$v_{tot} = v + P\frac{T_r}{E_c A} \tag{2.22}$$

The former is the contribution due to lateral displacement, obtained substituting Equation (2.19) and Equation (2.20) in Equation (2.16) and applying the same assumptions as for the horizontal stiffness K_H, while the latter is a contribution due to the compression load P.

Further assumptions can be made to simplify the expression for the vertical stiffness. In particular, considering $h \approx T_r$ and $P >> GA$ the vertical stiffness can be expressed as:

$$K_v = \frac{E_c A}{T_r}\left[\frac{1}{1 + \frac{3}{\pi^2}(\frac{u}{r})^2}\right] \tag{2.23}$$

Where E_c is the compression modulus of the rubber and r is the radius of gyration of the bonded rubber area, defined as:

$$r = \sqrt{\frac{I}{A}} \tag{2.24}$$

The physical model has been validated by Warn and Whittaker [2006]: several experimental results demonstrate that Equation (2.23) provides a good representation of the vertical stiffness and that the accuracy of the Two-spring model formulations is acceptable. The Two-spring model provides results that are close to the continuous beam model formulated by Kelly [1993].

Chapter 3

Mathematical and Numerical Model of Elastomeric Bearings for 3D Seismic Isolation

This chapter investigates the fundamental behaviour of elastomeric bearings and the way in which it is implemented in a numerical code. Thus, it can be considered as split in two parts: the former concerns the mechanical behaviour in the principal directions and the latter concerns the numerical implementation. Section 3.1 describes the mathematical model of a bearing in vertical direction, followed by Section 3.2 that describes the mathematical model in horizontal directions. Then, the torsional and rotational behaviour is discussed in Section 3.3. Once the mathematical model is established, the numerical model implemented on OpenSees is treated in Section 3.4. OpenSees is an open source software for earthquake engineering simulation. For a better comprehension of the numerical model, Section 3.4.1 introduces to the operating principles of the software whereas Section 3.4.2 explains the coordinate reference systems present on OpenSees. Finally, Section 3.4.3 describes the Element object that OpenSees provides to model an elastomeric bearing. The dissertation is completely referred to circular elastomeric bearing, due to the widespread use and the simplification of the problem thanks to the symmetry of this geometry.

3.1 Mechanical Behaviour in Vertical Direction

The stiffness in vertical direction of elastomeric bearings mainly controls the vertical frequency of a seismically isolated structure. Therefore, to design a three-dimensional isolation system that protect the structure also from vibrations in vertical direction (in addition to horizontal directions), the need to predict the behaviour under compressive loads becomes fundamental [Kelly, 1993]. In case of major earthquakes, large variations in axial loads are expected due to extreme shaking of the ground and the coupling of horizontal and vertical responses needs to be considered.

The coupling between horizontal and vertical responses of elastomeric bearings consists in three contributions:

- the axial stiffness K_v reduces for increasing lateral displacement u_h;
- the shear stiffness K_H reduces for increasing axial load P;
- the reduction of the axial stiffness implies a reduction of the critical buckling load P_{cr} which in turn causes a reduction of the shear stiffness.

Concerning the first of the three contributions listed above, two models have been proposed: the Two-spring model by Koh and Kelly [1988] and the continuous beam model by Kelly [1993]. Both models are based on the Haringx [1949b] stability theory. In the following, reference is made to the former due to the fact that gives results similar to the latter but it is a simplified model, so the analyzed problem becomes easier through some assumptions. As discussed in detail in Section 2.5, the vertical stiffness of the elastomeric bearing is given by:

$$K_v = \frac{E_c A}{T_r}\left[1 + \frac{3}{\pi^2}\left(\frac{u_h}{r}\right)^2\right]^{-1} = K_{v0}\left[1 + \frac{3}{\pi^2}\left(\frac{u_h}{r}\right)^2\right]^{-1} \tag{3.1}$$

Where

- E_c is the compression modulus of the rubber bearing;
- A is the area of the bonded rubber layers;
- T_r is the total height of the rubber;
- r is the radius of gyration, as defined in Equation (2.24);
- K_{v0} is the vertical stiffness at zero lateral displacement, i.e. $u_h = 0$.

Several formulations are proposed for the computation of the compression modulus of the rubber bearing, E_c. Two of the possible analytical expressions derive from two different formulations, both proposed by Gent and Lindley [1959]: the incompressible formulation and the compressible one. The former is based on the *"strict incompressibility"*, i.e. Poisson ratio ν equal to 0.5. The approximate relationship for circular bonded rubber is:

$$E_c = E(1 + 2S^2) \tag{3.2}$$

Where E is the Young modulus of the elastomer and S is the shape factor, as defined in Equation (2.1). To derive this formulation, three assumptions are made: (a) horizontal plane section parallel to the rigid plate remains plane and parallel, (b) lateral surface deforms in a parabolic shape configuration and (c) the normal stress components are equal to the mean pressure in all three orthogonal directions.

The compressible formulation includes the effect of the volume compressibility. The relation becomes:

$$\frac{1}{E_c'} = \frac{1}{E_c} + \frac{1}{K} \tag{3.3}$$

Being E_c the compression modulus as defined in Equation (3.2) and K is the bulk modulus of compression, which commonly used value in the analysis of elastomeric bearings is $K = 2000\ MPa$. However, the incompressible formulation is considered acceptable for low shape factor rubber bearings [Pinarbasi and Akyuz, 2004].

Constantinou et al. [2006] proposed another analytical expression for the compression modulus of a circular elastomeric bearing with finite compressibility:

$$E_c = \left(\frac{1}{6GS^2} + \frac{4}{3K} \right)^{-1} \tag{3.4}$$

It is worth noting that the variation of the vertical stiffness due to increasing lateral displacement u_h influences also the value of the instantaneous critical buckling load P_{cr}. Figure 3.1 shows the axial load-deformation curve in compression. For zero lateral displacement, the elastomeric bearing exhibits a vertical stiffness equal to K_{v0} that leads to a critical buckling load P_{cr0} computed by means of Equation (2.14), as discussed in detail in Section 2.4. Once the bearing deforms in shear, the vertical stiffness assumes a lower value that means a lower inclination of the curve. The reduction of

K_v leads to a stress softening, i.e. a reduction of the instantaneous critical buckling load P_{cr}.

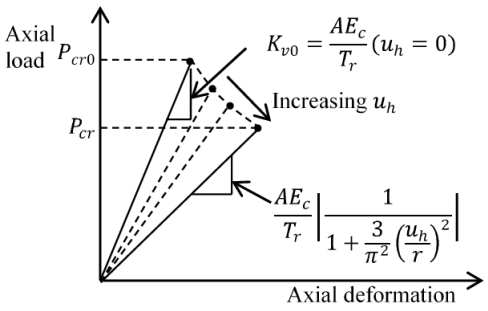

Figure 3.1: Axial load-deformation curve in compression (adapted from Kumar et al. [2015]).

The critical buckling load in deformed configurations can be computed through the area reduction method that provides a decreased value of P_{cr} as a function of the overlap area. In particular:

$$P_{cr} = P_{cr0}\frac{A_r}{A} \tag{3.5}$$

Where P_{cr0} is the critical buckling load at zero displacement, as defined in Equation (2.14), A is the bonded area and A_r is the overlap between the top and bottom areas of the deformed elastomeric bearing, shown in Figure 3.2 and computed as:

$$A_r = \frac{D^2}{4}(\delta - \sin\delta) \tag{3.6}$$

Being

$$\delta = 2\cos^{-1}\left(\frac{\Delta}{D}\right) \tag{3.7}$$

Noting that Δ corresponds to the lateral displacement of the bearing, previously defined as u_h. According to this method, zero capacity is expected for the bearing when $\Delta = D$. However, it has been demonstrated that, for lateral displacement equal to the diameter of the bearing, the capacity is not completely lost but a residual value is still present. To take into account this important experimental result, Warn and Whittaker [2006] proposed a linear approximation of the area reduction method that provides a constant critical buckling load when the ratio A_r/A assumes values lower than 0.2. As shown in Figure 3.3, the reduced critical buckling load can be computed as:

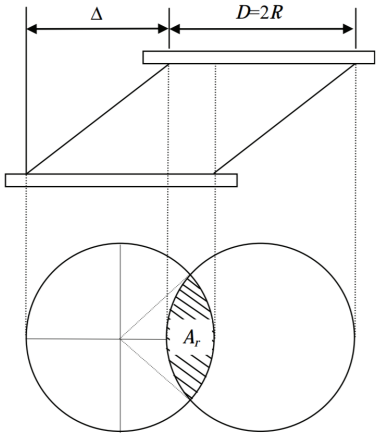

Figure 3.2: Reduced area of elastomeric bearing (adapted from Warn and Whittaker [2006]).

$$P_{cr} = \begin{cases} P_{cr0}\frac{A_r}{A}, & \frac{A_r}{A} \geq 0.2 \\ 0.2P_{cr0}, & \frac{A_r}{A} < 0.2 \end{cases} \tag{3.8}$$

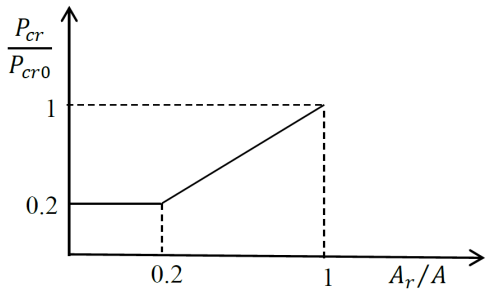

Figure 3.3: Bi-linear variation of buckling load (adapted from Kumar et al. [2015]).

The mechanical behaviour of elastomeric bearings in vertical direction is not symmetric in compression and in tension. For tensile loading, the behaviour is characterized by the formation of cavities in rubber volume that leads to a reduction of the vertical stiffness. A detailed discussion on this topic is provided by Kumar et al. [2015] and omitted here because not required to reach the scope of this thesis.

3.2 Mechanical Behaviour in Horizontal Direction

The horizontal stiffness of an elastomeric bearing is computed considering the influence of the axial load. According to the approximation proposed by Kelly [1993] of the Two-spring model formulation, the analytic expression of the horizontal stiffness is given by:

$$K_H = \frac{GA}{T_r}\left[1 - \left(\frac{P}{P_{cr}}\right)^2\right] = K_{H0}\left[1 - \left(\frac{P}{P_{cr}}\right)^2\right] \tag{3.9}$$

Where K_{H0} is the horizontal stiffness when the axial load P is equal to zero and P_{cr} is the critical buckling load computed as defined in Equation (3.8). It is worth noting that the effect of the axial load becomes significant for values of P close to the buckling load capacity.

The coupling between vertical and horizontal is included in the model that describes the coupling between horizontal directions. In particular, the model for elastomeric bearing in horizontal shear is a bidirectional smooth bi-linear hysteretic one, showed in Figure 3.4, and is based on the formulation by Park et al. [1986].

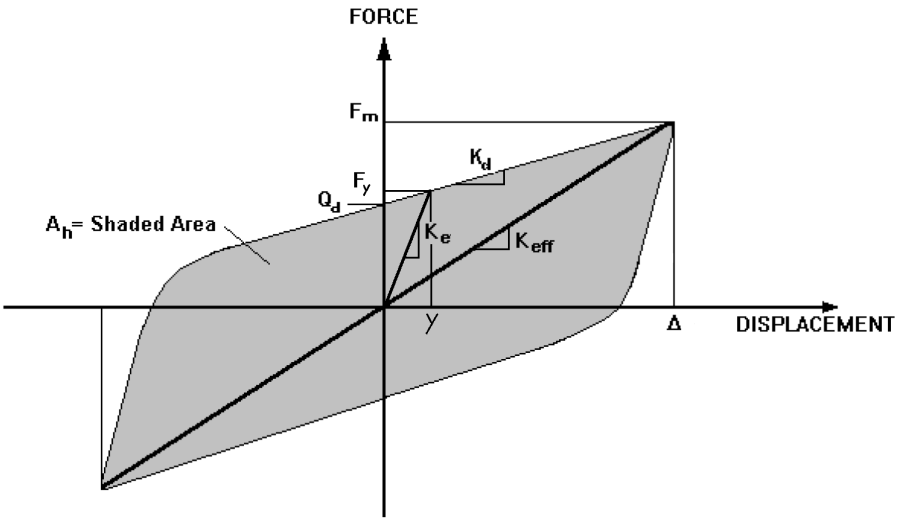

Figure 3.4: Idealized smooth behaviour of elastomeric bearing in shear (adapted from Kelly [2001]).

The hysteresis loop is characterized by parameters typical of seismic isolation design:

– The initial elastic stiffness, K_e;

– The post-elastic stiffness, K_d;

– The effective stiffness, K_{eff};

– The yield strength, F_y;

– The yield displacement, Y;

– The characteristic strength, Q_d;

– The maximum displacement, Δ;

– The maximum force, F_m.

The effective stiffness of an elastomeric bearing is computed from experimental data as:

$$K_{eff} = \frac{|F_m^+| + |F_m^-|}{|\Delta^+| + |\Delta^-|} \tag{3.10}$$

Where "+" and "-" are referred to positive and negative values. Then the effective shear modulus could be obtained through:

$$G_{eff} = \frac{K_{eff} T_r}{A} \tag{3.11}$$

However, despite the fact that the shear modulus depends on shear strain and axial load, a constant value is typically assumed. As the axial pressure increases, the shear modulus reduces. As the shear strain increases, the shear modulus decreases up to 100% and then remains almost constant till 200%. Thus, to take into account these dependencies, the constant value of the shear modulus is determined from testing at large strains and nominal axial pressure.

The restoring forces in orthogonal directions, F_x and F_y, are derived from the isotropic formulation of the model and result:

$$\begin{bmatrix} F_x \\ F_y \end{bmatrix} = c_d \begin{bmatrix} \dot{U}_x \\ \dot{U}_y \end{bmatrix} + K_d \begin{bmatrix} U_x \\ U_y \end{bmatrix} + Q_d \begin{bmatrix} Z_x \\ Z_y \end{bmatrix} \tag{3.12}$$

Being U_x and U_y the displacements, $\dot{U}_x$ and $\dot{U}_y$ the velocities, c_d a parameter of the viscous energy dissipation in rubber. Z_x and Z_y represent the hysteretic components of the restoring forces and depend on the displacements through the relation:

$$Y \begin{bmatrix} \dot{Z}_x \\ \dot{Z}_y \end{bmatrix} = \left(A[I] - \begin{bmatrix} iZ_x^2 & jZ_xZ_y \\ iZ_xZ_y & jZ_y^2 \end{bmatrix} \right) \begin{bmatrix} \dot{U}_x \\ \dot{U}_y \end{bmatrix} \tag{3.13}$$

Where

$$\begin{cases} i = \gamma Sign(\dot{U}_x Z_x) + \beta \\ j = \gamma Sign(\dot{U}_y Z_y) + \beta \end{cases}$$

γ and β define the shape of the hysteresis loop and A the amplitude of the restoring forces. The parameters fulfill the condition $A/(\gamma + \beta) = 1$. Once the system yields, the solution is provided by:

$$\begin{cases} Z_x = \cos\theta \\ Z_y = \sin\theta \end{cases} \tag{3.14}$$

Where $\theta = \tan^{-1}(\dot{U}_y/\dot{U}_x)$ is the angle between the resultant force and the direction of the motion.

It is worth noting that the first two terms of Equation (3.12) provide the viscoelastic contribution of the rubber while the third term is the hysteretic contribution. The hysteretic term depends on the characteristic strength Q_d of the elastomeric bearing that is related to the definition of an effective damping of the system as the ratio between the dissipated energy per cycle and the dissipated energy enclosed by the maximum displacement in each cycle. The US codes define the effective damping β_{eff} as:

$$\beta_{eff} = \frac{1}{2\pi} \left(\frac{E_D}{K_{eff}\Delta^2} \right) \tag{3.15}$$

Being E_D the energy dissipated per cycle, i.e. the area enclosed by the loop, that for the idealized behaviour in Figure 3.4 can be approximated as:

$$E_D = 4Q_d(\Delta - Y) \tag{3.16}$$

Considering that $(\Delta - Y) \leq \Delta$ and $K_{eff} \geq K_d$, the effective damping results:

$$\beta_{eff} = \frac{1}{2\pi} \left(\frac{4Q_d(\Delta - Y)}{K_{eff}\Delta^2} \right) \leq \frac{2Q_d}{\pi K_d \Delta} \tag{3.17}$$

The shape of the cycle shows that $Y << \Delta$ and $K_{eff} \approx K_d$. These considerations allow to invert the previous relationship and the characteristic strength of the elastomeric bearing can be approximated as:

$$Q_d = \frac{\pi}{2}\beta_{eff} K_d \Delta \tag{3.18}$$

The mechanical behaviour described above follows the formulation for low damping rubber bearings. However, it is considered valid also for high damping rubber bearing due to the fact that the force-displacement response of HDR bearing is similar to that shown in Figure 3.4 but with larger energy dissipated per cycle, so the same path of reasoning can be followed [Constantinou et al., 2006]. It is worth noting that the formulation described above holds on the assumption that $Y << \Delta$; if this condition is not fulfilled, other assumptions are needed leading to higher level of approximation.

3.3 Mechanical Behaviour in Rotation and Torsion

Fortunately, opposite to the complexity in understanding and describing the behaviour in vertical and horizontal directions, behaviour in torsion and rotation of a bearing can be easily modelled by means of linear elastic springs. The linear elasticity is acceptable because of the low influence of torsional and rotational behaviours on the overall response of the whole system.

The stiffness of the rotational spring is given by:

$$K_r = \frac{E_r I_r}{T_r} \tag{3.19}$$

Where E_r is the rotation modulus and is equal to a third of the compression modulus of the elastomeric bearing, i.e. $E_c/3$ [Kelly, 1993]. I_r is the moment of inertia about an axis of rotation in the horizontal plane and T_r is the total height of the rubber layers.

The stiffness of the torsional spring is given by:

$$K_t = \frac{G I_t}{T_r} \tag{3.20}$$

Where G is the shear modulus of the elastomeric bearing and I_r is the moment of inertia about the vertical axis. The perpendicular axis theorem implies that for symmetrical bearings $I_t = 2I_r$ [Kumar et al., 2015].

It is worth noting from Equation (3.19) and Equation (3.20) that any type of coupling is not present in the formulations for rotational and torsional stiffness. Hence, in addition to the linear elasticity, the decoupling of these behaviours make the model easier than the vertical and the horizontal directions.

3.4 Numerical model in OpenSees

Numerical model for elastomeric bearings has been implemented in several structural software, e.g. ABAQUS or OpenSees. The development of the latter is sponsored by the Pacific Earthquake Engineering Research Center (PEER). Since the use of OpenSees is less widespread than other commercial structural software, a description of it and its main object used for the analysis of elastomeric bearings is reported in the following.

3.4.1 OpenSees Framework

The word *OpenSees* stands for **Open S**ystem for **E**arthquake **E**ngineering **S**imulation. OpenSees is an open source software framework that allows users to create application for nonlinear analysis of structural and soil systems. The possibility of sharing improved analysis and developed results makes OpenSees a research-oriented application. It is designed to be flexible, extensible and object-oriented, i.e. Opensees makes extensive use of object composition allowing users to combine components in manners that are not available in commercial or other research codes [McKenna, 2011]. However, OpenSees is not much user-friendly because it does not have a graphical interface but it is an interpreter, i.e. inputs are contained in a file that is run through this. The input file is actually a program written in Tcl programming language extended for finite element analysis. Each command is associated to a C++ procedure. An important characteristic of OpenSees is the high level of modularity that enables developers to modify and improve the code without needing to know the whole framework. This advantage permits to reduce the repetition of the same command and the possibility of error, due to the fact that nothing is automatically assigned or defined. Nevertheless, this software shows limited features in modelling complex structures that, in some cases, leads to the impossibility to perform a dynamic analysis on a structure isolated with elastomeric bearings.

The main modules for the code implementation of a dynamic analysis on a structure are:

1. **ModelBuilder**: used to construct the objects of the structure in the model.
2. **Recorder**: used to select the quantities to be monitored during analysis procedures and the outputs of results.
3. **Analysis**: used to define the solution procedure to advance the model from state at time t_i to state at time $t_i + dt$.

The command that allow to enter in the first module requires the definition of the number of dimensions and the number of degrees of freedom (dofs) of the system. The model of a structure consists of elements created in a 2D or 3D space having 3 or 6 dofs, respectively. The high modularity of the software leads to the definition of an Element object through different steps. In fact, OpenSees does not allow to create an element with a single command containing all its properties but it is necessary to formerly define the materials with the corresponding properties, then define the nodes to place the element in the correct position. To apply any kind of constraint to an element, a specific command relates the node to the degree of freedom that must be fixed, i.e. displacements or rotations of an end of the considered element is impeded through the application of constraints to the corresponding node. A specific command assigns mass to a node in the directions of the corresponding degrees of freedom. Once materials, nodes, mass and constraints are defined, the element can be finally created. The main function of an element is to provide the nodal force vector and stiffness matrix.

Similarly, the procedure to model the loads acting on the structure is split in two passages: a first command to set a value or a time series of the loading and a following commands to apply the defined loads through a load pattern. Whenever a object is introduced, it must be identified by a tag that must be unique.

The Analysis objects are responsible for performing the analysis that may vary from a simple static linear analysis, e.g. for the gravity loads, to a transient non-linear analysis. The analysis moves the model along from state at time t to state at time $t + dt$. In OpenSees each Analysis object is composed of several component objects, as shown in Figure 3.5 which define the type of analysis [Mazzoni et al., 2006].

The results of the analysis are provided by output files through Recorder objects. A Recorder command monitors the state of a component (e.g. node

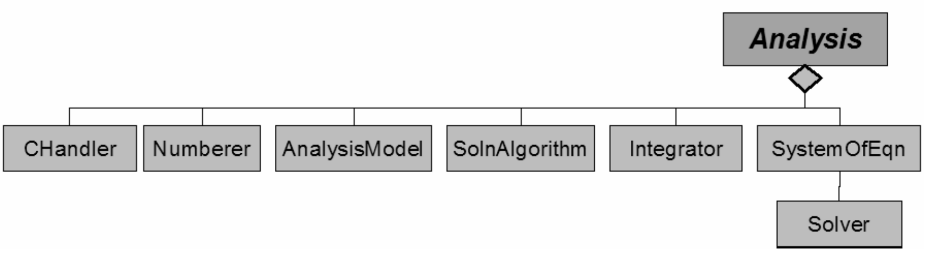

Figure 3.5: Analysis objects on OpenSees (adapted from Mazzoni et al. [2006]).

or element) during a previously defined analysis, writing the states at selected intervals. Example of a typical Recorder objects are the displacements of a node in horizontal directions or the basic forces of an element.

3.4.2 Reference Coordinate Systems

In the OpenSees framework, three different reference coordinate systems are present (Figure 3.6):

- Basic coordinate system;
- Local coordinate system;
- Global coordinate system.

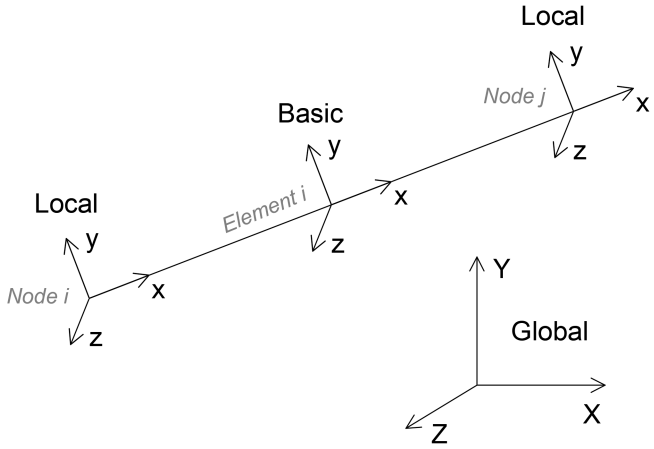

Figure 3.6: Reference coordinate systems in OpenSees.

Each reference system is related to different aspects of the model and its response. In particular, the element forces, displacements and stiffness matrices are expressed in the basic coordinate system while the nodal response

is expressed in the local coordinate system. Moreover, the system of equations for the whole model is solved in the global coordinate system [Kumar et al., 2015]. Transformation matrices can be found expressing deformations and forces in one reference system as a function of deformations and forces in another reference system, so they allow to pass from one coordinate system to another. The procedure to obtain the response of the model is analogous to any software for finite element analysis: OpenSees starts from the element force vector and stiffness matrix in the basic coordinate system and transforms them formerly from basic to local coordinates and latterly from local to global coordinates. The solution of the system of equations is found and then the procedure is performed backward, computing the nodal response in the local coordinate system.

In the global coordinate system the vertical axis is the Y-axis whereas X-axis and Z-axis lie in the horizontal plane. However, for most of the Element objects, the x-axis is a vector which links the two nodes that define the considered element (obtainable as a unit vector through the difference of the nodal coordinates divided by its norm) while y-axis and z-axis lie in the plane normal to the element axis (one of them must be formerly assumed and latterly the other one is found as a cross-product of the two known axis). Different orientation of the basic axes can be defined specifically inside the `Element` command. Considering the specific and most common case of a vertical element, i.e. an element which nodes have the same location in the horizontal plane but different quotes in vertical axis, the orientation of the axes of the local and the basic coordinate systems coincides. Nevertheless, the x-axis in the local and in the basic coordinate systems corresponds to the Y-axis in the global reference system. Consequently, the y-axis in the local and in the basic coordinate systems corresponds to the X-axis in the global reference system, as shown in Figure 3.7.

3.4.3 Element ElastomericX

Kumar et al. [2015] proposed an Element object in OpenSees, the so-called `ElastomericX`, that reproduces the actual behaviour of an elastomeric bearing, as an extension of the bidirectional formulation of the Bouc-Wen existing model. The physical model of an elastomeric bearing consists of a two-nodes, twelve dofs discrete element as illustrated in Figure 3.8.

The two nodes are connected by six springs that represent the mechanical behavior in the six basic directions of a bearing (Figure 3.9), highlighted by the general form of element basic force vector in the basic coordinate system:

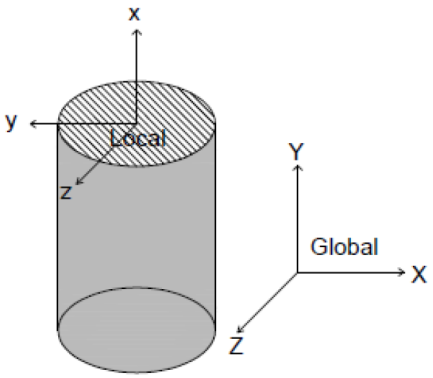

Figure 3.7: Coordinate systems of a vertical element in OpenSees (adapted from Kumar et al. [2015]).

$$f_b = \begin{bmatrix} Axial \\ Shear1 \\ Shear2 \\ Torsion \\ Rotation1 \\ Rotation2 \end{bmatrix} \tag{3.21}$$

The springs that reproduce the mechanical behaviour in axial and shear directions are nonlinear while the ones for the torsional and rotational behaviour are linear.

The general form of the element stiffness matrix in the basic coordinate system for the model shown above results:

$$K_b = \begin{bmatrix} Axial & 0 & 0 & 0 & 0 & 0 \\ 0 & Shear1 & Shear12 & 0 & 0 & 0 \\ 0 & Shear21 & Shear2 & 0 & 0 & 0 \\ 0 & 0 & 0 & Torsion & 0 & 0 \\ 0 & 0 & 0 & 0 & Rotation1 & 0 \\ 0 & 0 & 0 & 0 & 0 & Rotation2 \end{bmatrix} \tag{3.22}$$

It is worth noting that only the coupling between the two horizontal directions is explicitly present in the element stiffness matrix. On the base of the Two-spring model [Koh and Kelly, 1988], discussed in detail in Section 2.5, the coupling of vertical and horizontal responses is considered indirectly

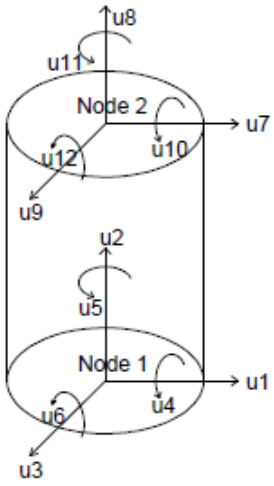

Figure 3.8: Model of the 3D continuum geometry of an elastomeric bearing (adapted from Kumar [2016]).

through Equation (3.1) and Equation (3.9) that vary the vertical and the shear stiffness as a function of the lateral displacement and axial load, respectively. As specified in Section 3.3, the linear elastic springs for torsion and rotations remain uncoupled because their behaviour is not expected to significantly influence the model response. The mechanical behaviour is discussed in detail in the previous sections of this chapter so in the following the focus is put on the way the `ElastomericX` element is implemented.

Axial direction Starting from the displacements in basic coordinates the shear displacement of the elastomeric bearing is found as:

$$u_h = \sqrt{u_b(2)^2 + u_b(3)^2} \tag{3.23}$$

Where 2 and 3 are referred to the y-axis and the z-axis of the basic coordinate system, denoted with the pedix b. The lateral displacement is computed at each step of the analysis.
The displacement u_h influences both the overlap area A_r, calculated through Equation (3.6) (the dependence is contained in the computation of the angle δ by means of Equation (3.7)), and the vertical stiffness K_v. The quantities present in Equation (3.1) are obtained as follows:

- E_c computed through Equation (3.4);
- A computed as a function of the defined internal and external diameters;

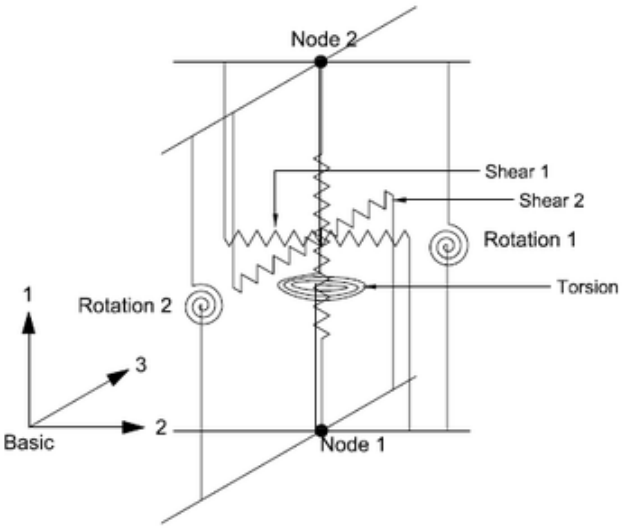

Figure 3.9: Degrees of freedom and discrete spring representation of an elastomeric bearing (adapted from Kumar [2016]).

- T_r equal to the product between the height of a single layer of rubber and the number of layers;
- u_h computed through Equation (3.23);
- r computed through Equation (2.24).

The value of the overlap area A_r influences the critical buckling load capacity of the bearing by means of the relation in Equation (3.8). As the lateral displacement u_h changes at each analysis step, also the vertical stiffness K_v and the critical buckling load P_{cr} are computed at each analysis step. Failure in buckling occurs when the axial load exceeds the value of P_{cr}. A small value of post-buckling axial stiffness, $K_{post-buckling} = K_v/1000$, is assumed to avoid numerical problems in the analysis but, actually, the bearing shows no more resistance.

Horizontal directions The numerical model of the mechanical behaviour in horizontal directions is based on the Bouc-Wen formulation that considers the response as the sum of two contributions: a viscoelastic component, having elastic stiffness k_e, and a hysteretic component, having an initial elastic stiffness k_0. The sum of the two contributions leads to a resulting initial stiffness $k_e + k_0$ and a post-yield stiffness k_e (Figure 3.10), the ratio of which defines the parameter α. In particular:

$$\alpha = \frac{k_e}{k_e + k_0} \tag{3.24}$$

The stiffness k_e corresponds to the elastic horizontal stiffness for zero axial load, previously referred as K_{H0} (Equation (3.9)). For a given value of α, the previous relation can be used to express k_0 as a function of known quantities:

$$k_0 = \left(\frac{1}{\alpha} - 1\right) k_e \tag{3.25}$$

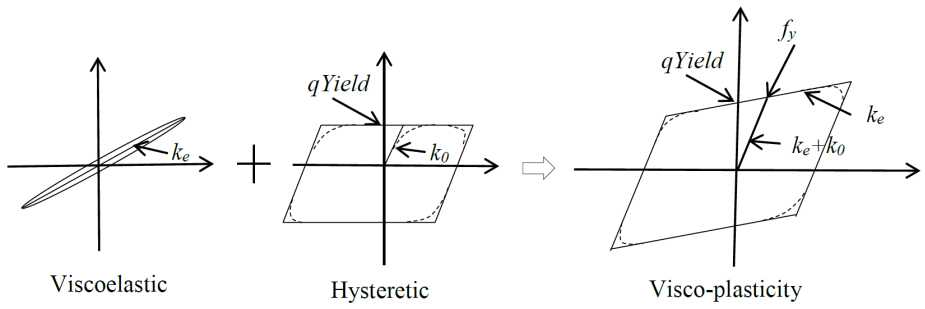

Figure 3.10: Numerical model of the response in shear (adapted from Kumar et al. [2015]).

The yield strength of the bearing is computed as a function of the characteristic strength, Q_d ($qYield$ in Figure 3.10):

$$f_y = \frac{Q_d}{1 - \alpha} \tag{3.26}$$

The value of the characteristic force can be found referring to Equation (3.18). In fact, considering a constant value of the shear modulus G, obtained from experimental test at a reference level of shear strain equal to 100% that means $\Delta = T_r$, K_d is obtained from Equation (3.11) and turns out to be GA/T_r. For a given value of β_{eff}, Q_d is easy to compute.
The constant value of the characteristic strength must be calculated also to obtain the restoring forces through Equation (3.12), where Q_d is computed as described above. The value of K_d corresponds to the aforementioned k_e and is computed through Equation (3.9) at each analysis step. As the characteristic strength, also the parameter c_d is a constant value and it describes the damping of the elastomeric bearing. The aforementioned effective damping β_{eff} represents the ratio between the damping of the bearing c_d and the critical damping $c_{cr} = 2\sqrt{k_e m}$, where m is the mass above the elastomeric

bearing. Inverting the definition, the parameter of the viscous energy dissipation in the rubber results:

$$c_d = \beta_{eff} 2\sqrt{k_e m} \tag{3.27}$$

The effects of geometric non-linearity are included in the computation of the axial stiffness and of the two shear stiffnesses of an elastomeric bearing. The overturning moment due to the axial load of the superstructure at horizontal displacement u_h is split between the two ends of the bearing.

Torsion and Rotations The linear elastic springs, having stiffness as in Equation (3.19) and Equation (3.20), for torsion and rotations remain uncoupled because their behaviour is not expected to significantly influence the model response, as deeply discussed in Section 3.3.

Command An elastomeric bearing is created on OpenSees through the `Element` command:

```
element ElastomericX $eleTag $Nd1 $Nd2 $Fy $alpha $Gr $Kbulk
$D1 $D2 $ts $tr $n <$x1 $x2 $x3> <$y1 $y2 $y3> <$kc> <$PhiM>
<$ac> <$sDratio> <$m> <$cd> <$tc> <$tag1> <$tag2> <$tag3>
<$tag4>
```

Where the symbol $ means *"the value of"* the following parameter and the symbols <> denote an optional input. If an optional input is not specified, the default value is assigned.
The input arguments are reported in Table 3.1.

The element is created and located with the inputs `$eleTag`, `$Nd1` and `$Nd2`. `$Fy`, `$alpha`, `$Gr` and `$Kbulk` define the material properties of the rubber. Typically, the assumed value for the bulk modulus is $K = 2000\ MPa$. The geometrical properties are defined by `$D1`, `$D2`, `$ts`, `$tr` and `$n`. `$x1 $x2 $x3` and `$y1 $y2 $y3` represent the orientation of the local axes with respect to the global reference system. The parameters `$kc`, `$PhiM` and `$ac` are related to the implementation of the behaviour in tension, activated with `$tag1`. Additional properties of the bearing are `$sDratio`, `$m`, `$cd` and `$tc`. Finally, the four tags allow to consider or neglect some aspects of the mechanical bearing behaviour, discussed in the previous sections. Assigning the value 1 to the tag means including the corresponding aspect. On the contrary, assigning the value 0 to the tag means neglecting the effects of the corresponding behaviour on the bearing response. If the variation in

the buckling load capacity is not considered, the reduction of P_{cr} with the increase of the overlap area (as reported in Section 3.1) is not performed and the constant value at zero lateral displacement P_{cr0} is assumed. The same path of reasoning holds for the vertical and horizontal stiffness. If the influence of the axial load is not significant and `$tag3` is set to 0, the horizontal stiffness is not computed at each step because it assumes always the constant value corresponding to zero axial load, K_{H0}. Analogously, if `$tag4` is set to 0, i.e. the effects of the lateral displacement is neglected, the vertical stiffness is not computed at each step and the constant value K_{v0}, corresponding to zero lateral displacement u_h, is assumed.

Table 3.1: Input arguments of `ElastomericX`.

Input	Definition
`$eleTag`	tag associated to the bearing (unique)
`$Nd1`	bottom end node
`$Nd2`	top end node
`$Fy`	yield strength
`$alpha`	post-yield stiffness ratio
`$Gr`	shear modulus
`$Kbulk`	bulk modulus
`$D1`	internal diameter
`$D2`	external diameter
`$ts`	thickness of a single steel shim
`$tr`	thickness of a single layer of rubber
`$n`	number of rubber layers
`$x1 $x2 $x3`	vector components in global coordinates defining local x-axis
`$y1 $y2 $y3`	vector components in global coordinates defining local y-axis
`$kc`	cavitation parameter (default=10.0)
`$PhiM`	damage parameter (default=0.5)
`$ac`	strength reduction parameter (default=1.0)
`$sDratio`	distance of the shear centre from the bottom node, as a fraction of the element length (default=0.5)
`$m`	mass of the isolator (default=0.0)
`$cd`	viscous damping parameter (default=0.0)
`$tc`	thickness of the rubber cover (default=0.0);
`$tag1`	tag to include the cavitation and post-cavitation behaviour in tension
`$tag2`	tag to include the variation in the buckling load capacity due to lateral displacement
`$tag3`	tag to include the variation in horizontal shear stiffness with axial load
`$tag4`	tag to include the variation in vertical stiffness with lateral displacement

Chapter 4

Design of a 3D Elastomeric Bearing-based Isolation System

The design of a three-dimensional elastomeric bearing-based isolation system must fulfill conditions and requirements imposed by national codes. This chapter describes formerly a design procedure according to European Standards in Section 4.1 and then, in Section 4.2, an alternative design approach that follows the former procedure but it is based on a hypothesis that could allow to reach the beneficial effects of the 3D seismic base isolation relaxing the conservative requirement while maintaining a relatively high level of safety.

4.1 Design Procedure according to European Standards

A three-dimensional isolation system is designed to protect the superstructure from the damaging effects of strong ground motions in the three principle directions. In particular, vertical isolation is aimed to reduce the sensitivity of the structure to vibrations in vertical direction while horizontal isolation is aimed to reduce the seismic response of the lateral-force resisting system, principally by shifting the fundamental natural period of a structure to the long period range and to decrease the participation factors of the modes for which isolation is required. In fact, the introduction of isolators between the foundation, referred as *substructure*, and the structure above the isolation plane, referred as *superstructure*, makes the whole system more

flexible and leads to a reduction of the overall stiffness. The deformation is concentrated on the isolation interface, thereby allowing the superstructure to behave elastically and to experience relatively uniform accelerations over the height. A decrease of the accelerations with respect to the corresponding non-isolated structure implies a decrease of the top drifts. A full isolation is reached if the response of the superstructure is kept in the elastic, or nearly elastic, range. Nevertheless, a reduced stiffness means also larger displacements that must be controlled and maintained within an established range. Therefore, sufficient space between the structure and the surrounding environment, in particular existing constructions, must be provided to allow the lateral deformation of the structure in every direction during earthquakes. In addition to this, codes require a sufficient space between the superstructure and the substructure to allow inspection, maintenance and replacement of the devices during the lifetime of the structure. Together with the flexibility in case of major earthquakes, the isolation system provides rigidity for service loads, as wind or low-intensity earthquakes, thereby the structure results as fixed at the base in ordinary conditions. Moreover, isolation system guarantees a significant dissipation of the energy induced by earthquakes, enhancing the reduction of the seismic-induced forces on the superstructure. In particular, high damping rubber bearings provide a high level of energy dissipation due to filler materials added to the rubber compounds during manufacturing process.

To the aim of designing a three-dimensional isolation system, i.e. a seismic isolation system that protect the structure from damaging effects of earthquakes in horizontal and vertical directions, elastomeric bearing characterized by low shape factor has been selected. The shape factor S is introduced to consider the shape of the elastomer in strength and deflection calculations and it is defined as the ratio between the plan area common to elastomer and steel shims and the force-free area. For circular bearings, the shape factor depends on the diameter of the bearing and on the thickness of a single rubber layer. To consider an elastomeric bearing to have a low shape factor, the value of S must be lower than 5.

The design procedure described in the following is based on the Eurocode for the design of structures for earthquake resistance EN1998-1:2004, hereinafter referred as EC8 for short, on the European standards for anti-seismic devices EN15129:2018, hereinafter simply referred as EN15129, and on the European standards for elastomeric bearings EN1337-3:2005, hereinafter referred as EN1337 for short.

The starting point of designing a high damping rubber bearing-based isolation system is the assumption on the period of the whole structure, T_0. The aforementioned long period range, in which the fundamental natural period of the non-isolated structure is shifted through the introduction of the isolation system, corresponds to the interval of time between 2 *sec* and 4 *sec*. Actually, the suggested interval is restricted between 2 *sec* and 3 *sec* because higher period implies lower stiffness, so lower restoring forces, which in turn implies higher displacements. The reduction in horizontal stiffness leads to an increase of the thickness of a single rubber layer. As a consequence, both the vertical stiffness and the critical buckling load reduce, raising the importance of the stability problem.

Once the period of the isolated structure is assumed, the natural frequency can be calculated through the relation:

$$\omega = \frac{2\pi}{T_0} \tag{4.1}$$

Then, if the mass of the structure is known, the stiffness of the whole isolated structure can be obtained by means of the definition of the natural frequency as:

$$\omega = \sqrt{\frac{K_{eff}}{m_t}} \quad \Longrightarrow \quad K_{eff} = \omega^2 m_t \tag{4.2}$$

According to EC8 §10.9.2, the effective stiffness K_{eff} of the isolation system is the sum of the effective stiffnesses of the isolator units. Thus, considering an isolation system made of bearings with the same geometrical and material properties, the stiffness in horizontal direction of a single isolator is computed as:

$$K_H = \frac{K_{eff}}{n_i} \tag{4.3}$$

Where n_i is the number of bearings of the 3D isolation system.
The horizontal stiffness is provided by the rubber, having area A and total height T_r, and it is computed according to the definition reported in Section 3.2 referring to K_{H0}. In particular:

$$K_H = \frac{GA}{T_r} \tag{4.4}$$

Therefore, an assumption on the material properties is needed. According to EN15129 §8.2.2.1, the shear modulus G at a shear strain of 100% can

assume values between 0.3 MPa and 1.5 MPa. Thus, the value of the shear modulus is assumed on the base of the values suggested by Kelly [2001] as a function of the hardness of the rubber compound, as reported in Table 4.1.

Table 4.1: Values of the shear modulus suggested by Kelly [2001].

Hardness IRHD± 2	**Shear Modulus G**
37	0.40 MPa
40	0.45 MPa
45	0.54 MPa
50	0.64 MPa
55	0.81 MPa
60	1.06 MPa

Furthermore, the elastic compression modulus is computed according to EN15129 §8.2.3.3.2 through:

$$E_c = 3G(1 + 2S^2) \tag{4.5}$$

The difference between the compression modulus obtained by means of Equation (4.5) and the one obtained through Equation (3.4) is negligible. Knowing the horizontal stiffness K_H and the shear modulus G, a constant value for the ratio A/T_r is found out and the design of the bearing geometry can be performed assuming a value of the diameter D and a value of the thickness of a single rubber layer t_r. At this point, the shape factor can be computed and it is possible to verify that it results lower than 5. The known diameter allows to calculate the area of the bearing A and, through this, to derive the total height of the rubber T_r. The latter can be used to find the number of rubber layers n. In fact, the total height of rubber is defined as the thickness of a single rubber layer t_r multiplied by the number of layers n, i.e. :

$$T_r = n\, t_r \tag{4.6}$$

The value of T_r found from Equation (4.4), as a consequence of the assumptions on the shear modulus G and the diameter of the bearing D, is a decimal number whereas the number of rubber layers n is an integer. Hence, the relation in Equation (4.6) is inverted and an exact value of n is obtained,

which must be approximated to the unit. This approximation causes slightly different value of the total height T_r that leads to slightly different values of the horizontal stiffness K_H and of the effective horizontal period T_{eff}. Therefore, it is needed to perform the procedure backward to obtain the actual value of T_r (through Equation (4.6)), K_H (through Equation (4.4)) and T_{eff} (through Equation (4.2) and Equation (4.1), where now the period is not the assumed one T_0 but the effective one) and to check the acceptability of these modified actual values.

The last step consists in the computation of the vertical period of the isolated structure. Analogously to the horizontal direction, the 3D isolation aims at the shifting of the fundamental natural period of the non-isolated structure to the long period range also for the vertical direction. Thus, the vertical effective period T_v can be computed following the same path of reasoning of the horizontal effective period and it could result in the corresponding long period range.

Once the geometry and the material properties of a single bearing are established, deformations and stability must be verified according to EN15129 §8.2.3.3 and §8.2.3.4.

Deformation Requirements EN15129 prescribes that the maximum total design shear strain $\varepsilon_{t,d}$ satisfies the requirement given by:

$$\varepsilon_{t,d} = K_L(\varepsilon_{c,E} + \varepsilon_{q,max} + \varepsilon_{\alpha,d}) \leq \frac{7.0}{\gamma_m} \tag{4.7}$$

Where

- K_L is a type loading factor equal to unity for buildings;
- $\varepsilon_{c,E}$ is the design local maximum shear strain due to compressive strain;
- $\varepsilon_{q,max}$ is the design shear strain due to maximum earthquake-imposed horizontal displacement;
- $\varepsilon_{\alpha,d}$ is the design strain due to angular rotation;
- γ_m is a partial factor for elastomer material, recommended value of 1.0.

The design shear strain due to compression by vertical loads $\varepsilon_{c,E}$ is defined as:

$$\varepsilon_{c,E} = \frac{6SN_{Ed,Max}}{A_r E_c} \tag{4.8}$$

Being:

- S the shape factor;
- $N_{Ed,Max}$ the maximum vertical load;
- A_r the reduced effective plan area due to non-seismic action only;
- E_c the compression modulus, computed through Equation (4.5).

The definition of the design strain due to angular rotation $\varepsilon_{\alpha,d}$ is established by EN1337 §5.3.3.4. Considering a circular bearing and assuming a minimum rotation angle $\alpha_d = 0.003\ rad$ for each orthogonal direction, the aformentioned strain results:

$$\varepsilon_{\alpha,d} = \frac{D^2 \alpha_d}{n t_r^2} \tag{4.9}$$

The shear strain due to maximum horizontal displacement $\varepsilon_{q,max}$ derives from the definition of the design shear strain, $\varepsilon_{q,E}$, due to earthquake-imposed horizontal displacement d_{bd} given as follows:

$$\varepsilon_{q,E} = \frac{d_{bd}}{T_r} \tag{4.10}$$

The shear strain due to maximum horizontal displacement $\varepsilon_{q,max}$ must satisfy the requirement:

$$\varepsilon_{q,max} = \frac{d_{Ed}}{T_r} \leq 2.5 \tag{4.11}$$

Where d_{Ed} is the maximum horizontal displacement induced by the seismic action and it is defined as:

$$d_{Ed} = \gamma_x d_{bd} \tag{4.12}$$

Being $\gamma_x = 1.2$ a magnification factor. The design horizontal displacement d_{bd} can be found from the horizontal elastic response spectrum $S_e(T)$ defined according to EC8 §3.2.2.2 as a function of the damping correction factor η.

This latter parameter depends on the viscous damping ratio of the structure, expressed as a percentage. The viscous damping ratio of the structure ξ is the equivalent of the effective damping of the bearing β_{eff}. In fact, if the bearings are the same for the whole isolation system, also the effective damping ratio is the same and it coincides with the overall viscous damping ratio. The damping correction factor η is defined in EC8 §3.2.2 as:

$$\eta = \sqrt{10/(5+\xi)} \tag{4.13}$$

It is worth noting that the parameter η results equal to 1 for viscous damping ratio $\xi = 5\%$. Entering in the elastic response spectrum with the value of the horizontal effective period T_{eff} and finding the corresponding $S_e(T_{eff})$ allows to modify it multiplying by the damping correction factor and obtaining $S_{e,\xi}(T_{eff}) = \eta\, S_e(T_{eff})$. Finally, the earthquake-imposed horizontal displacement can be computed as:

$$d_{bd} = \frac{S_{e,\xi}(T_{eff})}{\omega^2} \tag{4.14}$$

Stability Requirements EN15129 defines the buckling load capacity through the expression:

$$P_{cr} = \frac{\lambda G A_r D S}{T_r} \tag{4.15}$$

Being $\lambda = 1.1$ for circular bearing and $A_r = A$ for bearing without holes. It is worth noting that the values of the critical buckling load P_{cr} computed through Equation (4.15) gives results very similar to the values computed through Equation (2.14). Furthermore, the fundamental requirement for the stability check is:

$$N_{Ed,Max} \leq \frac{P_{cr}}{2} \tag{4.16}$$

Then, two different conditions have to be satisfied basing on the force interval in which $N_{Ed,Max}$ is comprised. In particular:

- For $P_{cr}/2 > N_{Ed,Max} \geq P_{cr}/4$ the condition to be fulfilled is:

$$1 - \frac{2N_{Ed,Max}}{P_{cr}} \geq 0.7\delta \tag{4.17}$$

- For $N_{Ed,Max} < P_{cr}/4$ the condition to be fulfilled is:

$$\delta \leq 0.7 \tag{4.18}$$

Where $\delta = \frac{d_{Ed}}{D}$.

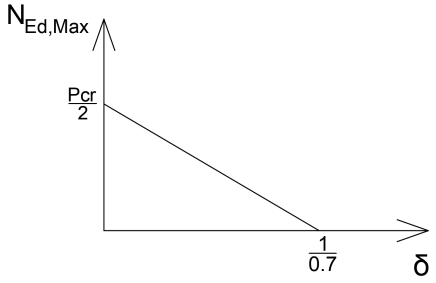

Figure 4.1: Stability domain for $P_{cr}/2 > N_{Ed,Max} \geq P_{cr}/4$.

It is worth noting that expressing $N_{Ed,Max}$ as a function of δ from Equation (4.17) is possible to individuate a stability domain, shown in Figure 4.1. The domain respects the correction of the area reduction method for the computation of the critical buckling load. In fact, it has been demonstrated that for horizontal displacement equal to the diameter of the bearing, a residual capacity of the bearing is present. To be aligned with this experimental results, for $\delta = 1$ the maximum vertical load assumes a value different from zero. The total loss of capacity is reached for $\delta = \frac{1}{0.7} > 1$.

To sum up, the design procedure can be subdivided in steps as illustrated in Figure 4.2. Except for the first two steps, if anyone of the following steps fails, it means that one of the initial hypotheses is not correct so it is necessary to go back to the Assumptions step.

4.2 Alternative Design Approach

The conservative design approach established by European Standards makes the aim of fully isolating large structures in both vertical and horizontal directions complex and difficult to be reached. The need of low value of the shape factor implies high value of the height of a single rubber layer. This leads to a decrease in both vertical and horizontal stiffnesses but also to an increase in importance of the stability problem. To increase the value of the critical buckling load capacity, a rubber with a higher value of the shear

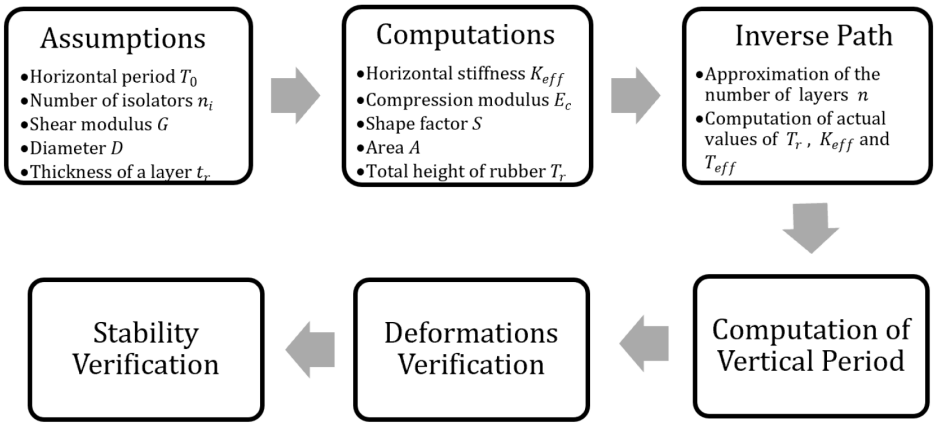

Figure 4.2: Design Procedure.

modulus can be selected. However, larger shear modulus means larger values of horizontal and vertical stiffnesses, tending to nullify the advantage taken from the low shape factor. Alternatively, a bearing having larger diameter can be selected. Also in this case, an increase in vertical and horizontal stiffness is expected. Notwithstanding, the critical buckling load is directly proportional to the shear modulus while depends on the cubic power of the diameter, so the latter allow to increase the critical buckling load capacity with a lesser increase in vertical and horizontal stiffnesses. However, the design of a three-dimensional isolation system is principally a matter of finding an equilibrium between stability requirements and stiffness values needed to isolate the structure and obtain values of the period belonging to the long period range.

EN15129 establishes that the maximum axial force $N_{Ed,Max}$, used in the definition of the deformation and stability requirements reported in the previous section, must be considered as the resultant of the static and dynamic loads, all acting simultaneously. Thus, the maximum axial force is computed as the sum of the contribution of the self-weight of the structure, the contribution of the rocking effects due to the horizontal component of the seismic action and the contribution of the axial force due to the vertical component of the seismic action. However, the long period range of the horizontal effective period is found to be between 2 *sec* to 3 *sec* while the long period range of the vertical effective period is around $0.3-0.5$ *sec*. The marked distance between the isolation periods in the two directions reduces the risk that the maximum damaging effects of the horizontal and vertical components of the seismic action occur simultaneously. In fact, the proba-

bility that the lateral displacement due to horizontal seismic action assumes the maximum value in the same instant of time when the maximum axial force due to vertical seismic action is experienced by the structure is low. Basing on this hypothesis, an alternative design approach is proposed.

The vertical and horizontal components of the seismic action are considered separately and two loading conditions are independently verified. The two different loading conditions are defined as:

- *Condition 1:* **Static load and Horizontal seismic action.** The structure is assumed to undergo the horizontal component of the seismic action in addition to the static load. The vertical component of the seismic action is neglected. Thus, the maximum axial force is computed as the sum of the contribution due to the self-weight and the contribution due to the overturning moment, i.e. the effects of rocking. The lateral displacement is equal to the maximum one;
- *Condition 2:* **Static load and Vertical seismic action.** The structure is assumed to undergo the vertical component of the seismic action in addition to the static load. The effects of rocking are neglected. The maximum axial force is computed as the sum of the contribution due to the self-weight and the contribution due to the vertical seismic action.

Then, the design procedure described in the previous section is performed considering one of the two loading conditions above and, successively, the deformation and stability verification are performed for the remaining condition. It is worth noting that the stability requirement reported in Equation (4.16) is defined to guarantee a safety factor equal to 2. This condition is strongly conservative and can be slightly relaxed, maintaining a great margin of safety.

Finally, once the 3D isolation system is designed, the initial assumption must be checked to assess the reliability of the design approach. Thus, it is necessary to verify that, when the maximum lateral displacement occurs, the axial force does not assume its maximum value. Moreover, for the sake of completeness, it is possible to perform the cross check, i.e. verify that, when the maximum axial load occurs, the lateral displacement does not assume its maximum value.

Chapter 5

Design of a 3D Seismic Base Isolation System for a Case Study

In this chapter, the design approach described in Chapter 4 is applied to design a three-dimensional seismic isolation system at the base of an important large structure containing research technology sensitive to vibrations, in particular to high frequency vibrations, in every direction, i.e. horizontal and vertical directions. The 3D isolation system is made of high damping rubber bearing characterized by low shape factor. This kind of seismic base isolation is very expensive and the prediction of its behaviour in case of intense earthquake is very complex. For these reasons, this system could be used only for special structures for which vertical isolation is considered essential [Kelly and Lee, 2018]. The selected structure is the E-ELT, described in Section 5.1, for which a possible scheme is proposed in Section 5.2. The loads acting on the structure are discussed in Section 5.3. Finally, a proposal for a 3D base isolation system made of high damping rubber bearing with low shape factor is reported in Section 5.4.

5.1 E-ELT Structure

The **E**uropean **E**xtremely **L**arge **T**elescope, **E-ELT** for short, is the most innovative and powered telescope in the world supported by ESO (European Southern Observatory), that is the European Organisation for Astronomical Research in the Southern Hemisphere. Extremely Large Telescope is considered worldwide as one of the highest priorities in ground-based astronomy. The telescope aims to vastly advance astrophysical knowledge and to reveal

the mysteries of the Universe. The ESO challenge consists of a 1083 million euro, 11-year project to construct a 39-meter diameter mirror that makes the E-ELT to be defined as *"the world's biggest eye on the sky"*. The segmented optical telescope allows to view an area on the sky about one ninth the size of the full Moon. A hemispherical dome with curved, laterally opening doors rotating atop a concrete pier is provided to house the telescope, as shown in Figure 5.1 where some vehicles are introduced below to further demonstrate how extremely large the telescope really will be.

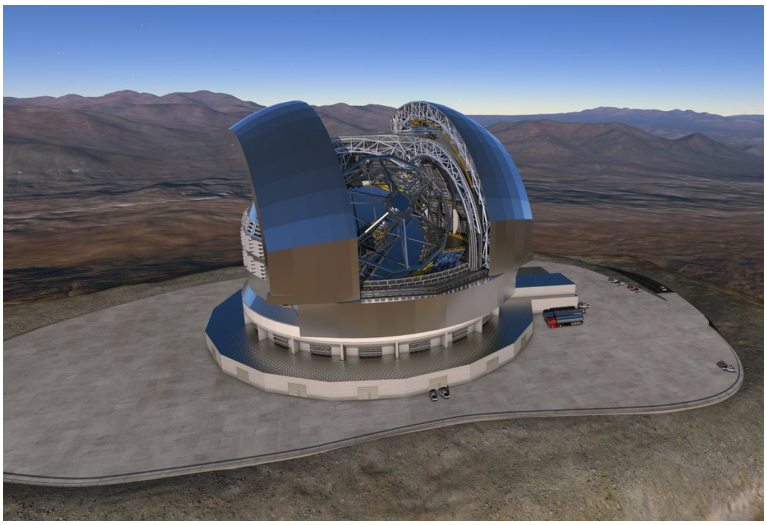

Figure 5.1: Rendering of the E-ELT (adapted from ESO [2019]).

The E-ELT will be placed on Cerro Armazones as part of the La Silla Paranal Observatory, proven to be one of the world's best astronomical sites. The altitude of the mountaintop is 3064 meters above the sea level. At this height, the operating temperatures are low with respect to the average temperature of a very hot zone such Chile and belong to the temperature range suitable for seismic protective systems, as elastomeric bearings. The E-ELT and its components are designed to deal with an earthquake that would couple with the structure at above $1g$ acceleration. A detailed analysis of the site seismicity has been performed and it leads to the elastic response spectrum shown in Figure 5.2 that confirms a maximum acceleration higher than $1g$. The airtight and watertight dome lets the telescope completely free to position itself whether the dome is open or closed. The size of the opening relative to the total dome size is very large. Four girders carry the tracks upon which the doors travel. A windscreen protects the telescope from high wind speeds whereas several louvers increase the ventilation of the internal

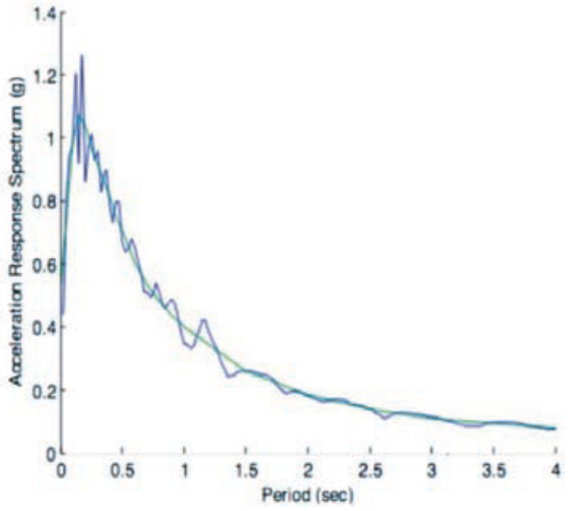

Figure 5.2: Horizontal elastic response spectrum (adapted from ESO [2011]).

volume. The dome is placed on its own foundations which also holds a concrete pier. The telescope concrete pier lifts the telescope azimuth structure above the ground level, ensuring that the primary mirror remains more than 10 metres above the ground.

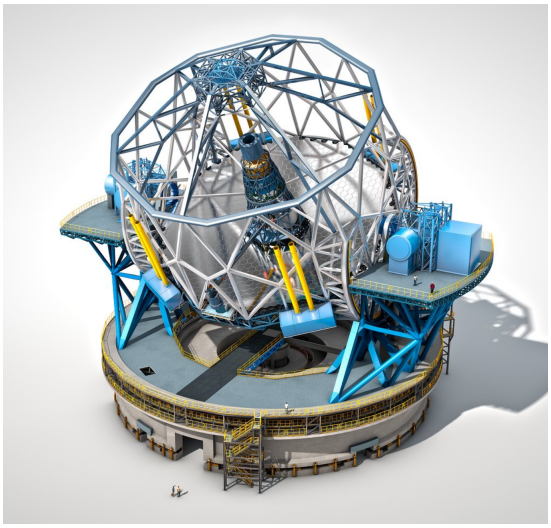

Figure 5.3: Rendering of the telescope (adapted from ESO [2019]).

The telescope and its sub-units constitute the so-called *Main Structure*. The sub-units consists of two azimuth tracks, that take the axial loads and allow the rotation of the telescope about the zenith, two Nasmyth platforms,

mounted at the side of the azimuth tracks to host additional instruments, and the altitude structure, i.e. the metallic component that hosts the telescope optics and rotates with them.

The telescope pier is 9.3-metre high and consists of two load-carrying annular rings for the interface with the azimuth tracks of the telescope. The external annular ring has the diameter equal to 51.5 metre whereas the internal one has the diameter equal to 34 metre. Both rings are 1 metre thick and have 2.2-metre-wide and 2.8-metre-deep crowns in which the azimuth tracks are installed. Additional stiffness is provided to the load-carrying beams by including radial walls every 15 degrees and 40 cm thick floor and 40 cm thick ceiling components that seal the foundations. The floor is located at the 8.125-metre level and extends outside the pier outer diameter to allow access to the lower part of the outer track for maintenance [ESO, 2011]. The cross section of the telescope pier is illustrated in Figure 5.4.

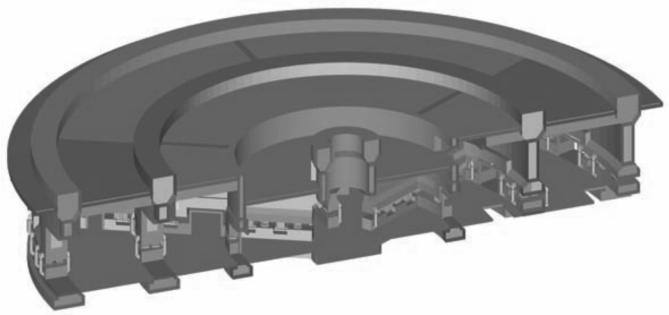

Figure 5.4: Telescope concrete pier (adapted from ESO [2011]).

ESO [2011] proposed a sophisticated isolation system composed by springs, viscous damper and pre-loaded unites that provide adequate stiffness performance under operational conditions. The baseline isolation system is located just above the bottom slab of the telescope foundation. The seismic protective system units provide an equivalent damping of 27% and shift the fundamental frequency of the building to 0.51 Hz, corresponding to the long period range. Therefore, the structure is no longer coupled with the high accelerations of the earthquake. Hence, the horizontal acceleration experienced by the structure is reduced to $0.14g$ obtained from the NCR (No-Collapse Requirement) response spectrum and assuming 27% damping of the isolation system, as shown in Figure 5.5.

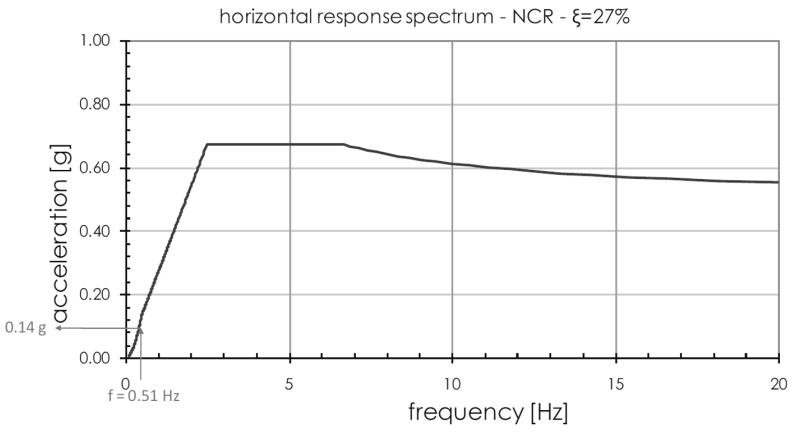

Figure 5.5: Horizontal response spectrum due to equivalent damping of 27% (adapted from ESO [2011]).

5.2 Scheme of the Structure

As mentioned above, an elastomeric bearing-based protective system that guarantees vertical and horizontal isolation is very expensive and rarely adopted. The E-ELT is considered a special construction for which a three-dimensional isolation system is required to protect the telescope, that is an instrument sensitive to both horizontal and vertical vibrations. Due to this fact, the 3D isolation system, described in the following section, is designed to isolate only the main structure, thus positioned just under the telescope pier and the elastomeric bearings are placed along the annular rings.
The telescope pier is assumed to be rigid and to act as a fixed constraint for the main structure. The mass of the concrete walls, slabs and floors is all concentrated in the centre of gravity, located at the centre of the rings and at half of the total height of the concrete pier.
The mass of the main structure can be concentrated in the centre of gravity of the telescope and its sub-units, assumed to coincide with the point around which they rotate. The rotation point is located at the centre of the rings and at the height of the Nasmyth platforms. Knowing that the external ring has diameter of 51.5 m, the height of the rotation point is computed through a proportion and it results equal to 18.84 m, as shown in Figure 5.6.

The main structure can be approximated as an elastic beam of length $L = 18.84\ m$, which properties are derived from the eigenfrequencies obtained through a modal analysis on a detailed finite element model of the telescope and its sub-units.

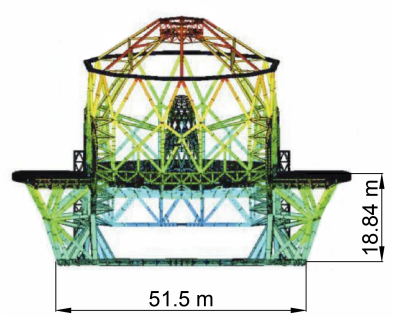

Figure 5.6: Dimensions of the main structure (adapted from ESO [2011]).

Table 5.1: Eigenfrequencies of the main structure (adapted from ESO [2011]).

Mode	Frequency	Mode shape
1	2.91 Hz	Horizontal in Y
2	3.19 Hz	Horizontal in X
8	5.17 Hz	Vertical

The significant modes are the ones that represent the main structure response as a whole. They are reported in Table 5.1 where the coordinate reference system has the Z-axis as the vertical one. The first and the second modes are in orthogonal horizontal directions and the eighth mode is in vertical direction. Intermediate modes involve deformation of components or, in general, part of the main structure, so they are not considered of interest for the design of the isolation system. The deformed shapes of the three relevant modes are shown in Figure 5.7.

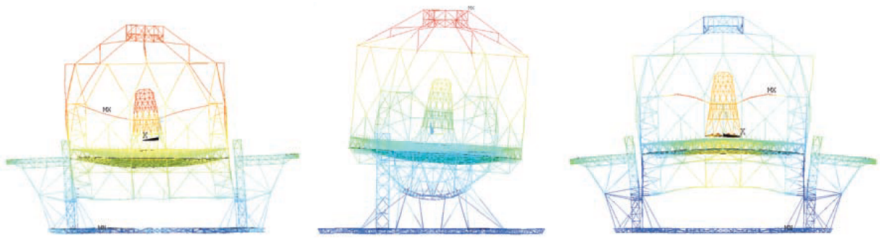

(a) First horizontal mode (b) Second horizontal mode (c) Vertical mode

Figure 5.7: Deformed shape of the mode 1, mode 2 and mode 8 of the main structure (adapted from ESO [2011]).

Starting from the values of the eigenfrequeciences, it is possible to compute the corresponding natural frequencies and then, from the definition of ω, to derive the horizontal and vertical stiffnesses. The absence of torsional modes, at least in the first ten modes of vibration of the main structure, allows to consider as zero the torsional mass and the torsional moment of inertia. Assuming that the main structure has an average Young's modulus of $E_{Young} = 200\ GPa$, close to the modulus of elasticity of the steel, the geometrical properties of the equivalent elastic beam result:

$$\begin{cases} I_x = 12.668\ m^4 \\ I_y = 15.223\ m^4 \\ A = 0.338\ m^2 \end{cases} \tag{5.1}$$

5.3 Acting loads

The significant importance and magnificence of the E-ELT is evident even from the size of the structure. However, the huge size implies high gravity loads. The main structure is about 3400 *ton*, including 700 *ton* of opto-mechanics and electronics. The mass of the described components are reported in Table 5.2.

Table 5.2: Mass budget (adapted from ESO [2011]).

Component	**Description**	**Mass**
Telescope Pier	Concrete walls and slabs	17815 ton
	Concrete floors	794 ton
Main Structure	Telescope and sub-units	3400 ton

To design a single isolator, the mass of the whole structure can be equally divided among the elastomeric bearings, i.e. each isolator sustains a mass equal to m_{tot}/n, where m_{tot} is the total mass of the telescope pier and the main structure and n is the number of isolators.
The design of the isolation system is performed considering the seismic event as the predominant variable action on the structure. The actual values of the seismic actions in horizontal and vertical directions should be obtained through a numerical dynamic analysis. However, to apply the design procedure, it is possible to initially consider the seismic actions as equivalent static loads and, successively, perform the numerical dynamic analysis.
The initial assumptions of the design procedure are based on the required horizontal response of the bearing, i.e. the dimensioning of the bearing is

performed to obtain a required value of the horizontal stiffness. Reminding that the 3D isolation system is made of high damping rubber bearing characterized by low shape factor, an effective damping ξ equal to 10% is selected. This assumption allows to compute the maximum horizontal displacement induced by seismic action d_{Ed}. According to Equation (4.13), the damping correction factor for an effective damping $\xi = 10\%$ is $\eta = 0.816$. Entering in the elastic response spectrum, shown in Figure 5.2, with the value of the isolation period assumed to be $T_H = 2.5\ sec$, the corresponding value is $S_e(T_H) = 0.18g$. The damping correction factor must be applied to the elastic response spectrum to obtain the actual value of the acceleration of the damped system. In particular:

$$S_{e,\xi}(T_{eff}) = S_e(T_{eff})\ \eta = 0.147g \tag{5.2}$$

Therefore, the design horizontal displacement is computed through Equation (4.14) and it results:

$$d_{bd} = 0.231\ m \tag{5.3}$$

Then, the maximum horizontal displacement induced by the seismic action is computed as $d_{Ed} = \gamma_x d_{bd} = 0.277\ m$, with $\gamma_x = 1.2$.

Hence, the effects of the horizontal components of the seismic action in horizontal direction are considered through the initial assumptions.Then, the effects of the horizontal components of the seismic action in vertical direction must be computed to account for the effects of rocking. On the base of the elastic response spectrum illustrated in Figure 5.2, the shear force at the base can be computed as:

$$V_b = m_t\ S_{e,\xi}(T_{eff}) \tag{5.4}$$

The effects of the base shear is distributed on the two masses: the mass of the telescope pier m_{tp}, concentrated at the height h_{tp} equal to half of the pier height, and the mass of the main structure m_{ms}, concentrated at height h_{ms} equal to the total height of the telescope pier added to the length of the equivalent elastic beam L. For this reason, the portion of the base shear acting on the telescope pier and on the main structure are computed, respectively, as:

$$V_{tp} = \frac{m_{tp}}{m_{tp} + m_{ms}} V_b \tag{5.5}$$

$$V_{ms} = \frac{m_{ms}}{m_{tp} + m_{ms}} V_b \tag{5.6}$$

Therefore, the overall overturning moment due to the shear forces acting on the two masses is given by:

$$M_{rock} = V_{tp} h_{tp} + V_{ms} h_{ms} \tag{5.7}$$

Finally, to compute the axial force on the i-th bearing, the structure is assumed to behave as a rigid beam lying on elastic springs, one for each elastomeric bearing, subjected to a bending moment that causes a rigid rotation around the middle point. Making reference to the Navier formulation, the axial force N_{rock} on the i-th bearing depends on the distance between the middle point and the position of the i-th spring and on a factor that account for the stress distribution. The expression of N_{rock} turns out to be:

$$N_{rock} = \frac{x_i - x_g}{\sum_i (x_i - x_g)^2} M_{turn} \tag{5.8}$$

Being x_i the coordinate of the i-th bearing and x_g the coordinate of the middle point, that coincides with the centre of the rings, due to the symmetry of the structure. The overturning moment defines two zones with opposite effects: one subjected to compressive load and the other subjected to tensile load. The maximum effect is sustained by the farthest bearing, i.e. the bearing for which the term $(x_i - x_g)$ is maximum.

Due to the huge size of the telescope pier and the main structure, the number of units that compose the isolation system is fixed as $n_i = 120$ and the distribution of the devices is defined: 70 of which are placed on the external ring of diameter $D_{ext} = 51.5\ m$ and the remaining 50 are placed on the internal ring of diameter $D_{int} = 34m$. The computation of the exact position of each isolator is performed to allow the computation of the overturning moment contribution to the maximum axial load. The reference coordinate system is selected with origin in the common centre of the azimuth rings. The exact position of each isolator is computed as a function of the radius of the corresponding ring and of the angle θ between the considered isolator and the one of the two adjacent isolators, i.e. $\theta = 2\pi / n_{ring}$ with n_{ring} equal to the number of isolator on the corresponding ring. Increasing the number of isolators implies a decreasing of the stiffness demand on each unit.

Once the device locations are known, the overturning moment M_{rock} can be computed. The masses and the lever arms used for the computation are listed in the following.

$$\begin{cases} m_{tp} = 18609\, ton \\ h_{tp} = 4.65\, m \\ m_{ms} = 3400\, ton \\ h_{ms} = 28.14\, m \end{cases}$$

Starting from the value of the base shear obtained by means of Equation (5.4) and equal to $V_b = 32347\ kN$, the overturning moment results $M_{rock} = 267590\ kNm$.
Finally, the axial force is computed as discussed above and turns out to be:

$$N_{rock} = 226\ kN \tag{5.9}$$

The last contribution of the axial force to be computed is due to the vertical component of the seismic action. Referring to Figure 5.5, which is the only spectrum available from the design data, it is possible to conclude that the response spectrum of the E-ELT is analogous to the elastic response spectrum defined be EC8 for a *Soil Type A*. In fact, the frequency corresponding to the point where the plateau starts is around $2.5\,Hz$, that means a period of 0.4 *sec*. Following the same path of reasoning, the frequency corresponding to the point where the plateau finishes is around $7\ Hz$, that means a period of $0.15\,sec$. The obtained values of the period coincide with the values of T_B and T_C specified in Table 3.2 in EC8 §3.2.2.
Assumed that the horizontal response spectrum is related to a *Soil Type A*, the vertical response spectrum is assumed to be the corresponding defined by EC8 §3.2.2.3. Thus, the periods that define the vertical response spectrum are $T_B = 0.05\ sec$, $T_C = 0.15\ sec$ and $T_D = 1\ sec$ while the peak ground acceleration in vertical direction is equal to 90% of the one in horizontal direction, according to Table 3.4 in EC8 §3.2.2.3.
Moreover, according to the vertical elastic response spectrum defined by EC8, it is possible to compute the axial force due to the seismic action in vertical direction. In particular, considering that the damping in vertical direction is equal to the 80% of the damping in horizontal direction, i.e. $\xi_v = 8\%$, the damping correction factor is computed through Equation (4.13) and it results $\eta_v = 0.877$. The vertical peak ground acceleration can be computed according to EC8 §3.2.2.3 as:

$$a_{vg} = 0.9\, a_g = 0.4\, g \tag{5.10}$$

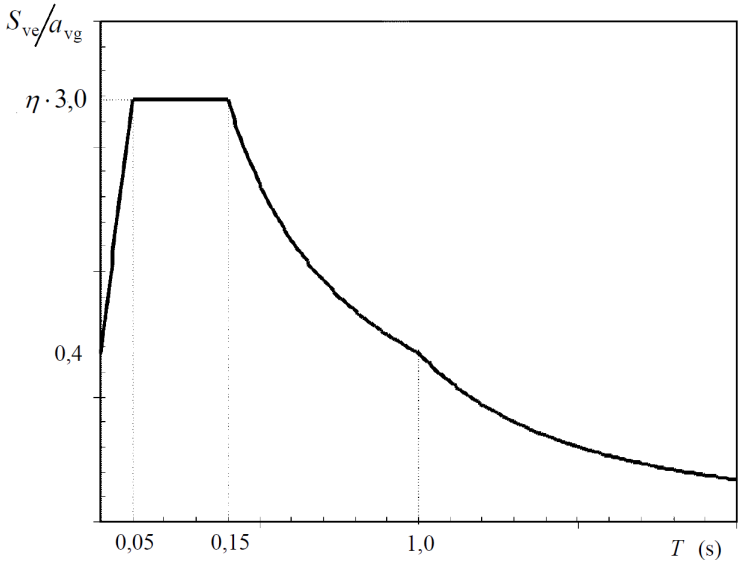

Figure 5.8: Vertical elastic response spectrum (adapted from EC8).

Then, the value of the acceleration of the damped system is obtained entering with the vertical period, assumed to be equal to 0.3 *sec*, in the vertical elastic response spectrum, shown in Figure 5.8, or, more precisely, according to the definition of the vertical elastic response spectrum reported in EC8 §3.2.2.3 for $T_C \leq T \leq T_D$:

$$S_{ve,\xi}(T_v) = 3.0\, a_{vg}\, \eta_v\, \frac{T_C}{T} = 0.52\, g = 5.1\, \frac{m}{s^2} \tag{5.11}$$

The contribution of the vertical component of the seismic actions on the total axial force acting on a single bearing, obtained from the elastic response spectrum in vertical direction, turns out to be:

$$N_{ve} = \frac{m_{tot}\, S_{ve,\xi}(T_v)}{n} = 935\ kN \tag{5.12}$$

The maximum axial force $N_{Ed,Max}$, as defined by EN15129 and acting on a single bearing, can be obtained as the sum of the contribution of the self-weight, the contribution of the rocking and the value of N_{ve} computed above, as expressed in Equation (5.13).

$$N_{Ed,Max} = \frac{m_{tot}g}{n} + N_{rock} + N_{ve} = 2995\ kN \tag{5.13}$$

Analogously, the minimum axial force can be computed as the difference between the first two aforementioned terms and the last one due to the vertical seismic action, resulting in a positive value. Thus, it is possible to conclude that the elastomeric bearings for the 3D isolation of the E-ELT main structure are not subjected to tensile stresses.

5.4 Design of the 3D Isolation System

The elastomeric bearing system proposed herein is designed to provide both vertical and horizontal isolation of the main structure of the E-ELT. The system is placed at the interface between the dome foundation and the telescope pier and the isolators are located along the concentric rings, in a number different for the internal and the external rings but uniformly distributed on each ring. Thus, according to EC8 §10.5.2, the torsional effects can be neglected because the effective stiffness centre and the centre of damping of the isolation system coincide with the projection of the centre of mass on the isolation interface. The isolation system consists of high damping rubber bearings with a shape factor sufficiently low to allow vertical isolation. The high damping is provided by an effective damping of a single isolator of 10%.

Performing a design procedure according to European Standards means considering the maximum axial force equal to the value computed in Equation (5.13). Applying the design procedure described in Section 4.1, a 3D isolation system for the E-ELT case study can be proposed starting from the initial assumptions and obtaining the resulting quantities reported in Table 5.3.

As an alternative, the design approach described in Section 4.2 is now applied and discussed in detail following the passages reported in Figure 4.2. It is worth noting that the aforementioned approach is based on the hypothesis that the horizontal and vertical components of the seismic action can be considered separately due to the marked distance between the vertical and the horizontal isolation period. The non-simultaneity of the maximum lateral displacement with the maximum axial force must be checked through dynamic analysis performed on the commercial structural software used to

Table 5.3: Parameters designed according to European Standards.

Assumptions	**Results**
$D = 1.35\ m$	$K_v = 112890\ \frac{kN}{m}$
$n = 7$	$K_H = 1369\ \frac{kN}{m}$
$t_r = 0.09\ m$	$T_h = 2.29sec$
$S = 3.64$	$T_v = 0.24sec$
$G = 0.64\ MPa$	

model the whole structure and subjected to the simultaneous seismic action in every direction.
For the E-ELT case study, the two loading conditions described in Section 4.2 are:

- *Condition 1:* **Static load and Horizontal seismic action.** The maximum axial force is the sum of the contribution of the self-weight and the contribution of the effects of rocking, i.e. :

$$N_{cond1} = \frac{m_{tot}g}{n_i} + N_{rock} = 2025\ kN \tag{5.14}$$

  While the horizontal displacement is equal to the maximum one computed in Equation (4.14);

- *Condition 2:* **Static load and Vertical seismic action.** The maximum axial force is the sum of the contribution due to the self-weight and the contribution due to the vertical seismic action, i.e. :

$$N_{cond2} = \frac{m_{tot}g}{n_i} + N_{ve} = 2734\ kN \tag{5.15}$$

  While the horizontal displacement is assumed to be a low value, e.g. $d = 0.03\ m$.

Design basing on the alternative design approach

- *Assumptions.* The effective horizontal period is initially assumed to be $\boldsymbol{T_{eff,0} = 2.5\ sec}$. Thus, the natural frequency results:

$$\omega_0 = \frac{2\pi}{T_{eff,0}} = 2.51\ \frac{rad}{s} \tag{5.16}$$

According to the values reported in Table 5.3, the value of the shear modulus is assumed to be $\boldsymbol{G = 0.64\,MPa}$. A lower value of the shear modulus means a lower value of the critical buckling load capacity and a lower values of the vertical and horizontal stiffnesses, due to the dependence on the compression modulus E_c and on the shear modulus G, respectively.

The diameter of the bearing is assumed to be $\boldsymbol{D = 1.2\,m}$, considering the huge size of the structure and the large value of the acting loading. The thickness of a single rubber layer is assumed to be $\boldsymbol{t_r = 0.09\,m}$ to obtain a sufficient low value of the vertical stiffness. The geometrical properties are selected taking into account the influence of them on the shape factor, that must be lower than 5.

- *Computations.* Reminding Equation (5.16) and the definition of the natural frequency, the effective stiffness of the whole structure is computed as:

$$K_{eff,0,tot} = \omega_0^2\, m_{tot} = 138659\ \frac{kN}{m^2} \tag{5.17}$$

Where $m_{tot} = 22009\ ton$ is the total mass of the entire structure.

From the $K_{eff,0,tot}$, the effective horizontal stiffness of a single bearing is obtained through:

$$K_{eff,0} = K_{eff,0,tot}/n_i = 1155.5\ \frac{kN}{m^2} \tag{5.18}$$

The shape factor results $S = \frac{D}{4t_r} = 3.333 < 5$.

The compression modulus E_c can be calculated by means of Equation (4.5) and it results $E_c = 44.6\ MPa$.

The area of the bearing is easily computed and it results:

$$A = \frac{\pi D^2}{4} = 1.13\ m^2 \tag{5.19}$$

Finally, the total height of the rubber can be calculated inverting the definition of horizontal effective stiffness, i.e.:

$$T_{r,0} = \frac{GA}{K_{eff}} = 0.626\ m \tag{5.20}$$

- *Inverse Path.* From $T_{r,0}$, the exact value of n, that is the number of rubber layers, results:

$$n = \frac{T_{r,0}}{t_r} = 6.95555 \tag{5.21}$$

This value must be approximated with the closest unit, in this case $n = 7$. Now, the total height of the rubber T_r, the horizontal effective stiffness K_{eff}, the natural frequency ω and the horizontal period T_{eff} must be recomputed following the inverse path of reasoning of the previous steps. The aforementioned quantities result:

$$\begin{cases} T_r = 0.63\ m \\ K_{eff} = 1148\ \frac{kN}{m^2} \\ \omega = 2.5\ \frac{rad}{s} \\ T_{eff} = 2.51\ sec \end{cases} \tag{5.22}$$

- *Computation of Vertical Period.* Analogously to the procedure for the computation of the horizontal period T_{eff}, the vertical period must be computed from the value of the vertical stiffness of a single bearing. The vertical stiffness for a single bearing is defined as:

$$K_v = \frac{E_c A}{T_q} = 80041\ \frac{kN}{m} \tag{5.23}$$

Thus, the vertical period results:

$$T_v = 2\pi\sqrt{\frac{m_{tot}}{nK_v}} = 0.3\ sec \tag{5.24}$$

Hence, the vertical period of the isolated main structure belongs to the long period range for vertical elastic response spectrum. Therefore, both vertical and horizontal period respect the required values for a three-dimensional isolation system made of high damping rubber bearings.

Verification of Loading Condition 1

- *Deformations.* The deformation verification can be performed, according to Equation (4.7), Equation (4.8), Equation (4.9) and Equation (4.11). The values of the deformation satisfy the requirements established by EC8. In particular:

$$\begin{cases} \varepsilon_{c,E} = 0.000803 \\ \varepsilon_{\alpha,d} = 0.0762 \\ \varepsilon_{q,max} = 0.369 \leq 2.5 \\ \varepsilon_{t,d} = 0.446 \leq 7.0 \end{cases} \tag{5.25}$$

- *Stability.* According to Equation (4.15), the critical buckling load capacity is $P_{cr} = 5055\ kN$.

  Thus, the situation belongs to the case $P_{cr}/ > N_{Ed,Max} \geq P_{cr}/4$ and the condition reported in Equation (4.17) is fulfilled, in particular $0.198 \geq 0.161$.

Verification of Loading Condition 2

- *Deformations.* The values of the deformation satisfy the requirements established by EC8. In particular:

$$\begin{cases} \varepsilon_{c,E} = 0.000108 \\ \varepsilon_{\alpha,d} = 0.0762 \\ \varepsilon_{q,max} = 0.0463 \leq 2.5 \\ \varepsilon_{t,d} = 0.124 \leq 7.0 \end{cases} \tag{5.26}$$

- *Stability.* According to Equation (4.15), the critical buckling load capacity is $P_{cr} = 5055\ kN$.

  Thus, the fundamental requirement expressed in Equation (4.16) is not fulfilled. In fact, the maximum axial force turns out to be the 10% higher of $P_{cr}/2$. However, the result is considered acceptable because of the relaxation of the conservatively required safety factor equal to 2.

To conclude, it is worth noting that the elastomeric bearing, designed following the design approach proposed in Section 4.2 and basing on the same assumptions of the elastomeric bearing designed following the design procedure described in Section 4.1, has smaller diameter but leads to higher value of the isolation periods.

Chapter 6

Analyses on OpenSees of the Case Study

This chapter is devoted to the analyses on OpenSees of a single elastomeric bearing, the design of which is reported in Section 5.4. The aim of these analyses consists in understanding the bearing response when subjected to strong ground motions, on the base of the mechanical behaviour described in Chapter 3. Formerly, Section 6.1 describes the code implementation performed to create the model and to analyze it. Then, in Section 6.2 the analyses and the corresponding results are shown and discussed. Finally, Section 6.3 briefly discusses problems arose in the modelling of the whole structure.

6.1 Model of the Single Bearing

The OpenSees model of the designed bearing is created referring to the formulation of Kumar et al. [2015] and the element implemented by Kumar [2016]. However, the parameters required as input arguments of the element need to be selected such that represent the actual behaviour of the isolation device.

In particular, it is worth nothing that the expression for the computation of the restoring forces, based on the formulation by Park et al. [1986] and reported in Equation (3.12), describes in a correct manner the behaviour of lead rubber bearings, in which the hysteretic component is exploited by the internal lead core, but makes a mistake for what concerns elastomeric bearings. In fact, using that expression, the energy dissipation exploited by the rubber is taken into account twice: firstly by means of the parameter c_d of the viscous energy dissipation, that represents the defined percentage of

the critical damping of the bearing, and then by means of the characteristic strength Q_d, i.e. the intercept of the hysteresis cycle curve with the y-axis. Both quantities depend on the effective damping β_{eff}, that is the ratio between the energy dissipated per cycle and the elastic strain energy, so it is evident that the contribution of the damping is doubled. The major energy dissipation mechanism of the elastomer used for high damping rubber bearing is hysteretic rather than viscous. Due to this, the parameter c_d is assumed to be zero.

The predominant contribution of hysteretic energy dissipation leads to non-linear hysteresis in the force-displacement graph. The behaviour is modelled as a bi-linear curve, with initial elastic stiffness and then a strain-hardening branch. The post-elastic stiffness ratio α, i.e. the ratio between the the post-elastic stiffness and the elastic stiffness, is suggested by Kelly [2001] to be in the range of $1/3 - 1/4$ for high damping rubber bearing, so the elastic stiffness is from three to four times the post-elastic one. Therefore, the value of the parameter α is assumed to be 0.33.

The high damping rubber bearing has been designed to isolate the super-structure to an horizontal period $T_H = 2.51\ Hz$ and to a vertical period $T_v = 0.3\ sec$. The elastomeric bearing has a 1.2-metre diameter and consists of seven, 0.09-metre-thick layers of rubber, characterized by a shear modulus equal to $G = 0.64\ MPa$, and of a 4-millimetre-thick steel shims. The bulk modulus of the rubber is assumed as the most common value of $K = 2000\ MPa$. The mass over a single isolator is assumed to be equal to the n-th part of the total mass of the main structure. The value of the effective damping is set to 10%.

Elastomeric bearing are usually subjected to large strains, so the design of their properties is usually carried out at shear strain of 100%. In the case of the E-ELT, the aim to reach a vertical isolation, in addition to the horizontal isolation, has implied thick layers of rubber that means a high value of the total height of the bearing. Due to this, the design horizontal deformation corresponds no longer to shear strain of 100% but to less than 50%. In fact, the design horizontal displacement reported in Equation (5.3) is far from $T_r = 0.63\ m$, so the bearing subjected to high-intensity earthquakes will not reach the level of deformation assumed by Kumar et al. [2015]. Therefore, attention must be paid to the definition of the hysteresis cycle. In fact, the expression to compute the characteristic strength (Equation (3.18)) depends on quantities determined for $\Delta = T_r$, i.e. shear strain of 100%, but in this case $\Delta = T_r$ can not be reached, so the value of Q_d computed by means of Equation (3.18) can not be used.

To shed light on the reasons for this, the idealized bi-linear behaviour in shear, shown in Figure 6.1, is considered, with u_{max} corresponding to the maximum lateral displacement, here referred as Δ.

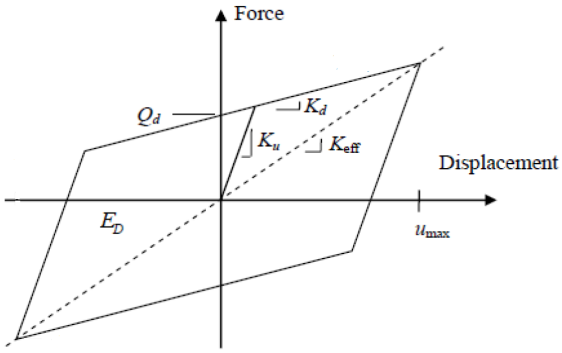

Figure 6.1: Idealized behaviour of elastomeric bearings in shear (adapted from Warn and Whittaker [2006]).

The area enclosed in the curve represents the energy dissipated per cycle and it can be computed in an approximate manner through Equation (3.16), that is a linear function of the maximum displacement Δ. The elastic strain energy is defined as $K_{eff}\Delta^2$ that is a square function of the maximum displacement. Thus, if the maximum displacement Δ decreases, both energies decrease but the elastic strain energy decreases faster than the energy dissipated per cycle, so the value of the effective damping β_{eff} results higher than the initial one, as evident from Equation (3.15). Moreover, since the effective stiffness is computed through Equation (3.10), if the maximum displacement Δ decreases, the effective stiffness K_{eff} increases. Kumar et al. [2015] assumes the effective stiffness K_{eff} to be very similar to the post-elastic stiffness K_d such that it has no influence if it is considered the latter rather than the former and this is acceptable for a shear strain of 100%. Conversely, for lower shear strain, the effective stiffness must be computed as:

$$K_{eff} = K_d + \frac{Q_d}{\Delta} \tag{6.1}$$

Hence, for value of the shear strain lower than 100%, the system turns out to be stiffer ($K_{eff} > K_d$) and more damped ($> \beta_{eff}$), so the procedure proposed by Kumar et al. [2015] leads to a hysteresis cycle that does not represent the actual behaviour of the designed bearing. In particular, due

to the fact that the post-elastic stiffness K_d is defined as a function of the geometrical and material properties of the bearing, that are fixed, and the elastic stiffness is computed as the product between the post-elastic stiffness K_d and the post-elastic stiffness ratio α, that are fixed, the characteristic strength Q_d remains the only quantity that can be modified to define a correct force-deformation curve.

Therefore, the definition of the characteristic strength is performed through an iterative procedure that aims at finding a value of Q_d for which the effective damping at a shear strain corresponding to the design horizontal displacement results as the designed value, i.e. $\beta_{eff} = 10\%$. The geometrical and material properties of the bearing are known and the post-elastic stiffness ratio is fixed. Considering $\Delta = d_{bd}$, the procedure starts assuming a value of the characteristic strength Q_d, from which it is possible to compute the yield strength F_Y through Equation (3.26) and the corresponding yield displacement Y as the ratio between the yield strength and the lateral displacement Δ. Then, the area enclosed in the hysteresis cycle can be obtained by means of Equation (3.16) and, once the post-elastic stiffness has been calculated as $K_d = GA/T_r$, the effective stiffness K_{eff} is found through Equation (6.1). Finally, the effective damping can be computed using Equation (3.15) and the result must be in accordance with the initial hypothesis of $\beta_{eff} = 10\%$. If the check is fulfilled, the initially assumed value of the characteristic strength Q_d describes correctly the energy dissipation of the bearing. Conversely, if the effective damping β_{eff} does not match with the initial hypothesis, another value of the characteristic strength must be assumed and the procedure must be repeated. In particular, if the effective damping β_{eff} results lower than the required one, a higher value of the characteristic strength Q_d has to be selected.

To sum up, the procedure can be performed in the following steps:

- **Known parameters.** The quantities known from the design of the bearing are:
  - G, the shear modulus of the rubber;
  - A, the area of the bearing;
  - T_r, the total height of the rubber;
  - α, the post-elastic stiffness ratio;
  - Δ, the design horizontal displacement;
  - β_{eff}, the effective damping.

- **Derived parameters.** The quantities that can be computed from the known parameters are:
  - $K_d = \frac{GA}{T_r}$, the post-elastic stiffness;
  - $K_u = \alpha K_d$, the elastic stiffness.
- **Initial assumption.** A first tentative value of the characteristic strength $Q_{d,0}$ is assumed.
- **Calculations.** The quantities that can be computed as a consequence of the assumption are:
  - $F_Y = \frac{Q_{d,0}}{1-\alpha}$, the yield strength;
  - $Y = \frac{F_Y}{\Delta}$, the yield displacement;
  - $K_{eff,0} = K_d + \frac{Q_{d,0}}{\Delta}$, the effective stiffness;
  - $E_{D,0} = 4Q_{d,0}(\Delta - Y)$, the energy dissipated per cycle;
  - $\beta_{eff,0} = \frac{1}{2\pi}\frac{E_{D,0}}{K_{eff,0}\Delta^2}$, the effective damping.
- **Check.** If $\beta_{eff,0} = \beta_{eff}$ the procedure is finished and the correct value of the characteristic strength Q_d is found. Conversely, the procedure must be repeated with a modified initial assumption, i.e. a different value of Q_d must be selected.

Performing the procedure with the designed properties of the bearing, the characteristic strength results equal to $Q_d = 46.5\ kN$, from which the yield strength of the bearing is found to be $F_Y = 69.4\ kN$.
Finally, reminding that the designed properties are related to a shear strain equal to $d_{bd}/T_r\% = 37\%$, the actual effective damping of the rubber at 100% of the shear strain can be obtained performing the procedure described above for the computed value of Q_d and $\Delta = T_r$. For an effective damping of 10% at 37% of the shear strain, the corresponding effective damping at 100% of the shear strain is equal to 4%. Thus, it is possible to conclude that for the designed isolation device the needed rubber compound is closer to a natural or synthetic rubber compound typically used for low damping rubber bearing.

The model is created following the OpenSees operational principles, explained in Section 3.4.1, and making use of the element `ElastomericX` described in Section 3.4.3.
The model of the isolator is created through the definition of the 3D space and of the two end nodes with the corresponding constraints. In particular:

```
#Create Model Builder
model basic -ndm 3 -ndf 6
#Create nodes
node 1 0 0 0
node 2 0 $h 0
#Define single point constraints
fix 1 1 1 1 1 1 1
fix 2 0 0 0 1 1 1
```

The distance `h` between the two nodes, i.e. the height of the element, corresponds to the sum of the total height of the rubber layers and the total height of the steel shims. The upper node of the bearing has fixed rotations to be consistent with the Two-spring model, discussed in Section 2.5. The element is created through the element `ElastomericX` having inputs listed in Table 6.1, except for the value of the four tags because they vary during different analyses, as discussed in Section 6.2.

Table 6.1: Designed input arguments of `ElastomericX`.

Input	Value	Input	Value
`$eleTag`	1	`$n`	7
`$Nd1`	1	`$x1 $x2 $x3`	0 1 0
`$Nd2`	2	`$y1 $y2 $y3`	1 0 0
`$Fy`	69400 N	`$kc`	default
`$alpha`	0.33	`$PhiM`	default
`$Gr`	$0.64 \cdot 10^6\, N/m^2$	`$ac`	default
`$Kbulk`	$2000 \cdot 10^6\, N/m^2$	`$sDratio`	default
`$D1`	0	`$m`	default
`$D2`	$1.2\, m$	`$cd`	0
`$ts`	$4 \cdot 10^{-3}\, m$	`$tc`	$12 \cdot 10^{-3}\, m$
`$tr`	$0.09\, m$		

The gravity load pattern must be introduced taking into account that the maximum axial load is the sum of the contribution of the mass and the contribution of the overturning moment having value obtained as defined in Equation (5.13) and set with the tag `$Nmax`.

```
#Apply gravity load
set P $Nmax
#Create a plain load pattern for static analysis
pattern Plain 1 "Linear" {
load 2 0.0 [expr -$P] 0.0 0.0 0.0 0.0};
```

The dynamic analysis is performed to analyze the actual bearing behaviour under seismic loads due to a high-intensity earthquake. The Imperial Valley record from El Centro 1940 is selected as an example due to the fact that its elastic response spectra in horizontal directions are quite coincident with the horizontal response spectrum of El Cerro Armazones, shown in Figure 5.2, around the horizontal effective period for which the isolation system has been designed. For the sake of completeness, the three pseudoacceleration elastic response spectra are superimposed in Figure 6.2.

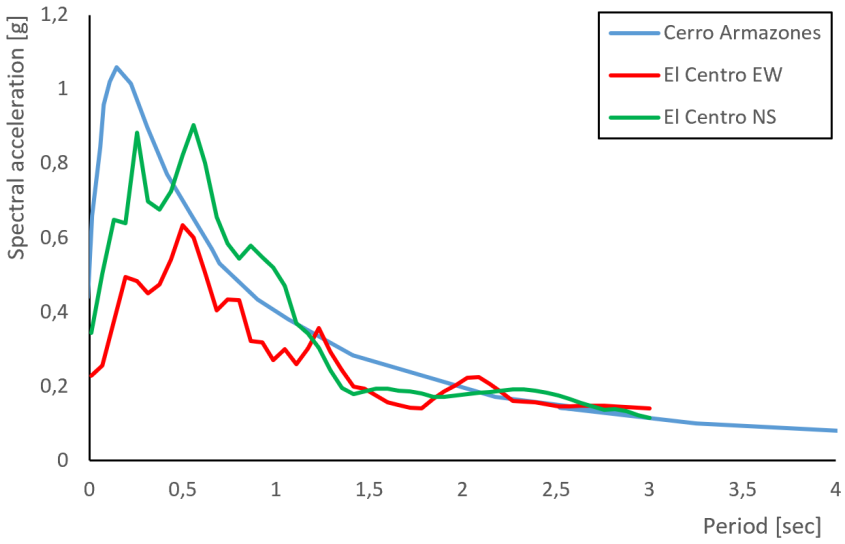

Figure 6.2: Superimposition of horizontal pseudoacceleration elastic response spectra.

The ground motion accelerograms in the three directions of El Centro earthquake are reported enterely in Figure 6.3 and detailed from 0 to 30 *sec* in Figure 6.4.

To show how the dynamic analysis data are defined, the implementation of El Centro excitation is reported in the following.

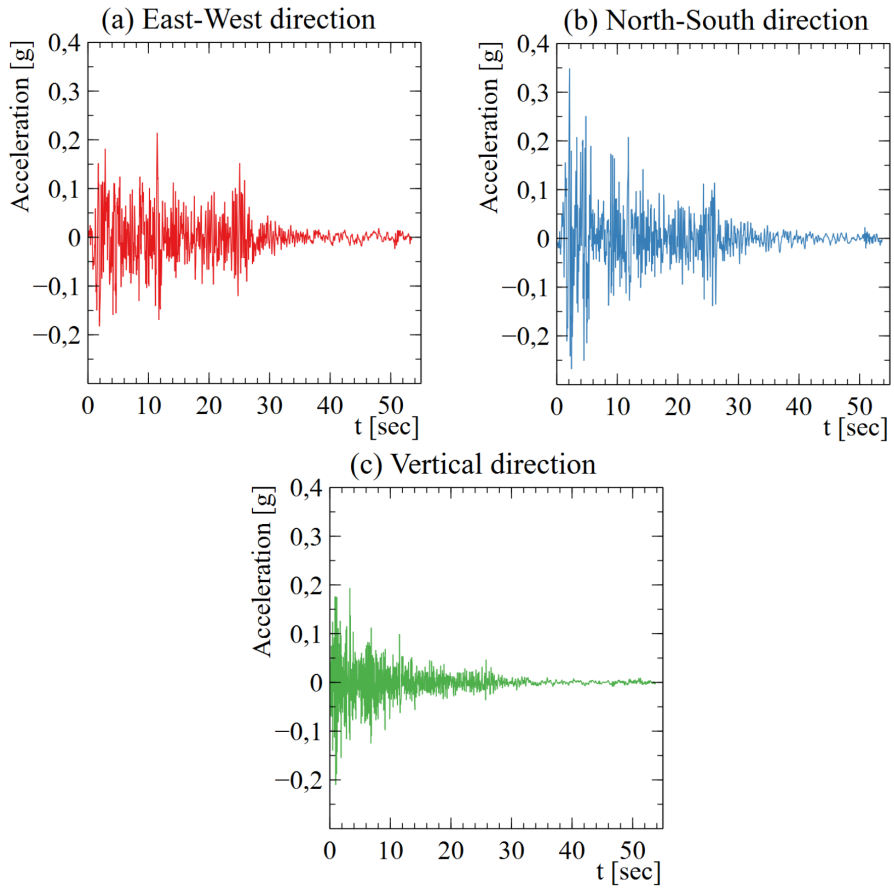

Figure 6.3: El Centro accelerograms in the three directions.

```
#Set constant gravity loads and reset time in the domain
loadConst -time 0.0
#Assign mass to node 2
mass 2 $M $M $M 0 0 0
#Define the time interval
set dt 0.02
#Define the time series path
timeSeries Path 1 -dt $dt -filePath elcentroNS.txt
-factor $g;
timeSeries Path 2 -dt $dt -filePath elcentroUP.txt
-factor $g;
timeSeries Path 3 -dt $dt -filePath elcentroEW.txt
-factor $g;
```

```
#Create load patterns for dynamic analysis
pattern UniformExcitation 2 1 -accel 1
pattern UniformExcitation 3 2 -accel 2
pattern UniformExcitation 4 3 -accel 3
```

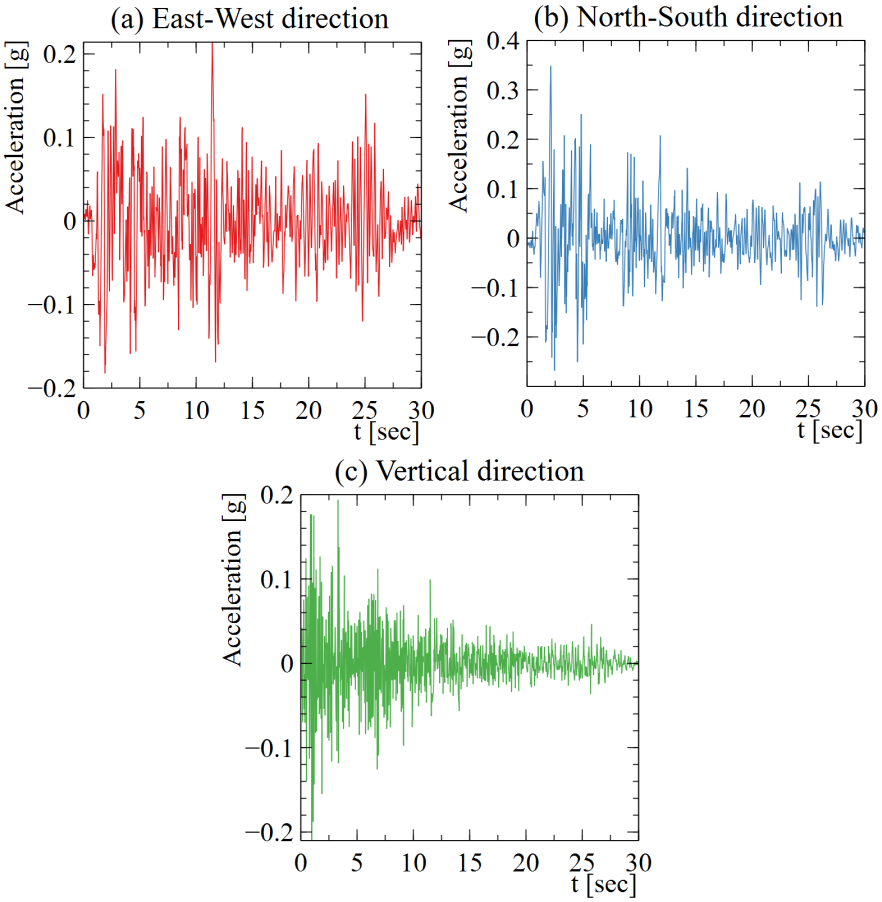

Figure 6.4: El Centro accelerograms detailed from 0 to 30 sec in the three directions.

The last passage for modelling the dynamic analyses on the designed bearing requires the definition of the recorder outputs. Through the `recorder` command, it is possible to ask OpenSees to monitor and print some quantities of the analysis at each analysis step. The procedure is implemented as follows:

```
#Create recorder to monitor outputs
recorder Node -file ELTNode2.out -time -node 2
-dof 1 2 3 4 5 6 disp;
```

```
recorder Element -file ELTForce.out -time
-ele 1 basicForce;
recorder Element -file ELTDisplacement.out -time
-ele 1 basicDisplacement;
recorder Element -file ELTParam.out -time
-ele 1 Parameters.
```

Therefore, the results are provided by OpenSees as text files. Then, the output values are put in graphs to be discussed.
Once the model of a single bearing subjected to gravity and dynamic loads is completed, several analyses can be performed to understand the variation in the bearing response with the inclusion of the behaviour aspects treated in Chapter 3.

6.2 Analyses and Results of the Single Bearing

The model of the single elastomeric bearing, which design is reported in Section 5.4, has been implemented as described above in Section 6.1 and then analyzed varying the four input tags that include the variation of significant properties of the device, as defined in Section 3.4.3. In particular:

- `$tag1` is set to 1 to include the cavitation and post-cavitation behaviour in tension;
- `$tag2` is set to 1 to include the variation in the buckling load capacity due to lateral displacement, according to Equation (2.14) and Equation (3.8);
- `$tag3` is set to 1 to include the variation in horizontal shear stiffness with axial load, according to Equation (3.9);
- `$tag4` is set to 1 to include the variation in vertical stiffness with lateral displacement, according to Equation (3.1).

The behaviour in tension of the elastomeric bearing is not of interest for the E-ELT case because of the huge gravitational loads due to self-weight of the main structure, that remove the possibility to have tension in the isolation devices. Therefore, `$tag1` is always set to zero during the analyses.
The other tags are changed to analyze the variation in the bearing response and the influence of each aforementioned aspect of the mechanical behaviour.

In the following, the performed analyses are described and the corresponding results are discussed. The two orthogonal horizontal directions are referred hereinafter as:

- *East-West direction*, the horizontal direction in which the East-West component of the El Centro earthquake acts;
- *North-South direction*, the horizontal direction in which the North-South component of the El Centro earthquake acts.

6.2.1 Analysis with no Variation

The first analysis on the model is performed without considering any aspects of the ones discussed in Chapter 3. Hence, the critical buckling load capacity is assumed to be constant and computed through Equation (2.14). Analogously, the horizontal stiffness is fixed as $K_H = K_{H0} = GA/T_r$ whereas the vertical stiffness is fixed as $K_v = K_{v0} = E_c A/T_r$. The input tags are set as reported in Table 6.2.

Table 6.2: Input tags for the analysis with no variation.

Input	Value
`$tag1`	0
`$tag2`	0
`$tag3`	0
`$tag4`	0

The analysis is performed and the results are shown in terms of force-displacement curve in each direction.

Figure 6.5 and Figure 6.6 evidence that the bearing behaviour in horizontal directions follows the bi-linear idealized behaviour, shown in Figure 6.1. Nevertheless the curves are smoother and less regular than the idealized one, it is possible to clearly recognize the same shape of the hysteresis cycles. Moreover, it is worth nothing that the resulting cycles are not perfectly symmetric as the idealized cycle is. The maximum displacement of the cycle for the East-West direction, along which the excitation has lower values of acceleration than the values of acceleration in North-South direction, reaches 0.15 m to which corresponds the maximum force of 200 kN. Referring to

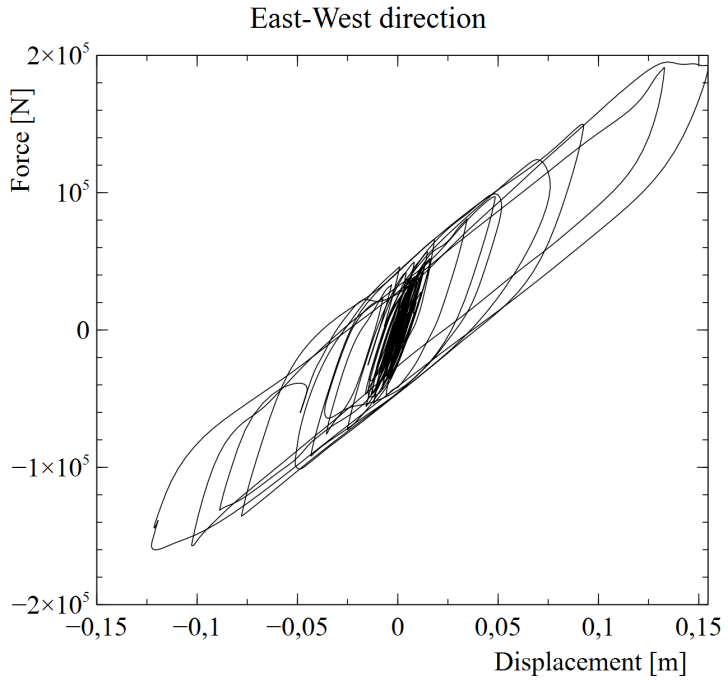

Figure 6.5: Force-displacement curve in East-West direction for no variation.

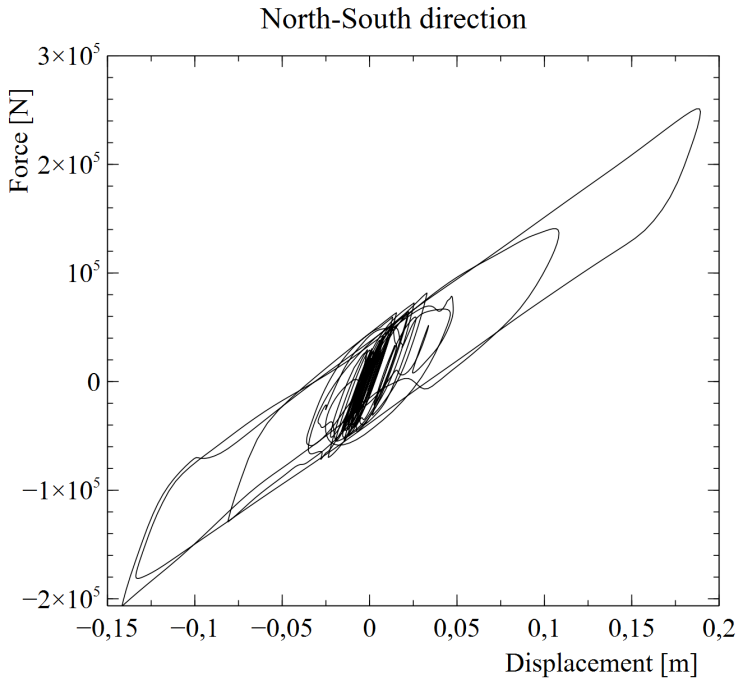

Figure 6.6: Force-displacement curve in North-South direction for no variation.

the North-South direction, the maximum displacement is 0.185 m at the maximum force of 250 kN.

The force-displacement curve in vertical direction is illustrated in Figure 6.7. As expected, the behaviour is perfectly elastic, with an inclination equal to K_{v0}. The values in the graph are all negative due to the presence of the gravity loads that are compression loads, so negative forces, and cause a shortening of the bearing under self-weight, so negative displacements.

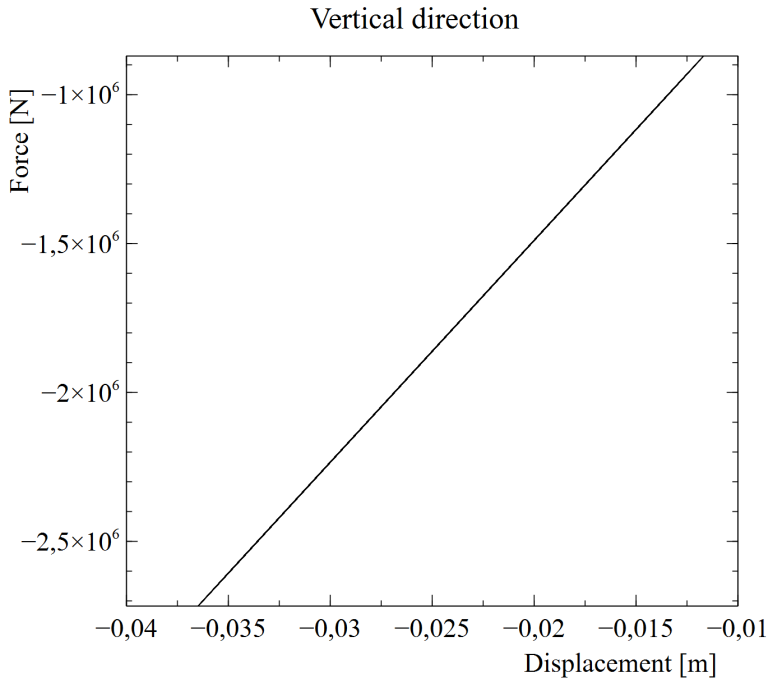

Figure 6.7: Force-displacement curve in vertical direction for no variation.

6.2.2 Analysis with Variation in Vertical Stiffness

The second analysis on the model is performed considering the variation in vertical stiffness, which is computed at each analysis step through Equation (3.1) and depends on the lateral displacement. The critical buckling load capacity is assumed to be constant and computed through Equation (2.14). The horizontal stiffness is fixed as $K_H = K_{H0} = GA/T_r$. The input tags are set as reported in Table 6.3.

Table 6.3: Input tags for the analysis with variation of K_v.

Input	Value
`$tag1`	0
`$tag2`	0
`$tag3`	0
`$tag4`	1

The force-displacement curve in vertical direction is illustrated in Figure 6.8.

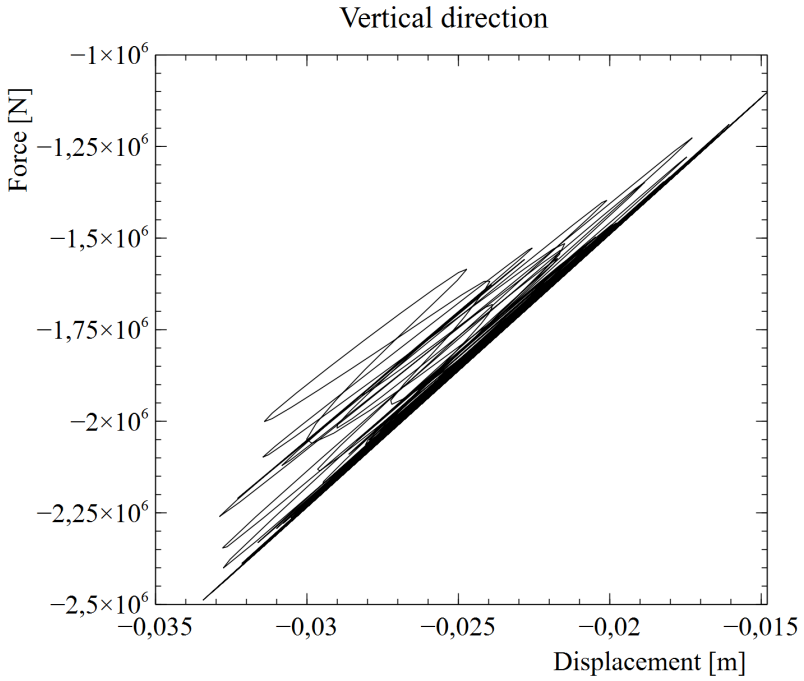

Figure 6.8: Force-displacement curve in vertical direction for variation in K_v.

In this case, the value of the vertical stiffness varies at each analysis step as a function of the lateral displacement. In particular, as the lateral displacement increases, the vertical stiffness reduces, so the inclination of the curve decreases too. Nevertheless the response is changing at each cycle, the curve consists of a series of straight, or almost straight, lines so the behaviour remains in the elastic range. Moreover, for increasing number of cycles, the behaviour tends to stabilize with an inclination similar to the

one in Figure 6.7, which has a range of displacements and a range of forces slightly wider than this.

As expected, nothing changes in the force-displacement curves for East-West and North-South directions that are not influenced by the variation in vertical stiffness, so the graphs of the two curves are not repeated here.

6.2.3 Analysis with Variation in Horizontal Stiffness

The third analysis on the model is performed considering the variation in horizontal stiffness for both horizontal directions. Each stiffness is computed at each analysis step through Equation (3.9) and depends on the axial load. Also in this analysis, the critical buckling load capacity is assumed to be constant and computed through Equation (2.14) whereas the vertical stiffness returns to be fixed as $K_v = K_{v0} = E_c A/T_r$. The input tags are set as reported in Table 6.4.

Table 6.4: Input tags for the analysis with variation of K_H.

Input	Value
`$tag1`	0
`$tag2`	0
`$tag3`	1
`$tag4`	0

Figure 6.9 and Figure 6.10 show that, including the variation in horizontal stiffness, the bearing response becomes sensitively more irregular. The decrease in the horizontal stiffnesses implies higher values of the maximum lateral displacement, in particular for the East-West direction that now reaches $0,18\ m$ while the maximum displacement in the North-South direction becomes equal to $0.19\ m$.

Thus, the direction with lower seismic excitation results more influenced by the horizontal stiffness reduction than the North-South direction. Nevertheless the axial load is the same for both horizontal directions, the seismic excitation is different so also the two graphs are different, according to the outcomes of the analysis with no considered variation, discussed in Section 6.2.1. However, the shape of the idealized cycle remains detectable also in these hysteresis cycles.

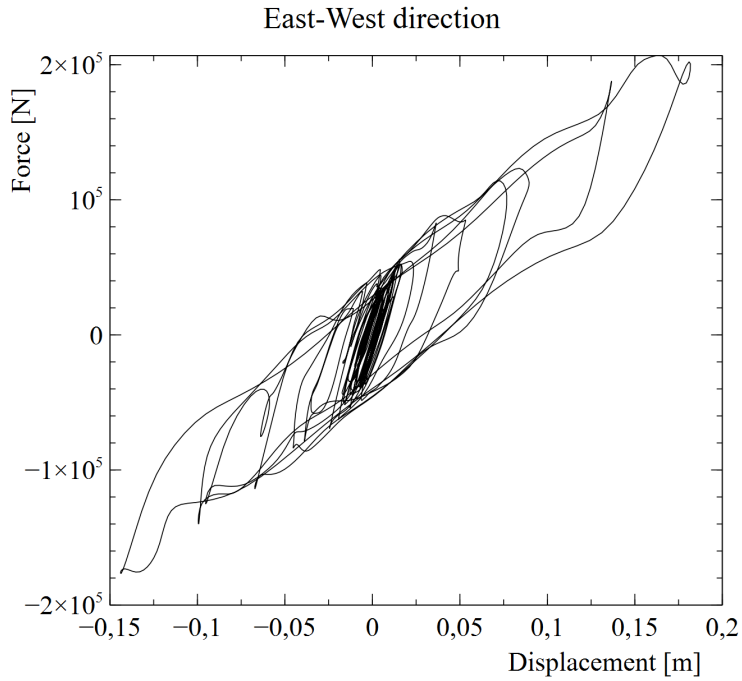

Figure 6.9: Force-displacement curve in East-West direction for variation in K_H.

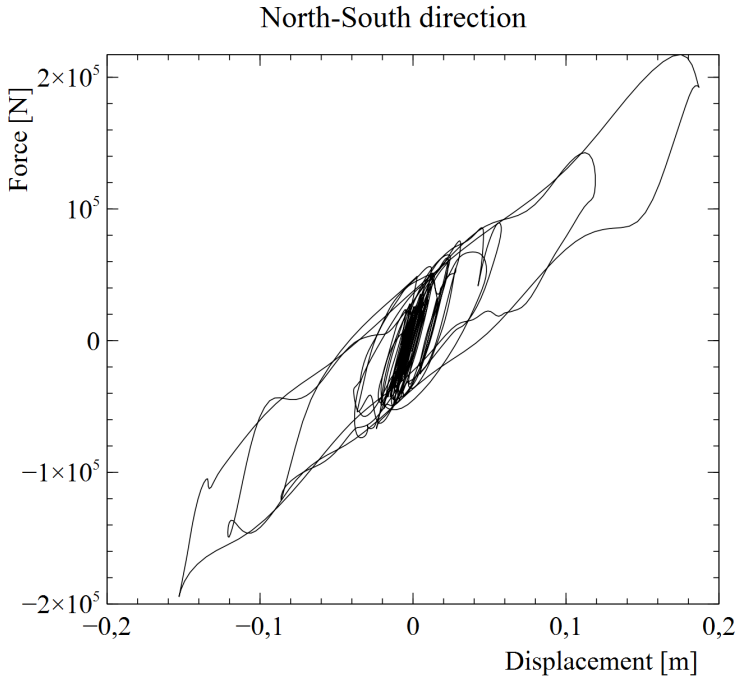

Figure 6.10: Force-displacement curve in North-South direction for variation in K_H.

As expected, the force-displacement curve in vertical direction is not influenced by the variation in horizontal stiffnesses, so the graph turns out to be equal to Figure 6.7 and the behaviour in vertical direction returns perfectly elastic.

6.2.4 Analysis with Variation in Critical Buckling Load and Horizontal Stiffness

The fourth analysis on the model is performed considering, in addition to the variation in horizontal stiffness for both horizontal directions as the previous analysis, also the variation in the critical buckling load capacity. As before, each horizontal stiffness is computed at each analysis step through Equation (3.9) but now it depends also on the critical buckling load, that is computed at each analysis step as a function of the lateral displacement, according to Equation (3.8), as discussed in Section 3.1. For what concerns the vertical stiffness, it is maintained fixed as $K_v = K_{v0} = E_c A/T_r$. The input tags are set as reported in Table 6.5.

Table 6.5: Input tags for the analysis with variation of P_{cr} and K_h.

Input	Value
`$tag1`	0
`$tag2`	1
`$tag3`	1
`$tag4`	0

In particular, the increase of maximum lateral displacement implies a decrease of the overlap area A_r, computed as Equation (3.6), so of the ratio A_r/A. As a direct consequence, the critical buckling load capacity P_{cr} decreases, which in turn cause a decreasing in the horizontal stiffness too.
The two hysteresis cycles, illustrated in Figure 6.11 and Figure 6.14, become very similar and, in correspondence with the maximum displacement of 0.195 m at around 200 kN as maximum force, the elastomeric bearing shows a sort of softening branch that makes the response difficult to be understood and expected. However, the values of the maximum force and maximum displacement have not undergone substantial changing.

As expected, also in this case the force-displacement curve in vertical direction is not influenced by the additional variation in critical buckling load

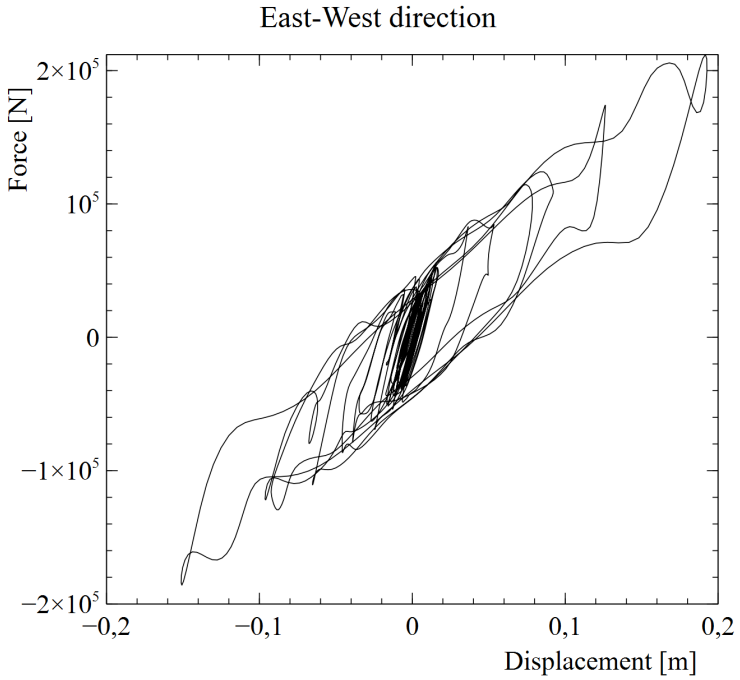

Figure 6.11: Force-displacement curve in East-West direction for variation in P_{cr} and K_H.

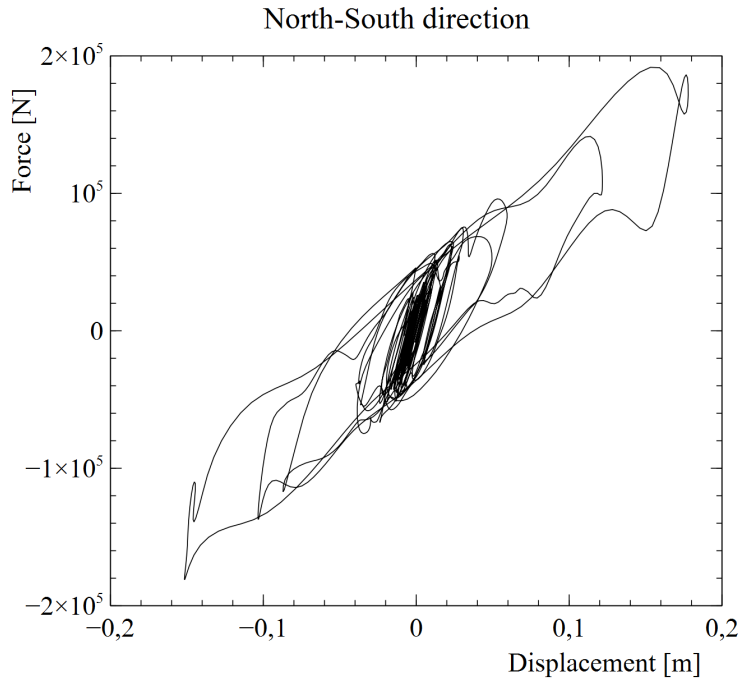

Figure 6.12: Force-displacement curve in North-South direction for variation in P_{cr} and K_H.

capacity because the value of K_v undergoes no variation, so the graph remains coincident to Figure 6.7 and the behaviour in vertical direction is still perfectly elastic.

6.2.5 Analysis with Variation in Critical Buckling Load, Horizontal and Vertical Stiffnesses

The last analysis on the model is performed considering all the behaviour aspects discussed in Chapter 3, simultaneously. In addition to the analysis reported in Section 6.2.4, the vertical stiffness is assumed to be computed at each analysis step through Equation (3.1), as considered in the analysis reported in Section 6.2.2. This case allows to analyze the bearing response that is expected to be the most adherent to the actual bearing response. Moreover, it allows to analyze the effect of the simultaneous variation in vertical and horizontal stiffnesses and how they influence each other. The input tags are set as reported in Table 6.6.

Table 6.6: Input tags for the analysis with variation of P_{cr}, K_H and K_v.

Input	Value
`$tag1`	1
`$tag2`	1
`$tag3`	1
`$tag4`	1

Figure 6.13 and Figure 6.14 represent the force-displacement curves in the two orthogonal horizontal directions when the influence of the vertical stiffness variation on the horizontal response of the bearing is considered.

The hysteresis cycles turn out to be in the middle between the outcomes of the analysis reported in Figure 6.9 and Figure 6.10 and the irregular results obtained through the analysis discussed previously (Figure 6.11 and Figure 6.12). In fact, the variation in vertical stiffness leads to a sort of regularization of the bearing response in horizontal directions, providing curves more similar to the first analysis results (Figure 6.5 and Figure 6.6) but characterized by values of the maximum displacement that are closer to the design horizontal displacement d_{bd}, suggesting that this is the case closest to the actual response of this device.

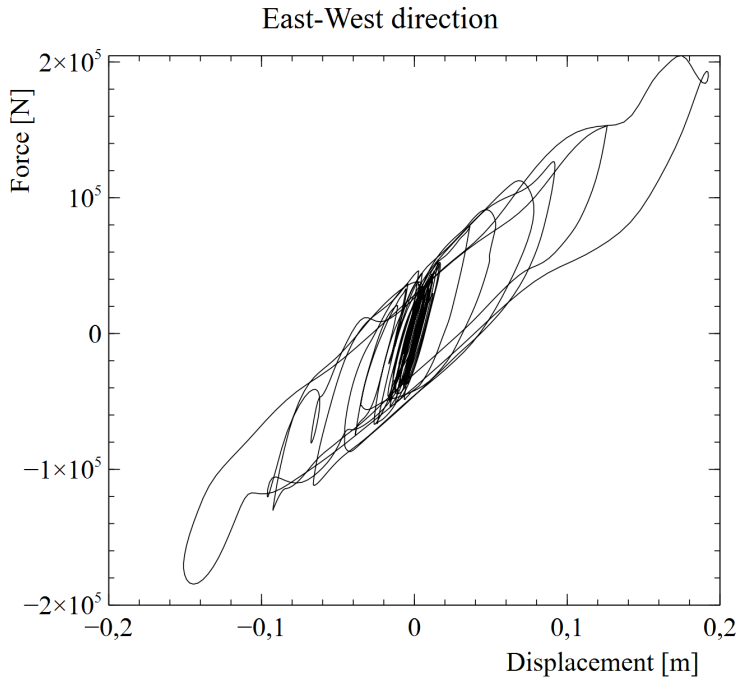

Figure 6.13: Force-displacement curve in East-West direction for variation in P_{cr}, K_H and K_v.

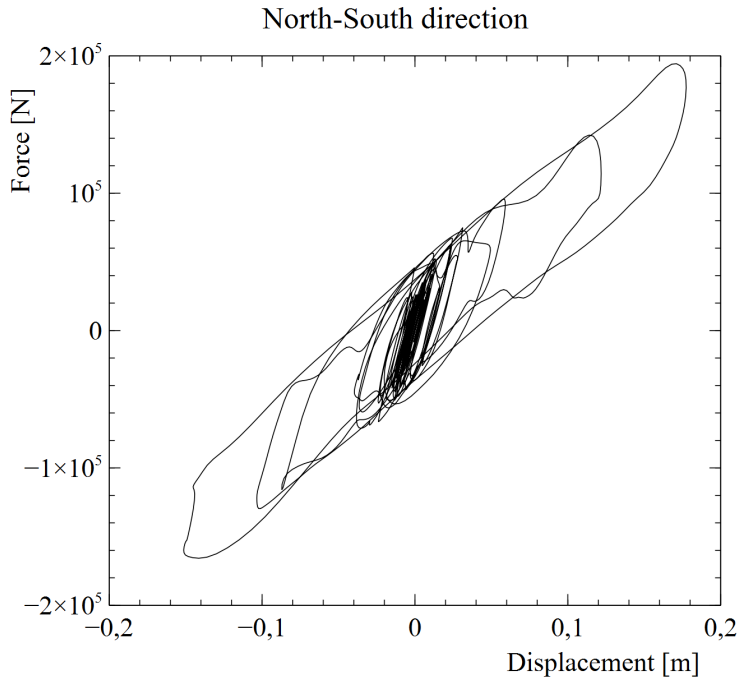

Figure 6.14: Force-displacement curve in North-South direction for variation in P_{cr}, K_H and K_v.

The bearing response in vertical direction results analogous to the analysis reported in Section 6.2.2, as shown in Figure 6.15. The increase in the maximum lateral displacement implies that lower values of the vertical stiffness are reached, so straight, or almost straight, lines more distant to the K_{v0} inclination are present. However, the graph shows that the bearing response in vertical direction is developed in the elastic, or almost elastic, range so it can be approximated as perfectly elastic.

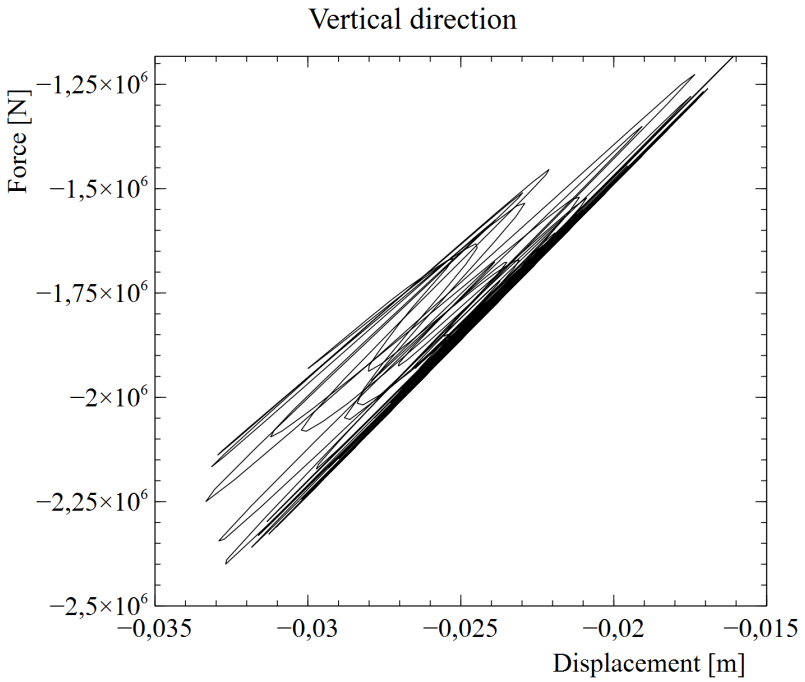

Figure 6.15: Force-displacement curve in vertical direction for variation in P_{cr}, K_H and K_v.

Finally, it is possible to conclude that all results reported in Section 6.2 evidence the complexity of elastomeric bearings response and the difficulty to predict the actual behaviour of these devices through a simplified model. However, the analyses on the model of a single bearing subjected to the static and dynamic loads of the E-ELT main structure demonstrate that the bearing response in horizontal directions fits with the bi-linear curve of the idealized hysteresis cycle while the bearing response in vertical direction can be modelled as elastic.

6.3 Problems in Modelling the Whole Structure

The work proceeds with the modelling of the whole structure. The designed isolation system is composed by 120 elastomeric bearing having the same material and geometrical properties as the model previously described. The devices are distributed along the two annular rings: 70 elastomeric bearings along the external ring and 50 elastomeric bearings along the internal ring. The isolators are located uniformly, i.e. at a constant distance one from each other. The telescope pier is assumed to behave rigidly so it is modelled through `rigidLink` elements of type `beam` between the centre of gravity of the telescope pier and the top node of each isolator. An additional `rigidLink` element is required between the centre of gravity of the telescope pier and its extrados to account for the upper half of the rigid body. The main structure is modelled as an `elasticBeamColumn` element having properties as described in detail in Chapter 5. The `ElastomericX` and `rigidLink` elements are created in the model through two `for` cycles.

Therefore, the first step of the modelling of the whole structure consists in the creation of the nodes for the centre of gravity and the extrados of the telescope pier and for the centre of gravity of the main structure, located at a distance $L = 18.84\ m$ from the extrados of the telescope pier. Then, the `rigiLink` between the centre of gravity and the extrados of the telescope pier and the `elasticBeamColumn` element, that models the E-ELT main structure, are created. Successively, the two `for` cycles are implemented, one for each annular ring. In particular, each `for` cycle contains the creation of the bottom and top nodes of the elastomeric bearing, the assignment of the corresponding constraints of the nodes and the creation of the `ElastomericX` element, that models the isolator, and of the `rigidLink` element between the centre of gravity of the telescope pier and the top joint of the isolator created in the considered step of the cycle. Finally, the gravity loads and the masses are assigned. The self-weight of the telescope pier is applied on the node corresponding to the centre of gravity of the telescope pier whereas the self-weight of the main structure is applied to the node corresponding to the centre of gravity of the main structure. The mass of the telescope pier is assigned to its centre of mass for all the translational and rotational directions whereas the mass of the main structure is assigned only for the translational directions, according to the results of the modal analysis on the main structure discussed in Chapter 5.

To be consistent with the Two-spring model discussed in Section 2.5, the three rotational degrees of freedom at the top node of each isolator must be

fixed. This condition implies a strong limit in the modelling of the whole structure. In fact, a `rigidLink` element can not be created between nodes that have fixed dofs. If this last rule is not fulfilled, OpenSees finds a compatibility error and directly eliminates the element. To solve this problem, two different paths have been followed: remove the constraint at the top joint of each isolator or assign the mass of the telescope pier only in the translational directions. Nevertheless, both solutions reveal to be ineffective. The former leads to the impossibility in analyzing the model of the whole structure due to the high sensitivity of the `ElastomericX` element, i.e. of the bearing model, to rotational deformations that implies too large displacements of the structure without any physical sense. The latter leads to the impossibility in analyzing the model of the whole structure due to the fact that the removal of the inertial mass in the rotational directions implies that the rocking effects are neglected in a structure for which they assume a relevant role that can not be disregarded.

An alternative to avoid the limit of the `rigidLink` element is substituting it with an `EqualDOF` command, that consists in a multi-point constraint between nodes. Notwithstanding, through the imposition of same deformations for different nodes, problems occur in the numeration of the degrees of freedom of the whole structure that leads to significant mistakes in the construction of the global stiffness matrix.

Another tentative to overcome the difficulties in modelling the whole structure is represented by the use of a `TwoNodeLink` element having reasonable high values of stiffness but also in this case OpenSees finds compatibility errors that cause a lack of convergence of the analysis, leading to an infinite loop situation.

Therefore, problems related to the enslavement of some specific nodes to other are not solved and the analysis can not be performed. To investigate the whole structure response, it has been decided to switch to SAP2000 and to model the whole isolated structure through the element provided by one of the most widespread software for structural and earthquake engineering. In fact, it has been proved that the bearing response can be reproduced through a `Plastic (Wen) Link` element on SAP2000 in a manner sufficiently adherent to the actual behaviour, analyzed in the previous section through the OpenSees model of the single elastomeric bearing. In particular, the hysteresis cycles obtained from SAP2000 analysis, described in the following chapter, substantially coincides with the hysteresis cycles obtained from OpenSees analysis of the `ElastomericX` element, neglecting the coupling between the horizontal and vertical response. However, the OpenSees

analysis demonstrate that the coupling between horizontal and vertical directions causes a maximum horizontal displacement that is slightly higher than the one obtained without considering the aforementioned coupling but it is still lower than the maximum displacement defined by EN15129, so it has been checked that the designed 3D elastomeric bearing fulfills all the code requirements and sustains the loads applied on the considered structure.

Chapter 7

Analyses on SAP2000 of the Case Study

Once the single elastomeric bearing designed to isolate in horizontal and vertical directions the main structure of the E-ELT has been modelled and analyzed on OpenSees, the analysis is performed on SAP2000 to construct the model of the whole structure. Thus, this chapter aims to verify the beneficial effects of the designed three-dimensional isolation system on the main structure response when it is subjected to strong ground motions. Due to the widespread use of SAP2000 as structural and earthquake engineering software, its framework and operational principles descriptions are not reported here. This chapter is split in two parts: formerly the model of the whole structure is developed, as described in Section 7.1, and then analyzed, discussing the outcomes in Section 7.2.

7.1 Model of the Whole Structure

The model of the designed single bearing is created on SAP2000 as a `Link` element between two nodes located in the same point of the horizontal plane but at a vertical distance equal to the height of the bearing. SAP2000 provides a `Plastic Link` based on the hysteretic behaviour proposed by Wen. The Bouc-Wen formulation has been already discussed in Section 3.4.3 due to the fact that also the element developed by Kumar [2016] is based on it to model the mechanical behaviour in horizontal directions.

A `Link` element on SAP2000 is assumed to be composed of six separate springs, one for each deformational degrees of freedom, that connect `Joint i` to `Joint j`. Figure 7.1 illustrates the springs for three of the deformations:

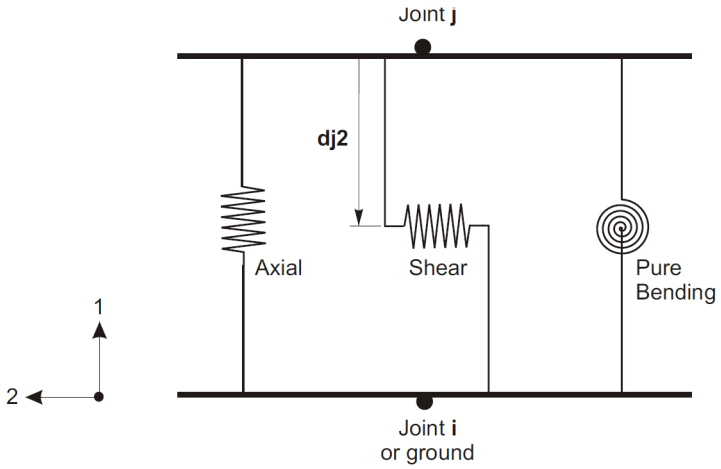

Figure 7.1: Three of the six independent springs of a Link element on SAP2000 (adapted from CSI [2016]).

axial, shear in the 1-2 plane, and pure-bending in the 1-2 plane. The other not-shown springs are for torsion, shear in the 1-3 plane, and pure-bending in the 1-3 plane.
The element has its own local coordinate system, with axes denoted as 1, 2 and 3, used to define force-deformation properties and output, as shown in Figure 7.2. The first is the longitudinal axis, directed along the length of the element and corresponding to extensional deformation. The other two axes, corresponding to shear deformations, lie in the plane perpendicular to the element and have a default orientation. However, SAP2000 allows to redefine a specified orientation of the local axes different from the default one.
The behaviour of a `Link` element is defined through a set of structural properties. The `Link Properties` contain linear properties, used by the element for linear analyses, and non linear properties, used for non linear analyses and for linear analyses that continue from non linear analyses [CSI, 2016].

In particular, `Plastic Link` has been selected to model the bearing behaviour. All internal deformations are independent and represented by springs that can be linear or non linear. If the spring is linear, the effective stiffness and the effective damping must be specified and they will be used for all types of analysis. These two quantities must be specified also if the spring is non linear. Thus, six uncoupled linear effective-stiffness coefficient k are required, which represent the total elastic stiffness for each dof, and six uncoupled linear effective-damping coefficients ce are required, which

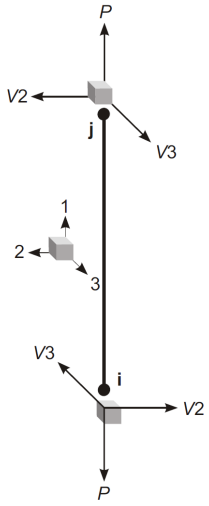

Figure 7.2: Local axes and internal forces at end joints of a `Link` *element (adapted from CSI [2016]).*

represent the total viscous damping for each dof that is used for response-spectrum analyses, for linear and periodic time-history analyses.
If the spring is non linear, in addition to the linear properties, non linear properties are required. In particular, for each deformational degree of freedom, independent uniaxial plasticity properties are defined to characterize the hysteresis cycle illustrated in Figure 7.3, that is analogous to the idealized cycle considered in the previous chapter and shown in Figure 6.1.

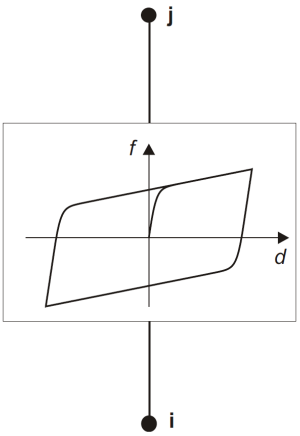

Figure 7.3: Hysteresis cycle for Wen uniaxial plasticity property (adapted from CSI [2016]).

The non linear properties that must be provided are listed in the following, making reference to Figure 7.4:

- *Stiffness,* **k**. The inclination of the elastic branch;
- *Yield strength,* **yield**. The value of the force that individuates the transition from elastic to plastic behaviour;
- *Post yield stiffness ratio,* **ratio**. The value of the ratio between the inclination of the elastic branch and the inclination of the plastic branch;
- *Yielding exponent,* **exp**. Parameter used to define the smoothness of the transition from elastic to plastic behaviour (default=2).

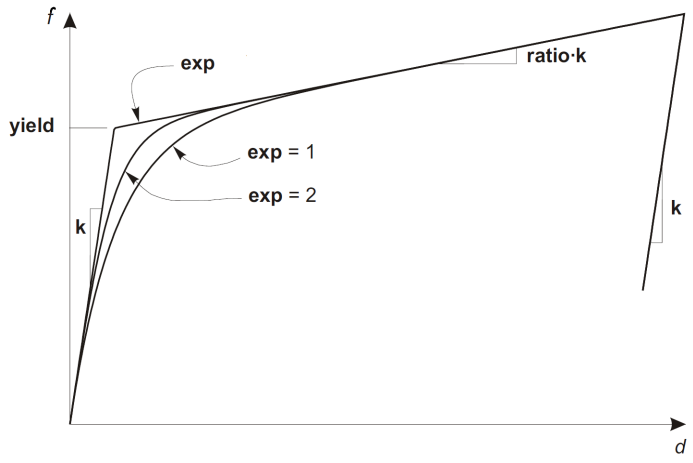

Figure 7.4: Parameters required for the definition of non linear properties (adapted from CSI [2016]).

Therefore, the designed bearing is modelled as a `Plastic (Wen) Link` having linear springs for torsion, rotations and axial deformations whereas shear deformations are characterized by non linear springs. The linearity of the torsional and rotational deformations is set according to the considerations reported in Section 3.3. The axial deformation is assumed to be linear according to the results of the analyses on the OpenSees model, reported in Section 6.2. The non linear properties of the shear deformations dofs are defined on the base of the hysteresis cycles obtained in Section 6.2. The bearing element is created through the procedure:

`Define > Section Properties > Link/Support Properties > Add New Property > Link/Support Type: Plastic (Wen)`

Then, the `Link/Support Property Data` window allows to select the degrees of freedom to be activated. Once a dof is activated, it could be fixed or not and non linear or not. Attention must be paid to fixed dof. In fact, `Link` elements with fixed dofs should not be connected to other fixed `Link` elements or connected to constrained joints. In this case, all the translational dofs are activated while the properties of the rotational and torsional ones are not specified because they are considered to not affect the response of the structure. Due to the choice of defining rigid link using `Link` element, as specified below, the rotational and torsional dofs can not be fixed to avoid mistakes during the analyses. The linear properties in the axial direction are defined according to Section 5.4 (in particular Equation (5.23)) and the OpenSees model described in Section 6.1, whereas the effective damping coefficient is computed such that the effective damping of the whole structure in vertical direction results equal to 8%, a little less than the effective damping in horizontal directions. Analogously, also the properties in the directions corresponding to shear deformations follow the results reported in previous chapters. The properties definition is shown in Figure 7.5. The `Shear Deformation Location` provides the distance between the upper joint of the `Link` element and the shear centre, where the shear deformations are assumed to be concentrated, analogously to the `$sDratio` input required on OpenSees for the definition of the `ElastomericX` element; this distance corresponds to the length **dj2** in Figure 7.1.

Once the two-joint link is created, all the degrees of freedom of the bottom joint are fixed whereas the rotational and torsional dofs of the top joint are fixed to be consistent with the Two-spring model discussed in Section 2.5. The static and dynamic loads are defined according both to the design procedure reported in Section 5.4 and to the OpenSees model described in Section 6.1. The El Centro seismic excitation is defined as a non linear time history `Load Case` solved by direct integration.

Thanks to the SAP2000 graphic interface feature, the model described above is illustrated in Figure 7.6. The global axes are shown in black at the bottom joint whereas the coloured axes correspond to the local axes. The red axis, green axis and cyan axis represent the local 1, 2 and 3 axes, respectively. It is worth noting that, as specified above, the first local axis is in the extensional direction and corresponds to the global Z-axis while the local axes of the top joint coincide with the global axes.

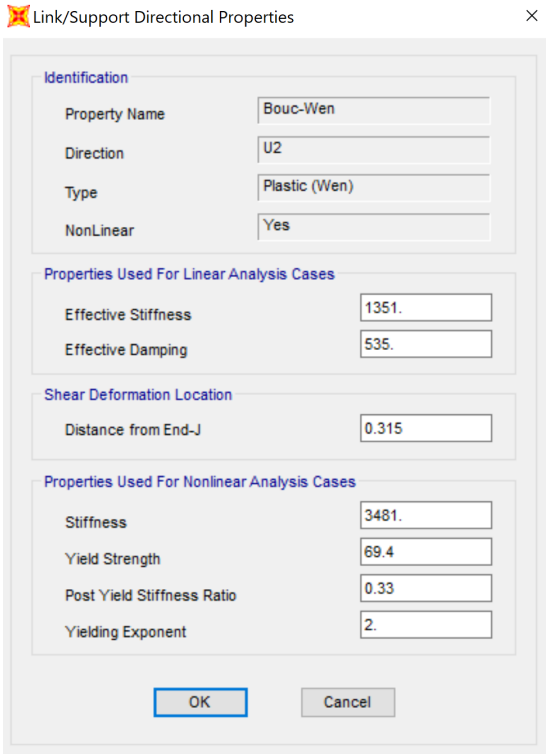

Figure 7.5: Definition of properties in shear deformation directions.

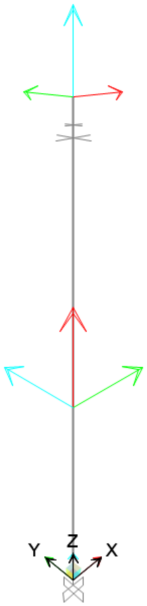

Figure 7.6: Model of a single bearing on SAP2000.

Once the model of a single bearing is assessed, the work proceeds to model the whole structure. The design base isolation system is composed by 120 isolators having the same geometrical and material properties of the model of a single isolator described above. The devices are put at the interface between the dome foundation and the telescope pier and distributed along the two annular rings of diameters 51.5 m and 34 m, as described in detail in Chapter 5. In particular, 70 elastomeric bearings are uniformly distributed under the external ring, i.e. located every $\Delta\theta_{ext} = 2\pi/70 = 0.09\ rad$, while the remaining 50 bearings are uniformly distributed under the internal ring, i.e. located every $\Delta\theta_{int} = 2\pi/50 = 0.125\ rad$. Therefore, two `Grid Systems`, one containing the coordinates of the bearing positions along the external ring and the other containing the coordinates of the bearing positions along the internal ring, are created on SAP2000 and 120 `Plastic (Wen) Link` elements are drawn in the corresponding location, having the same properties defined above. The top view of the created two-joint link elements is reported in Figure 7.7.

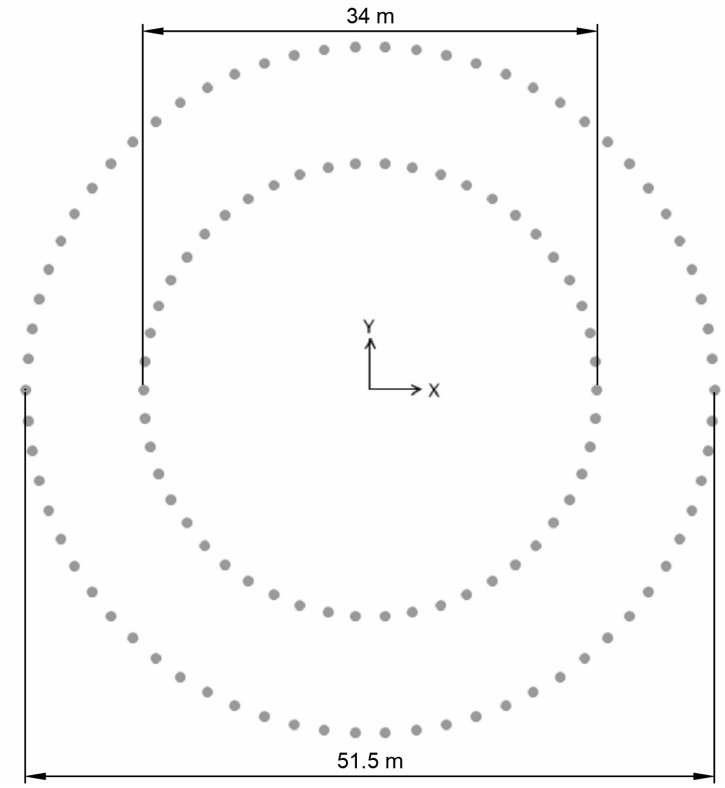

Figure 7.7: View in the X-Y plane of the isolation devices modelled on SAP2000.

The telescope pier has been assumed to be rigid so, instead of modelling a detailed and complex concrete annular system, it is possible to model it by means of simple rigid links. In particular, the mass of the telescope pier is concentrated in the common centre of the two annular rings and at half of their height. The mass must be linked to each isolator at the base of the telescope pier. Moreover, a vertical rigid link between the mass and the top extrados of the telescope pier allows to account for the upper half of the rigid body. The rigid link is created as a `Linear Link` element characterized by uncoupled stiffness in each direction equal to a reasonably large value, of the order of 10^{11}. Also in this case, the degrees of freedom are not fixed because a link with fixed dofs should not be directly connected to other objects with fixed dofs so, to avoid mistakes during the analysis, the value of the stiffness has been selected sufficiently high to model the `Linear Link` element as a rigid link.

For what concerns the model of the main structure, reference is made to the scheme described in Section 5.2. Thus, a `General Section` is created having length equal to $L = 18.84\ m$ and the properties listed in Equation (5.1) are assigned. The mass of the main structure is concentrated at the top joint of the beam and assigned in the translational directions. To obtain reasonable results from dynamic analysis, a nominal value of damping is assigned to the elastic beam. Thus, a `Linear Link` is created between the extrados of the telescope pier and the mass of the main structure, i.e. coincident with the elastic beam, having damping coefficients such that the three modes of vibration of the elastic beam, along the two orthogonal horizontal directions and the vertical direction, turn out to be damped of the 1% to avoid infinite oscillation. The damping coefficient is computed as $ce_i = 2\xi m_{ms}\omega_i = 2\xi m_{ms} 2\pi f_i$, where $m_{ms} = 3400\ ton$ is the total mass of the main structure (as reported in Table 5.2), $\xi = 0.01$ is the nominal effective damping and f_i is the frequency in direction i, as reported in Table 5.1.

It is worth noting that the X direction on SAP2000 corresponds to the horizontal direction previously referred as *East-West direction*, the Y direction on SAP2000 corresponds to the horizontal direction previously referred as *North-South direction* and the Z direction on SAP2000 corresponds to the vertical direction.

The model of the whole structure is shown in Figure 7.8 and Figure 7.9.

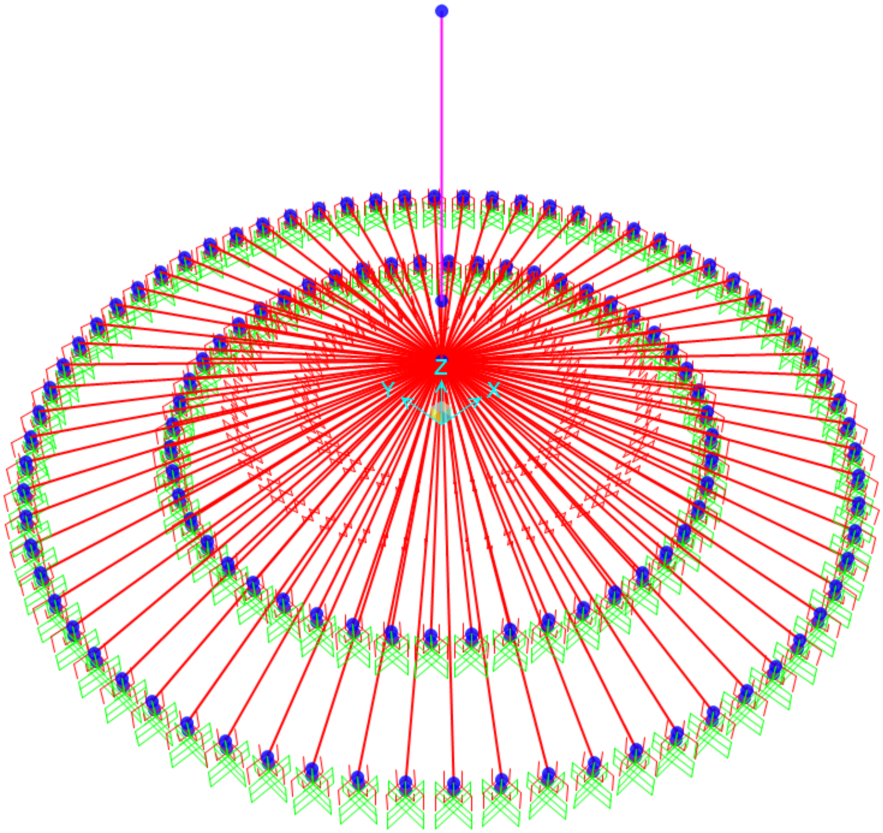

Figure 7.8: 3D view of the model of the structure on SAP2000.

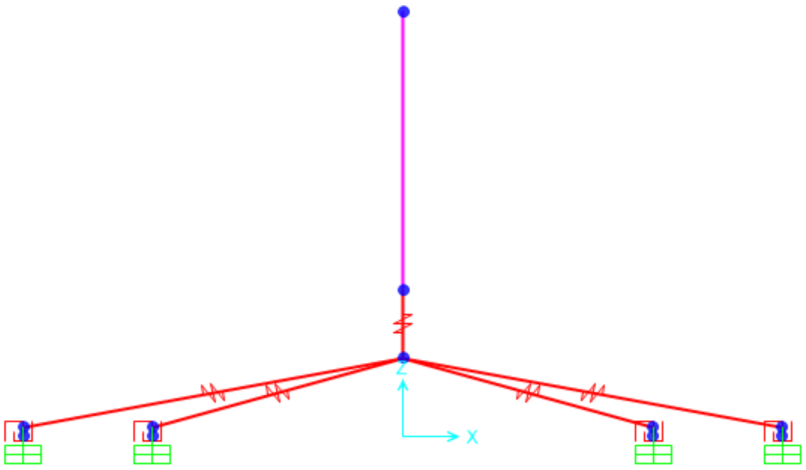

Figure 7.9: View in the X-Z plane of the model of the structure on SAP2000.

7.2 Analyses and Results of the Whole Structure

The model of the isolated main structure and the telescope pier of the E-ELT described above is analyzed on SAP2000 to investigate both the single bearing response and the overall effects of the isolation system on the whole structure response. The former is discussed in Section 7.2.2, whereas the latter is highlighted through the comparison with the model of the corresponding non-isolated structure. This model is obtained from the one described in the previous section by simply adding a joint constraint at the extrados of the telescope pier that fixes all the degrees of freedom. Thus, the elastic beam that models the E-ELT main structure results as a cantilever beam whereas the telescope pier and the isolation system under it results as totally fixed and they remain still.
Section 7.2.1 discusses the results of the modal analysis on both models whereas the results of the dynamic analysis are split in Section 7.2.2, where the single bearing response is reported, and in Section 7.2.3, where the whole structure response is described in term of Fourier spectra.

7.2.1 Results of Modal Analysis

The purpose of a modal analysis is to find the shapes and frequencies at which the structure will amplify the effect of loads. Thus, modal analysis allows to investigate the modes of vibrations of the structure and the corresponding periods.
In Table 7.1 are reported the first three modes of the isolated structure. Intermediate and higher modes involve only part of the structure, i.e. they are local modes of vibration, so they are neglected. The values of the period of the first modes result to be in accordance to the effective period selected during the design procedure, as discussed in Section 5.4. The vertical period turns out to be slightly higher than the design period so vertical isolation works as expected. Conversely, periods in horizontal directions turn out to be slightly lower than the design ones. However, they remains in the long period range, considered between 2 *sec* and 3 *sec*, so also horizontal isolation reaches the required performance.

To make a comparison, modal analysis is performed also on the model of the non-isolated structure. The first modes of vibration of the elastic beam are listed in Table 7.2. These results allow to verify that the elastic beam models the main structure of the E-ELT in a correct manner. In fact, the values of the frequencies are very similar to the eigenfrequencies of the main

Table 7.1: Eigenfrequencies of the isolated structure.

Mode	Direction	Frequency	Period
1	Y	0.43 Hz	2.33 sec
2	X	0.43 Hz	2.33 sec
5	Z	3.15 Hz	0.32 sec

structure reported in Table 5.1. Therefore, the elastic beam satisfies the aim to reproduce the actual behaviour of the main structure.

Table 7.2: Eigenfrequencies of the non-isolated structure.

Mode	Direction	Frequency	Period
1	Y	2.90 Hz	0.34 sec
2	X	3.18 Hz	0.31 sec
3	Z	5.15 Hz	0.19 sec

Comparing the two outcomes, it is worth noting that the introduction of the elastomeric bearings at the base of the telescope pier shifted the effective periods of the structure to the long period range. This beneficial effect is particularly significant in horizontal directions where the periods of the non-isolated structure belong to peak values range of the pseudoacceleration elastic response spectra, shown in Figure 6.2. Conversely, the horizontal periods of the isolated structure correspond to significantly lower values of spectral acceleration, far from the plateau defined by EC8. In vertical direction, the effective period underwent an increase of the 50% of the value of the corresponding non-isolated period.

7.2.2 Single Bearing Results of Dynamic Analysis

The single bearing response is discussed in terms of force-displacement curves, according to the analyses performed on OpenSees and reported in Section 6.2. The graphs, resulting from dynamic analysis of the model of the isolated structure on SAP2000, are shown in Figure 7.11 and Figure 7.10 for the two orthogonal horizontal directions.

The force-displacement curve for the vertical direction is not reported because the behaviour is modelled as linear elastic so the curve results as a line

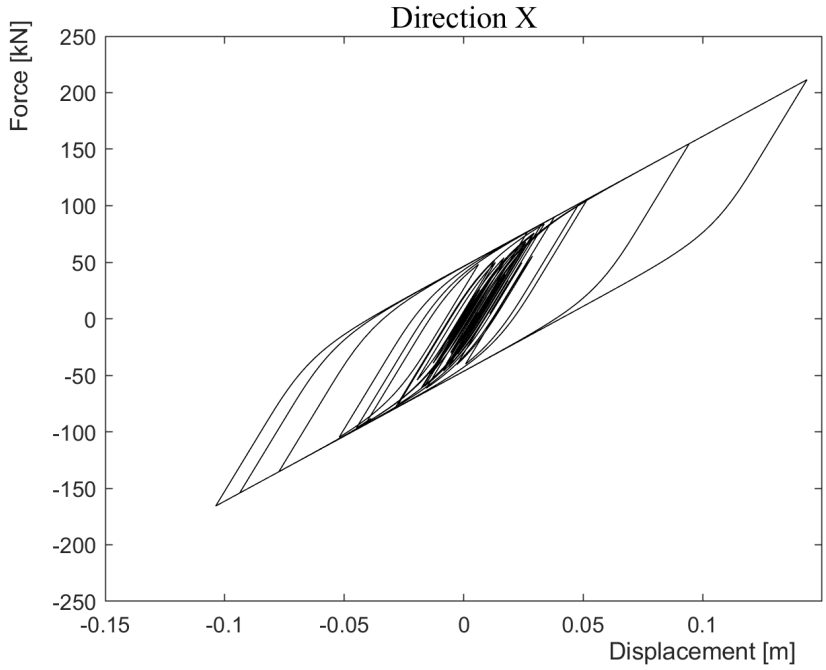

Figure 7.10: Force-displacement curve in East-West direction from SAP2000 analysis.

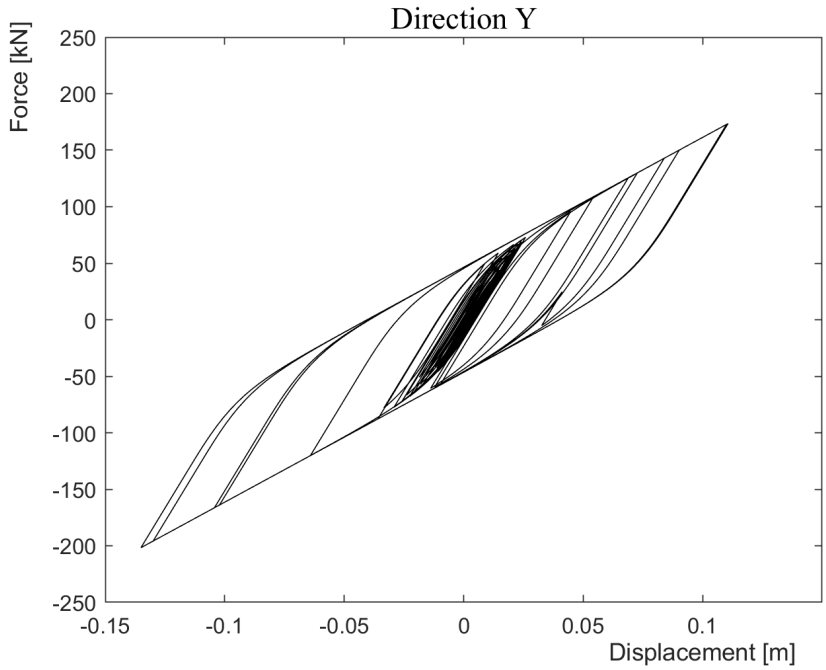

Figure 7.11: Force-displacement curve in North-South direction from SAP2000 analysis.

of inclination equal to the value of the vertical stiffness defined during the modelling procedure, as described in Section 7.1. In particular, the graph turns out to be coincident with the one shown in Figure 6.7. In horizontal directions, the hysteresis cycles respect both the idealized cycle shown in Figure 6.1 and the Wen cycle shown in Figure 7.3. Nevertheless the coupling between horizontal and vertical behaviour is not considered, the force-displacement curves prove to be in accordance with the results of the analyses on OpenSees.
In particular, it is worth noting that the hysteresis cycles in the two horizontal directions resulting from SAP2000 analysis are close to the ones resulting from OpenSees analysis considering the variation in critical buckling load, horizontal and vertical stiffnesses, shown in Figure 6.13 and Figure 6.14, with slightly lower displacements and forces but higher regularity. These results allow to conclude that the model is sufficiently adherent to the actual behaviour of the elastomeric bearing composing the 3D seismic base isolation system.

7.2.3 Whole Structure Results of Dynamic Analysis

The whole structure response is discussed firstly in terms of absolute acceleration time history of the mass of the main structure and then in terms of comparison between the resulting Fourier spectra for the isolated and non-isolated model.
Once the two models have been analyzed on SAP2000, the absolute accelerations of the top joint of the structure, corresponding to the centre of gravity of the E-ELT main structure where all its mass is concentrated, are extracted as a function of time. The time histories of the absolute acceleration of the top joint resulting from the analysis of the isolated and non-isolated models are superimposed and illustrated in the following.

The time histories highlights the beneficial effects of the designed isolation system. In fact, the absolute accelerations experienced by the E-ELT main structure have undergone an overall decrease. The substantial reduction is clear and unequivocal in horizontal directions, as shown in Figure 7.12 and Figure 7.13. In vertical direction, the advantages are less evident. However, the maximum value of the absolute acceleration for the non-isolated structure is never reached by the isolated structure and the other values are overall lower, as highlighted by Figure 7.14.

From the absolute accelerograms in each direction, it is possible to obtain the frequency spectrum through the Fourier Transform. The Fourier Transform

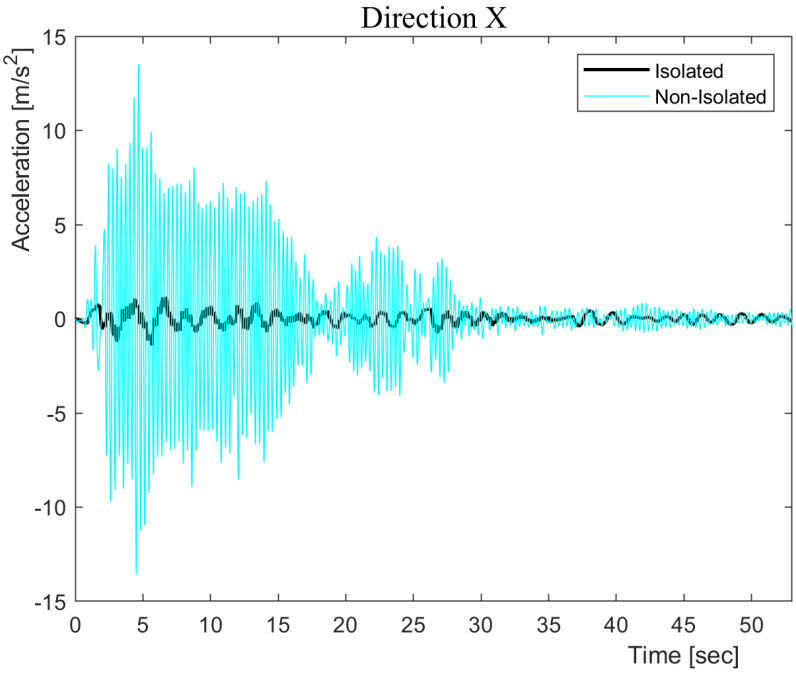

Figure 7.12: Absolute acceleration time history of the top joint of the structure in direction X.

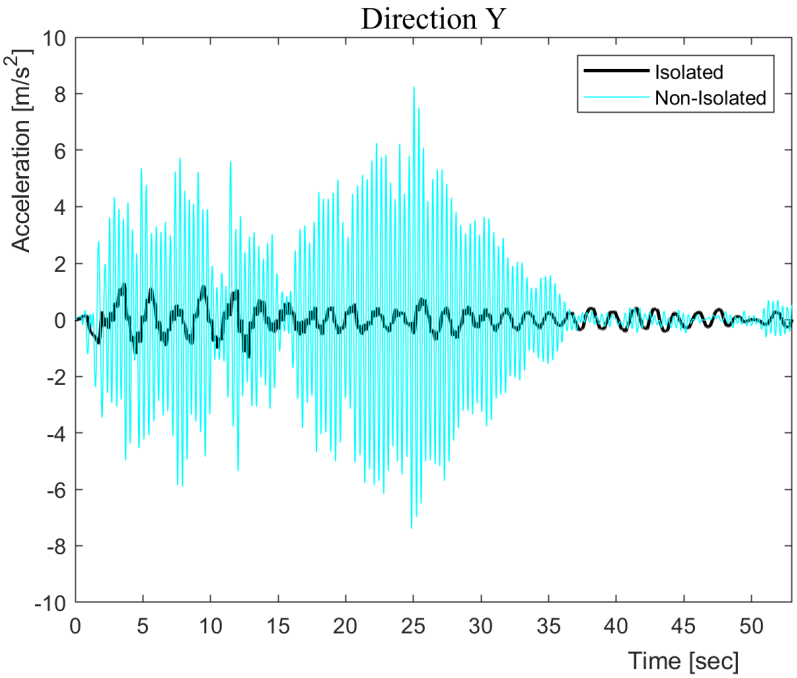

Figure 7.13: Absolute acceleration time history of the top joint of the structure in direction Y.

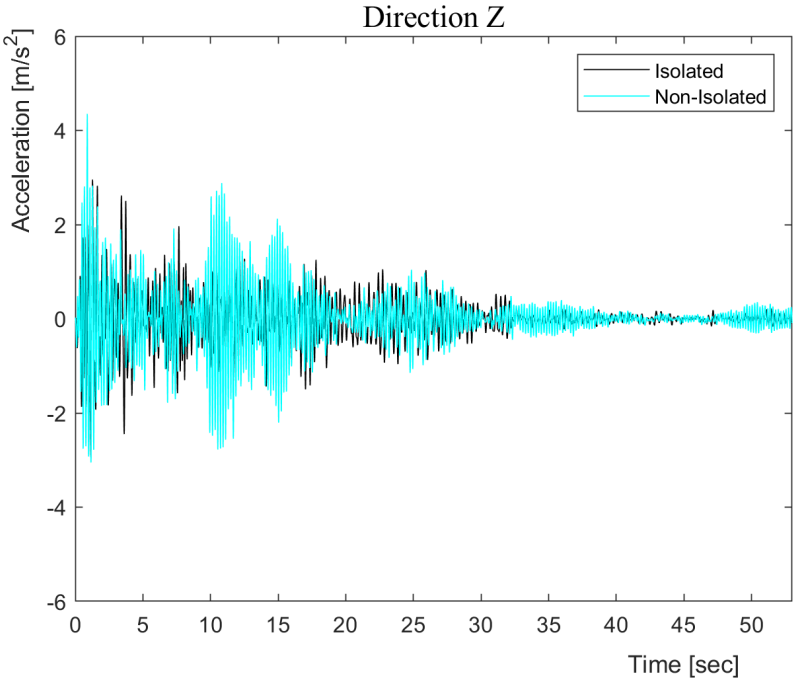

Figure 7.14: Absolute acceleration time history of the top joint of the structure in direction Z.

allows to pass from a function in the time domain to a function in the frequency domain. Then, the absolute value of the Fourier Transform is the so-called Fourier spectrum, which represents the density of frequency of the starting acceleration input.
The Fourier spectra of the non-isolated and the isolated structures modelled on SAP2000 are represented in Figure 7.15, Figure 7.16 and Figure 7.17 as superimposed in direction X, Y and Z, respectively.
The comparison between the Fourier spectra on each direction, resulting from the analysis of the two models, demonstrate the improvement in the seismic protection of the structure given by the introduction of the designed elastomeric bearing-based isolation system. As expected, the Fourier spectrum of the isolated structure has a peak in correspondence of the isolation frequency, that is a typical feature of isolation systems. However, except for the isolation frequency, the Fourier spectrum of the isolated structure remains below the corresponding Fourier spectrum of the non-isolated structure.

To give an example, considering the Fourier spectra in direction Y shown in Figure 7.16, the magenta line represents the spectrum of the isolated

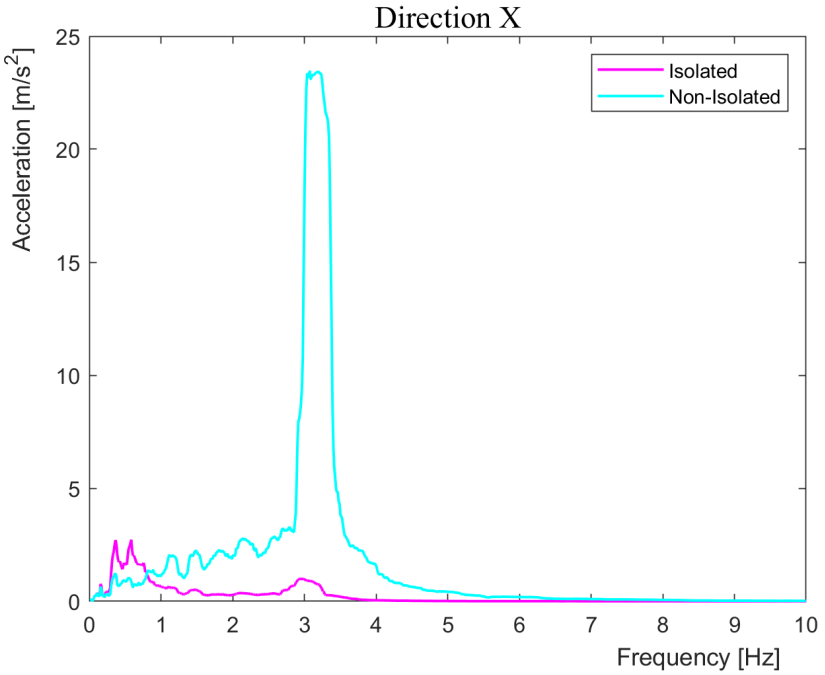

Figure 7.15: Fourier spectra of the isolated and non-isolated models in direction X.

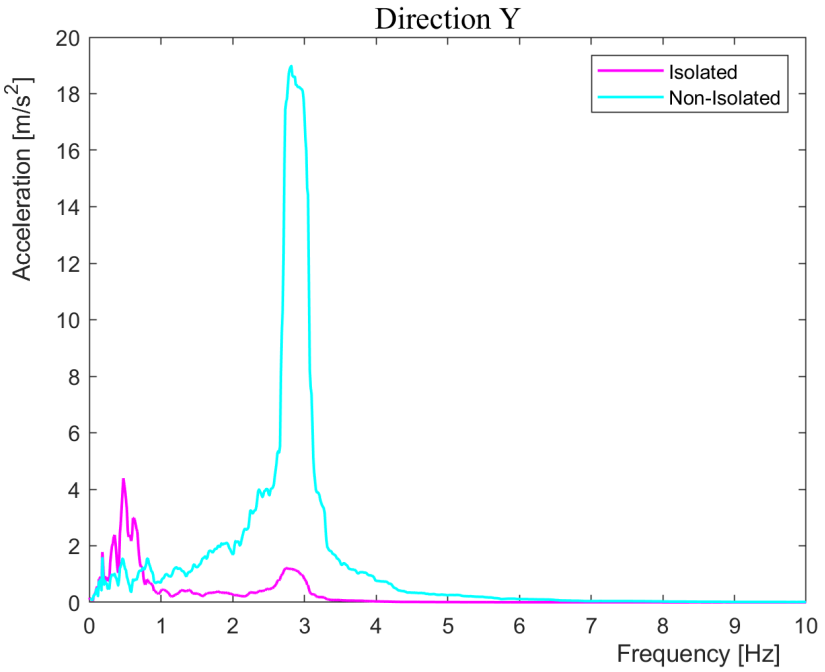

Figure 7.16: Fourier spectra of the isolated and non-isolated models in direction Y.

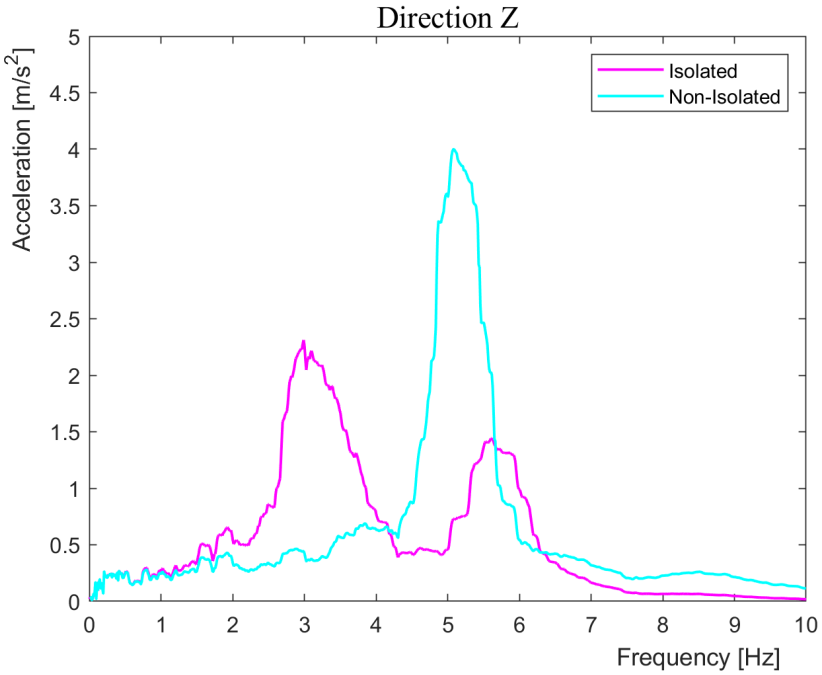

Figure 7.17: Fourier spectra of the isolated and non-isolated models in direction Z.

structure and it has a peak value around $f = 0.43\ Hz$, that is the isolation frequency in Y direction, as reported in Table 7.1. Then, it is kept below the cyan line that represents the spectrum of the non-isolated structure. The latter has only a high-value peak in correspondence of the mode of vibration in that direction, equal to $f = 2.90\ Hz$, as reported in Table 7.2, for which a very slight peak is present also in the magenta line, corresponding to a local mode of vibration.

Nevertheless the considerations discussed above are valid also in vertical direction, the difference between the two Fourier spectra is less marked than in the two orthogonal horizontal directions. This is in accordance with the conclusion deduced from the superimposition of the absolute accelerograms of the isolated and the non-isolated models in vertical direction and with the shifting of the vertical period. In fact, the vertical period is shifted from 0.19 *sec* to 0.32 *sec*, that is less relevant than from 0.34 *sec* to 2.32 *sec* in horizontal directions, and the difference between the accelerations in direction Z of the top joint of the two models, shown in Figure 7.14, is less marked than in horizontal directions. However, the vertical isolation is particularly effective in the high-frequency range where the distance between the Fourier spectrum of the isolated model and the Fourier spectrum of the non-isolated

model increases significantly, as illustrated in Figure 7.18 where the y-axis is in logarithmic scale. This is a great beneficial effect for structure in which instrumentation sensitive to high-frequency vibrations is present, as the case of the E-ELT. The high sensitivity of the machines, that is a common feature of research technology, combined with the designed vertical isolation guarantees the avoiding of resonance problems.

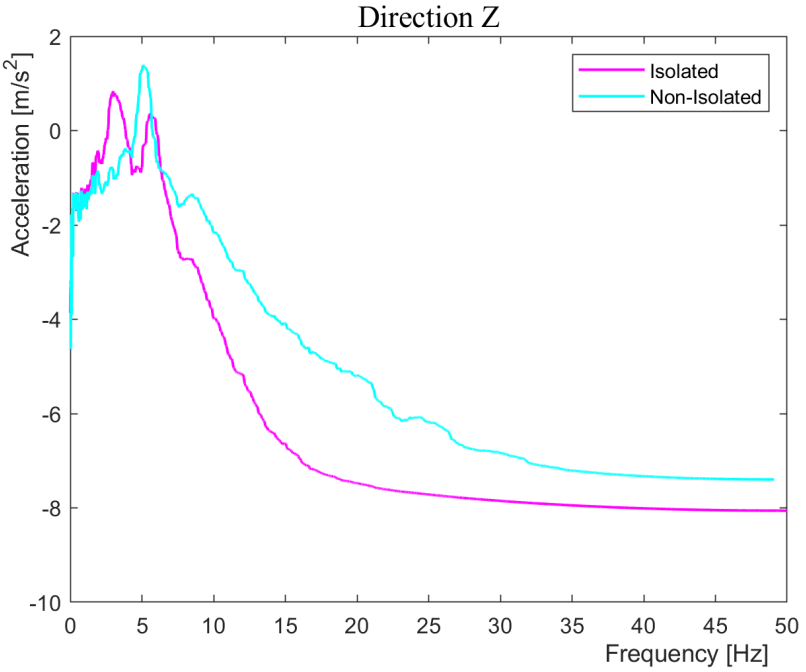

Figure 7.18: Fourier spectra of the isolated and non-isolated models in direction Z with accelerations in logarithmic scale.

Once the dynamic analysis results are discussed, the last step consists in verifying that the maximum axial force does not occur in the same instant of time when the horizontal displacement is maximum and that the corresponding value of axial force respect the European Standards requirements on the stability problem. To this aim, all bearings should be verified but, due to the fact that the two horizontal directions are considered separately, only eight devices are verified corresponding to the expected maximum lateral displacements: two on the external ring and two on the internal ring aligned with the y-axis while two on the external ring and two on the internal ring aligned with the x-axis, as shown in Figure 7.19. For the sake of clearness, the assessment procedure is reported in the following for one device as an example.

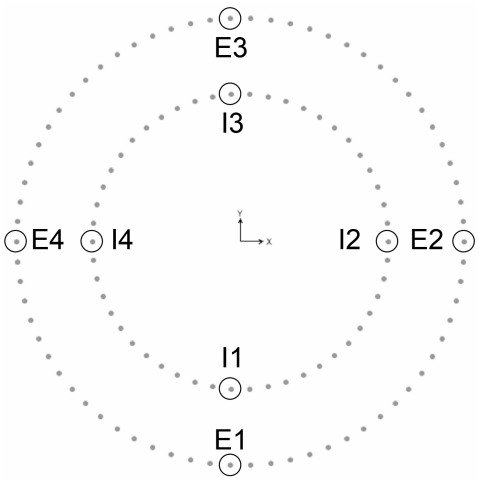

Figure 7.19: Selected elastomeric bearings for final verification.

Considering, for example, the elastomeric bearing in position E4 as illustrated in figure above, the lateral displacement time history in direction X is extracted from SAP2000 and shown in Figure 7.20.

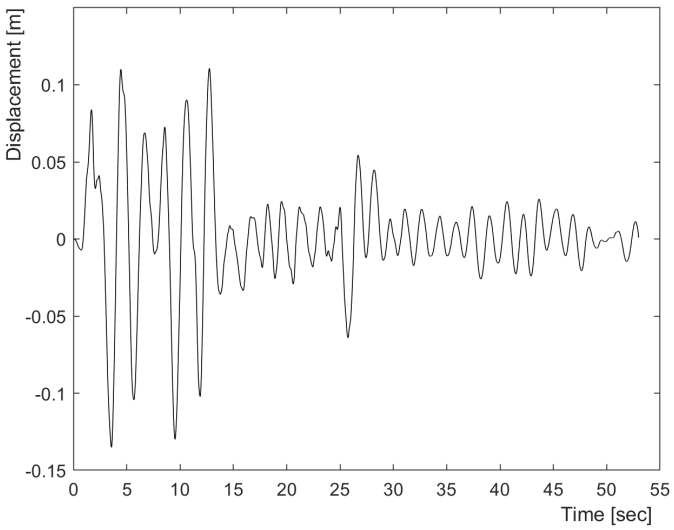

Figure 7.20: Lateral displacement time history in direction X of the E4 device.

The maximum lateral displacement is equal to $d_{max} = 0.144\ m$ at the corresponding instant of time $T_{d,max} = 5.61\ sec$.
Figure 7.21 shows the axial force time history of the same device. The maximum value of the axial force is $N_{max} = 2325\ kN$ at the corresponding

instant of time $T_{N,max} = 1.3\ sec$. However,the value assumed by the axial force at time $T_{d,max} = 5.61\ sec$, when the maximum lateral displacement occurs, is $N_{d,max} = 1719\ kN$.
Finally, the cross check can be performed verifying that the lateral displacement at time $T_{N,max} = 1.3\ sec$, when the maximum axial force occurs, is much lower than the maximum lateral displacement. In fact, it results equal to $d_{N,max} = 0.035\ m$.

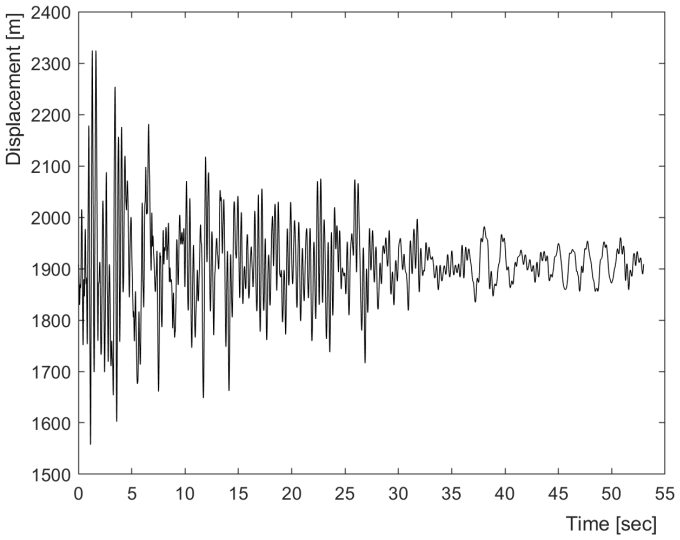

Figure 7.21: Axial force time history of the E4 device.

Then, the same procedure for the final verification and the cross check is repeated for the remaining devices and the results for the selected devices are reported in Table 7.3.

As expected, the maximum lateral displacement is coincident for aligned devices and occurs in the same instant of time. Conversely, the corresponding values of the axial force are different whether the devices are on the external or internal ring, due to the different distances from the centre that leads to a difference in the rocking contribution, and whether the contributions that define the total axial force on the devices are summed or subtracted.
For the same reasons, the maximum values of the axial force are different for each device while the lateral displacements in the corresponding instants of time are equal for devices on the internal ring and devices on the external rings, due to the rigid behaviour of the telescope pier.

Table 7.3: Final verification on maximum lateral displacement and axial force.

Device	$T_{d,max}$	d_{max}	$N_{d,max}$	$T_{N,max}$	N_{max}	$d_{N,max}$
E1	3.56 sec	0.135 m	1728 kN	3.44 sec	2306 kN	0.126 m
E2	5.61 sec	0.144 m	1969 kN	3.43 sec	2057 kN	0.042 m
E3	3.56 sec	0.135 m	1463 kN	1.64 sec	2287 kN	0.082 m
E4	5.61 sec	0.144 m	1719 kN	1.3 sec	2325 kN	0.035 m
I1	3.56 sec	0.135 m	1683 kN	3.44 sec	2256 kN	0.126 m
I2	5.61 sec	0.144 m	1927 kN	3.43 sec	2090 kN	0.042 m
I3	3.56 sec	0.135 m	1428 kN	1.64 sec	2246 kN	0.082 m
I4	5.61 sec	0.144 m	1681 kN	1.3 sec	2269 kN	0.035 m

Reminding that the fundamental requirement for the stability problem defined in EN15129 states that the maximum axial force must be lower than half of the critical buckling load, as expressed in Equation (4.16), with half of the critical buckling load for the designed 3D isolation system equal to $P_{cr}/2 = 2528\ kN$, the devices selected as the ones subjected to the worst loading condition result to be verified. Thus, it is possible to conclude that the designed approach proposed in Section 4.2 and applied to the E-ELT case study gives great results when the structure is subjected to the El Centro seismic excitation.

Moreover, the results listed in Table 7.3 demonstrate that the non-simultaneity hypothesis, on which the design approach proposed in Section 4.2 is based, is valid for the El Centro seismic excitation. However, it is worth noting that the El Centro vertical elastic response spectrum, shown in Figure 7.22, has an initial marked peak and then decreases rapidly such that the spectral acceleration corresponding to the isolation period $T_v = 0.3\ sec$ is lower than the peak ground acceleration. Thus, this vertical elastic response spectrum is not in accordance with EC8 so the resulting value of the maximum axial force is far from the value computed in Section 5.4 on the base of the vertical elastic response spectrum defined in EC8 §3.2.2.3.

Therefore, the 3D seismic isolation system proposed above can be considered only as a preliminary design. In fact, further dynamic analyses on the isolated E-ELT telescope pier and main structure model are required,

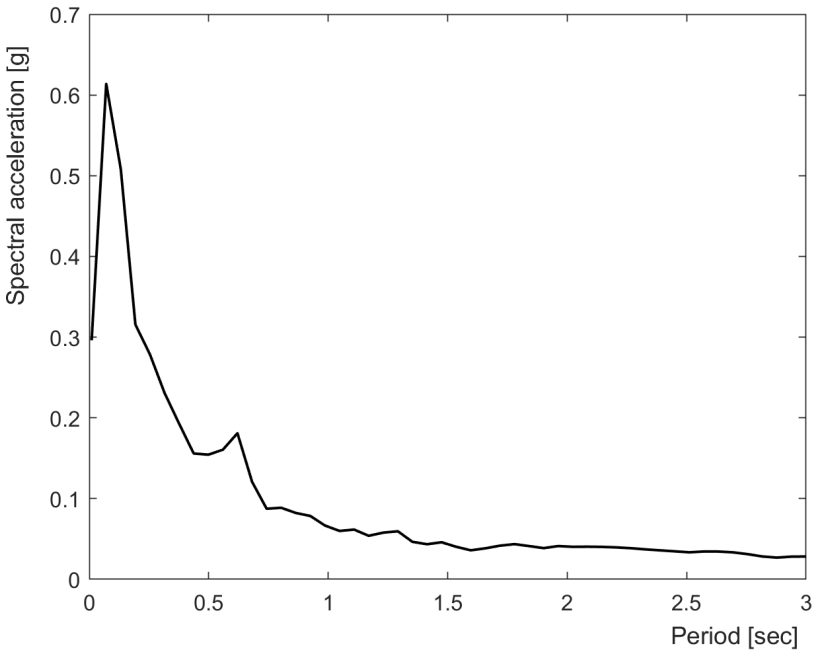

Figure 7.22: Vertical pseudoacceleration elastic response spectrum for El Centro earthquake.

subjecting the structure at least to seven different seismic excitations characterized by EC8-compatible vertical elastic response.

Chapter 8

Conclusions

A design approach for a three-dimensional seismic base isolation system using high damping rubber bearings with low shape factor ($S < 5$) has been proposed as an alternative to the approach defined by European Standards to protect large structures from damaging effects of intense earthquakes. Actually, it differs from the European Standards in an initial hypothesis that allow to relax the more conservative requirements of European codes. In particular, it is based on the assumption that, due to the marked distance between the vertical isolation period and the horizontal isolation period, it is possible to consider the probability that the maximum axial force occurs simultaneously with the maximum lateral displacement is sufficiently low to separate the effects of the components of the seismic action. It leads to the definition of two loading condition separately: the first assumes the bearing subjected to the static load and the horizontal component of the seismic action, neglecting axial force due to vertical seismic excitation, and the latter assumes the bearing subjected to the static load and the vertical component of the seismic action, neglecting rocking effects. Once the design is performed considering only one loading condition, both of the two conditions must be verified according to European Standards, maintaining a lower margin of safety. Then, the aformentioned design approach has been applied to a case study for which vertical isolation is considered to be essential. The European Extremely Large Telescope has been selected as suitable for this work due to its importance for the astronomy research, famous worldwide. The E-ELT consists of several instruments sensitive to vibrations, in particular high-frequency vibrations, both in horizontal and vertical vibrations. The elastomeric bearing response has been analyzed on the base of the mathematical and numerical model proposed by Kumar et al. [2015].

Kumar et al. [2015] suggested to obtain the restoring forces in orthogonal horizontal directions as the sum of a viscoelastic contribution and a hysteretic contribution, according to the isotropic formulation. The viscoelastic contribution is split in two terms: the former depends on a viscous damping parameter c_d and the latter depends on the horizontal stiffness K_d, computed considering the coupling between horizontal and vertical response. The hysteretic contribution depends on the characteristic strength of the bearing Q_d that allows to define the hysteresis cycles, which controls the energy dissipation mechanism. It has been noted that, computing the restoring forces according to this formulation, the damping effect is doubled. In fact, the effective damping of the elastomeric bearing β_{eff} enters in both the definition of the viscous damping parameter and of the characteristic strength. Thus, if both contributions are considered, the energy dissipation due to damping is counted twice.. Due to the fact that the major energy dissipation mechanism of the elastomer used for high damping rubber bearing is hysteretic rather than viscous, it is possible to conclude that the contribution due to the viscous damping parameter c_d must be neglected.

Elastomeric bearings for three-dimensional isolation systems require low value of the vertical stiffness, in concert with low value of the horizontal stiffness. To fulfill this condition, thick layers of rubber are required, that means high value of the total height of the rubber T_r. This geometrical property implies that, when an intense earthquake occurs, the elastomeric bearing reaches lateral deformations that are far from the 100% shear strain, considered as the reference deformation level. Therefore, attention must be paid to the definition of the parameters of the hysteresis cycle that are the post-elastic stiffness K_d, the post-elastic stiffness ratio α and the characteristic strength Q_d. Once the geometrical and material properties of the bearing are designed, the values of K_d and α are established. Thus, the value of the characteristic strength Q_d must be selected such that the energy dissipated per cycle corresponds to the percentage of the elastic strain energy defined by the effective damping β_{eff}, designed for a shear strain corresponding to the design maximum horizontal displacement. In fact, the effective damping β_{eff} is defined as the ratio between the energy dissipated per cycle and the corresponding elastic strain energy. However, the rubber compound properties, e.g. β_{eff}, are commonly defined for the 100% shear strain so it is necessary to pass from the designed properties at a shear strain corresponding to the design maximum displacement to the properties at the 100% shear strain. Due to this and to fact that the maximum lateral displacement increases, so the energy dissipated per cycle increases as

a function of it while the elastic strain energy increases as a function of the square of it, the effective damping β_{eff} decreases reaching low value (around 5%). Therefore, it is possible to conclude that the damping required to the rubber compound for elastomeric bearings used in 3D seismic base isolation could be closer to a natural or synthetic rubber compound typical of low damping rubber bearings.

The OpenSees analyses on the designed single elastomeric bearing, modelled using the `ElastomericX` element implemented by Kumar [2016], has been performed considering the coupling between horizontal and vertical responses. In particular, the variation in the critical buckling load capacity as a function of the lateral displacement, the variation in the horizontal stiffness as a function of the axial load and the variation in the vertical stiffness as a function of the lateral displacement have been progressively considered. The analyses evidence the complexity of elastomeric bearings response and the difficulty to predict the actual behaviour of these devices through a simplified model. However, for the E-ELT case study, it is possible to conclude that the bearing response in horizontal directions can be modelled by the bi-linear curve of the idealized hysteresis cycle whereas the bearing response in vertical direction can be modelled as linear elastic.

The SAP2000 analyses are performed on the model of the whole isolated structure and on the model of the corresponding whole non-isolated structure. The results of the modal analysis demonstrate that the designed 3D seismic base isolation system fulfills the shifting period requirement and the assumptions made during the design procedure. The results in terms of the single elastomeric bearing response of the dynamic analysis allow to conclude that the `Plastic (Wen) Link` element models the designed device with sufficient adherence to the actual behaviour. Nevertheless the coupling between horizontal and vertical responses is not considered, the hysteresis cycles turn out to be in accordance with the OpenSees analysis results with slightly lower displacements and forces but higher regularity. The results in terms of the whole structure of the dynamic analysis highlight the beneficial effects of the designed 3D isolation system. In fact, the absolute accelerations experienced by the centre of gravity of the main structure have undergone an overall reduction, in particular in horizontal directions. Expressing the results as absolute acceleration Fourier spectra, it is possible to conclude that the isolated model has a peak in correspondence of the isolation frequency, that is a typical feature of isolation systems made of elastomeric bearings, while the remaining values remain below the corresponding non-isolated model. Vertical isolation is particularly effective in

the high-frequency range, eliminating risks of resonance and protecting the research equipment sensitive to high-frequency vibrations.

Finally, the initial hypothesis on which the proposed design approach is based results to be verified for the El Centro seismic excitation. However, due to the fact that the vertical elastic response spectrum coming from the aforementioned earthquake is not compatible with the EC8 prescriptions, it is not possible to conclude that the proposed design approach is reliable in general. Therefore, the 3D seismic isolation system proposed above can be considered only as a preliminary design. In fact, further dynamic analyses on the isolated E-ELT telescope pier and main structure model are required, subjecting the structure at least to seven different seismic excitation characterized by EC8-compatible vertical elastic response.

Due to the complexity of the elastomeric bearing response prediction and the high expense of 3D isolation system made of these devices, these systems have not been fully accepted for civil constructions and they are adopted only for special structures, that require seismic protection not only in horizontal directions but also in vertical direction [Kelly and Lee, 2018].

Bibliography

E Blanford, E Keldrauk, M Laufer, M Mieler, J Wei, B Stojadinovic, and PF Peterson. Advanced seismic base isolation methods for modular reactors. Technical report, University of California Berkeley, 2010.

Ian G Buckle. Passive control of structures for seismic loads. *Bulletin of the New Zealand Society for Earthquake Engineering*, 33(3):209–221, 2000.

Ian G Buckle and Ronald L Mayes. Seismic isolation: history, application, and performance-a world view. *Earthquake spectra*, 6.2:161–201, 1990.

Michalakis C Constantinou, Tsu T Soong, and Gary F Dargush. Passive energy dissipation systems for structural design and retrofit. 1998.

Michalakis C Constantinou, AS Whittaker, Y Kalpakidis, DM Fenz, and Gordon P Warn. Performance of seismic isolation hardware under service and seismic loading. 2006.

Computer & Structures Inc Structural & Earthquake Engineering Software CSI. *CSI Analysis Reference Manual - For SAP2000, ETABS, SAFE and CSiBridge*. 2016.

EN1337-3:2005. Structural bearings-part 3: Elastomeric bearings. *Brussels: European Committee for Standardization.*

UNI EN15129:2018. Anti seismic devices. *Brussels: European Committee for Standardization.*

EN1998-1:2004. Eurocode 8: Design of structures for earthquake resistance-part 1: general rules, seismic actions and rules for buildings. *Brussels: European Committee for Standardization.*

European Southern Observatory ESO. The E-ELT construction proposal, 2011. URL `https://www.eso.org/public/archives/books/pdf/book_0046.pdf`. Accessed: 03.2019.

European Southern Observatory ESO. Extremely large telescope, 2019. URL `https://www.eso.org/public/images/archive`. Accessed: 03.2019.

Takafumi Fujita. Seismic isolation of civil buildings in japan. *Progress in Structural Engineering and Materials*, 1(3):295–300, 1998.

Alan Neville Gent. Elastic stability of rubber compression springs. *Journal of Mechanical Engineering Science*, 6(4):318–326, 1964.

AN Gent and PB Lindley. The compression of bonded rubber blocks. *Proceedings of the Institution of Mechanical Engineers*, 173(1):111–122, 1959.

Damian N Grant, Gregory L Fenves, and Ferdinando Auricchio. Modelling and analysis of high-damping rubber bearings for the seismic protection of bridges. 2005.

Johannes Adrianus Haringx. On highly compressible helical springs and rubber rods and their application for vibration-free mountings, i. *Philips Research Reports*, 3:401–449, 1948.

Johannes Adrianus Haringx. On highly compressible helical springs and rubber rods and their application for vibration-free mountings, ii. *Philips Research Reports*, 4:49–80, 1949a.

Johannes Adrianus Haringx. On highly compressible helical springs and rubber rods and their application for vibration-free mountings, iii. *Philips Research Reports*, 4:206–220, 1949b.

James M Kelly. Earthquake-resistant design with rubber. 1993.

James M Kelly and Jiang Jun Lee. Vertical flexibility in isolation systems. *Civil Engineering Research Journal*, 4(1), 2018.

James M Kelly, Ian D Aiken, and Frederick F Tajirian. Mechanics of low shape factor elastomeric seismic isolation bearings. *Earthquake engineering research center UCB/EERC-89/13*, 1989.

Trevor E Kelly. Base isolation of structures: design guidelines. *Holmes Consulting Group Ltd*, 2001.

Chan Ghee Koh and James M Kelly. A simple mechanical model for elastomeric bearings used in base isolation. *International journal of mechanical sciences*, 30(12):933–943, 1988.

Manish Kumar. ElastomericX, leadRubberX, and HDR: User elements in OpenSees for analysis of elastomeric seismic isolation bearings under extreme loading [computer program], 2016. URL `http://opensees.berkeley.edu/wiki/index.php`. Accessed: 02.2019.

Manish Kumar, Andrew S Whittaker, and Michael C Constantinou. Seismic isolation of nuclear power plants using elastomeric bearings. Technical report, MCEER, 2015.

Silvia Mazzoni, Frank McKenna, Michael H Scott, Gregory L Fenves, et al. Opensees command language manual. *Pacific Earthquake Engineering Research (PEER) Center*, 264, 2006.

Frank McKenna. Opensees: a framework for earthquake engineering simulation. *Computing in Science & Engineering*, 13(4):58–66, 2011.

YJ Park, YK Wen, and A H-S Ang. Random vibration of hysteretic systems under bi-directional ground motions. *Earthquake engineering & structural dynamics*, 14(4):543–557, 1986.

S Pinarbasi and U Akyuz. Investigation of compressive stiffness of elastomeric bearings. In *6th International Congress on Advances in Civil Engineering, Bogazici University October*, pages 6–8, 2004.

Michael D Symans. Seismic protective systems: seismic isolation. *Instructional material complementing FEMA*, 451, 2009.

Stephen P Timoshenko and James M Gere. *Theory of elastic stability*. McGraw-Hill Book, New York, 1961.

Gordon P Warn and Keri L Ryan. A review of seismic isolation for buildings: historical development and research needs. *Buildings*, 2(3):300–325, 2012.

Gordon P Warn and Andrew Stuart Whittaker. A study of the coupled horizontal-vertical behavior of elastomeric and lead-rubber seismic isolation bearings. 2006.

Victor Zayas, Stephen Mahin, and Michael Constantinou. Safe and unsafe seismically isolated structures. Technical report, University of California Berkeley, 2016.